Earth-Science Reviews 246 (2023) 104571

Contents lists available at ScienceDirect

Earth-Science Reviews

journal homepage: www.elsevier.com/locate/earscirev

Scaling behavior of bedload transport: what if Bagnold was right?

Christophe Ancey [a,*], Alain Recking [b]

[a] École Polytechnique Fédérale de Lausanne, Station 18, Lausanne 1015, Switzerland
[b] University of Grenoble Alpes, INRAE, CNRS, IRD, Grenoble INP, IGE, domaine universitaire, Saint-Martin-d'Hères 38400, France

ARTICLE INFO

Keywords:
Bedload transport
Bagnold
Flow resistance
Efficiency factor
Transport rate
Stream power

ABSTRACT

There is a paradox in the relationship between bedload transport rates and flow variables: laboratory and field studies have reported on how bedload transport rates depend on flow variables through a power law, but none of the empirical laws fitted to the data has managed to provide accurate predictions of bedload transport over a wide range of flow conditions. Inferring bedload transport's scaling behavior from data has remained a stubborn problem because the data are very noisy. It is, therefore, difficult to progress on this problem without some informed speculation about how bedload and flow interact. Ralph Bagnold proposed an original theory to resolve this problem. This paper reviews and updates Bagnold's model by separating the effects of flow resistance and efficiency (energy transfer from water to bedload) on dimensionless transport rates Φ. Both variables' contributions to transport rates can be parameterized separately for the three transport regimes that Bagnold defined (no transport, transitional, and sheet flow). We also consider two possible control variables: the dimensionless Shield stress τ^* and a dimensionless number related to stream power. In the transitional regime, the dimensionless bedload transport rate scales as $\Phi \propto \tau^{*3}$, whereas in the sheet-flow regime, it varies as $\Phi \propto \tau^{*5/3}$. We end up with two Bagnold equations: one based on physical principles and involving Shields stress τ^*, flow resistance f, a density ratio, and a bed slope; the other based on non-linear regression and stream power. Compared to a large set of laboratory and field data, predictions from Bagnold's model show reasonable accuracy when the bed is plane.

1. Introduction

If we had to sum up one century of research on bedload transport, the quest for a universal scaling law for bedload transport rates is certainly the one that has attracted the most attention in the last few decades. In a recent review paper, Gomez and Soar (2022) described this quest as a "Sisyphean task," in reference to Greek mythology's hero Sisyphus, who was condemned by Zeus to roll a boulder up to the top of a hill. Whenever Sisyphus reached the top, the boulder slipped from his hands and rolled down again, forcing him to resume his task endlessly.

Why is a scaling law interesting and relevant to the study of bedload transport, and why do we care so much about its potential existence? Bedload transport equations are of paramount importance to engineering, and that is why engineers took a keen interest in scaling laws as early as the mid 19th century: at that time, engineers started to build river training works and increase harbor capacities on a large scale across Europe, and they sought to quantify the relationships between water discharge and sediment flux of rivers and estuaries using power laws. Viewed from this perspective, practical approaches to bedload transport essentially fell into two categories: one category modeled how water carries sediment and used experiments to calibrate the model's parameters (du Boys, 1879; Forchheimer, 1914; Einstein, 1937; Kalinske, 1947), whereas the second category collected data and used it to fit a power law (Gilbert, 1914; Donat, 1929; Schoklitsch, 1934; Meyer-Peter et al., 1934; Thompson et al., 1935; Shields, 1936). Since the very beginning of research into bedload transport, the idea emerged that bedload transport rates q_s should vary as a power of the excess stress $\tau - \tau_c$ (du Boys, 1879; Donat, 1929; Shields, 1936; Meyer-Peter and Müller, 1948), excess water discharge (per unit width) $q - q_c$ (Gilbert, 1914; Schoklitsch, 1934; MacDougall, 1933; Thompson et al., 1935), excess stream power $\omega - \omega_c$ (Bagnold, 1966), or water velocity $u - u_c$ (Forchheimer, 1914; Kalinske, 1947), where τ [Pa], q [$m^2 \cdot s^{-1}$], ω [$W \cdot m^{-2}$], and u [$m \cdot s^{-1}$] denote the bed shear stress, flow discharge per unit width, stream power per unit width, and velocity, respectively, and the c subscript refers to incipient particle motion. As these power laws lack theoretical support, the exponents are not known in advance and

* Corresponding author.
E-mail addresses: christophe.ancey@epfl.ch (C. Ancey), alain.recking@inrae.fr (A. Recking).

https://doi.org/10.1016/j.earscirev.2023.104571
Received 23 March 2023; Received in revised form 15 September 2023; Accepted 19 September 2023
Available online 27 September 2023

must be fitted to the data, but as those data are fraught with variability and uncertainties, the exponents have been found to range from 1 (Cohen et al., 2010) to 16 (Paintal, 1971), with a consensual value around 3/2 (Meyer-Peter and Müller, 1948; Wong and Parker, 2006).

Apart from their usefulness in engineering, scaling laws are especially significant in helping us to understand how physical or biological systems self-organize in response to internal or external changes, and that is why they have been extensively studied since the early 20th century, giving rise to an abundant literature (Seshadri and Na, 1985; Turcotte, 1995; Bak, 1996; Solé et al., 1999; Sornette, 2000; Dodds and Rothman, 2000; Barenblatt, 2003). Scaling laws often reflect the persistence of intrinsic features or physical principles across scales, regardless of the specific dynamics of each process at a given scale (Barenblatt, 2003). For instance, Lacey (1930) found that for straight, self-formed channels over mobile beds, the wetted perimeter P_w [m] varied as the square root of the water discharge Q [$m^3 \cdot s^{-1}$], irrespective of bed slope and roughness: $P_w = 4.83Q^{1/2}$ in the metric system. A large body of data has confirmed this empirical law, often with the width as a substitute for the wetted perimeter and an exponent that may slightly deviate from 0.5 (Leopold and Maddock, 1953; Richards, 1977; Ferguson, 1986; Li et al., 2015; Métivier et al., 2017; Phillips et al., 2022). Lacey's equation holds over a wide range of water flow rates (spanning 6 orders of magnitude), from laboratory flumes to large real-world rivers. Like all power laws, it is scale-invariant, which means that the equation structure does not change when the water discharge is multiplied by any factor. It is also scale-free in its original form, which means that the perimeter's magnitude is not set by any particular length scale. At first glance, Lacey's law seems to contradict what we have learnt from flow resistance in straight channels—flow resistance equations show the interdependence of water discharge, bed roughness, bed slope, flow depth and wetted perimeter—but when we delve into the underlying mechanisms of channel formation, it is tempting to view Lacey's equation as the manifestation of general principles that rule how rivers adjust their cross-sections to drain water, transport excess sediment, and reach an optimal state in terms of energy and transport capacity. A large number of theoretical explanations have been advanced to explain Lacey's law, and although no consensus has been reached to date (Ferguson, 1986; Singh and Nott, 2003; Gleason, 2015), the criticisms raised in the debate about the origin of Lacey's equation (and other related forms) have prompted scientists to bounce ideas off each other and hone their respective arguments.

Bedload scaling equations are often criticized for their inaccuracies. Prediction errors exceeding one order of magnitude are often reported when comparing these equations with field or laboratory data (Ancey, 2020b). Their partial failure to summarize observations has pushed scientists to develop bedload equations for specific bed morphologies, grain size ranges, or flow conditions. The main problem with the development of specific equations is that we sacrifice universality to gain accuracy, thus leaving the question of bedload scaling unanswered. Naturally, the partial failure of existing scaling equations may mean that there is no such thing as a universal bedload transport scaling equation. Indeed, there are many reasons why sediment transport should not exhibit a universal behavior:

- the distinctive nature of sediment particles (bedload *vs.* suspended load) (Turowski et al., 2010),
- varied complex processes affecting the streambed (*e.g.*, partial mobility, bed armoring and arrangement, vegetation, cohesion) (Wilcock and McArdell, 1997; Pitlick et al., 2008; Yager and Schmeeckle, 2013; Yang and Nepf, 2019),
- uncontrolled boundary conditions (*e.g.*, bedrock, varying sediment supply) (Whiting and King, 2003; Yager et al., 2012; Recking, 2012; Turowski et al., 2013; Gomez and Soar, 2022; Schwindt et al., 2023),
- grain sorting (Parker, 1991; Lisle, 1995; Frey and Church, 2009),
- large fluctuations in transport rate time series (Kuhnle and Southard, 1988; Gomez, 1991; Nicholas et al., 1995; Dhont and Ancey, 2018; Gomez et al., 2022),
- overlapping or separate response times (bed *vs.* water stream response, scales of observation) (Gomez et al., 1989; Hoey, 1992; Recking et al., 2012; Heyman et al., 2013), and
- coupling between bedload transport, bedform, and water flow, and the influence of bed morphology (Church and Ferguson, 2015; Recking et al., 2016; Blondeaux et al., 2018).

Concurrently, there is ample evidence that laboratory and field data provide consistent power-law relationships between bedload transport rates and water discharge, thus supporting the idea of a single scaling law representing the first-order control of water discharge on bedload transport whose mean trend has to be corrected by higher-order terms accounting for more specific processes. The increasing accessibility of high-resolution bedload data and the development of data-driven approaches may soon overcome the current limitations of the regression analyses applied to bedload (Gomez et al., 2022). However, until then, we can attempt to move one step further towards elucidating bedload transport's scaling behavior by making an educated guess about what controls bedload transport.

This paper revisits the problem of bedload transport scaling by critically examining Bagnold's theory. Why Bagnold? Bagnold was associated with one of the few attempts to derive a scaling law based on physical principles—a law sufficiently versatile that it could be applied to a wide range of flow conditions. Over the years, Bagnold swung between rationalism (applying the principles of physics to derive a scaling law) and empiricism (applying regression analysis to a wide range of data). We follow him down both these avenues by building a bedload equation from Bagnold's ideas and the available information,and by fitting a power-law equation to experimental data.

In Sec. 2, we explain how Bagnold derived his equation relating bedload transport rate and stream power. We also express this equation by specifying its dependence on flow resistance, which leads us to propose an alternative formulation based on the bottom shear stress. Although Bagnold emphasized stream power as the main control variable, he also used the bottom shear stress to partition flow regimes (see § 2.5). It thus makes sense to have a more consistent formulation. We review three assumptions underpinning the derivation of Bagnold's equation: the local nature of transport in Bagnold's model (see § 2.2), bedload as a one-phase continuum at dynamic equilibrium (see § 2.3), and the equation's link with variational principles (see § 2.4). To close Bagnold's model, we need to supplement it with elements that were absent or only partially available in his time: parameterized energy transfer and flow resistance (see § 2.6); the detail about the calibration procedure has been left out of this paper and placed in the Supplementary Material (see § S1). We end the presentation of Bagnold's model by summarizing the three respective expressions of the dimensionless transport rate Φ for the three transport regimes Bagnold identified (see § 2.7, where the variables will also be defined): the no-transport, transitional, and sheet-flow regimes. We propose the complete expression $\Phi(\tau^*, i, f, s, \mu)$, specifying dependence of Φ on the Shields stress τ^*, bed slope i, the Darcy–Weisbach friction coefficient f, the density ratio s, and Bagnold's friction μ. We also propose a simplified expression referred to as Bagnold's master equation, where only the main trend $\Phi(\tau^*)$ is reported. We also revisit Bagnold's regression analysis and propose a scaling equation $\Phi(\Omega, \xi, R, s)$—referred to as Bagnold's scaling—in the form of a product M of the monomial powers of the scaled stream power Ω, relative submergence ξ, the particle Reynolds number R, and the density ratio s.

In Sec. 3, we compare predictions from Bagnold's model with laboratory data for the no-transport (see § 3.1), transitional (see § 3.2), and sheet-flow regimes (see § 3.3). The focus is on the $\Phi(\tau^*)$ relationship, but we also look at how the $\Phi(M)$ relationship performs using flume data

(see § 3.4) and how Bagnold's model compares with other theoretical models (see § 3.5). We then apply Bagnold's model to gravel-bed and sand-bed rivers for which sufficiently accurate records of bedload transport rates and hydraulic conditions are available (see § 3.6).

In Sec. 4, we examine how recent research in hydraulics and granular-flow dynamics sheds light on Bagnold's theory. We start by revisiting Bagnold's partitioning into three transport regimes (see § 4.1). Recent research has focused on microstructural theories of bedload transport. Within this framework, the existence of distinct transport regimes is seen as the consequence of the varied nature of particle contacts (see § 4.2). Finally, we examine how recent microstructural models of bedload transport shed further light on Bagnold's approach (see § 4.3).

2. Historical background and a reformulation of Bagnold's equation

2.1. Bedload transport equation

2.1.1. Derivation of Bagnold's model

All Bagnold's milestone papers, from 1956 to 1986, were predicated on the core assumption that water streams behave as "transporting machines." The word *machine* is significant here because it is closely related to thermodynamics, the science created in the 19th century to understand how energy could be extracted and converted to work in steam machines. For Bagnold, energy was the key concept to understanding the dynamics of sediment transport. Note that well before this time, a few scientists had intuited the part played by stream power in sediment transport (Seddon, 1886; Gilbert, 1914; Cook, 1935), but they had not developed the analogy of transport machines as Bagnold did.

Throughout Bagnold's papers, developed along two distinct avenues of research, energy was the driving variable. His earliest contributions focused on a microstructural analysis of stress generation and energy dissipation in a granular suspension (Bagnold, 1956, 1966, 1973). Later, by the 1970s, Bagnold simplified his approach to bedload and ended up with a holistic model based on general physical considerations, regression analysis, and experimental evidence (Bagnold, 1977, 1980, 1986).

The overarching idea of Bagnold's approach is simple. Let us consider a water column of depth h [m], flowing at a depth-averaged velocity $\bar{u}$ [m·s^{-1}], over a bed whose slope is denoted by $i = \tan\theta$ where θ is the bed angle with respect to horizontal; in the following, we will use the usual assumption of shallow slopes: $i = \tan\theta \approx \sin\theta$. In a steady uniform flow, the gravitational forces impart the driving power called *stream power* [W·m^{-2}]

$$\omega = \varrho g h \bar{u} i = \varrho g q i,$$

where $q = h\bar{u}$ is the water discharge per unit width [m^2·s^{-1}], ϱ is the water density [kg·m^{-3}], and g denotes the gravitational acceleration [m·s^{-2}]. This power is dissipated by friction. The dissipative power is $\mathscr{P} = \tau_b \bar{u}$ [W·m^{-2}], where τ_b denotes the bottom shear stress [Pa]. In the absence of bedload transport, the supplied energy is primarily dissipated by friction near the bottom, and thus, under steady-state conditions, $\mathscr{P} = \omega$ and $\tau_b = \varrho g h i$.

When the stream entrains particles, it imparts momentum to them, and thus part of the energy is dissipated by those particles. In his 1956 paper, Bagnold assumed that the power P [W·m^{-2}] dissipated by particles was related to the difference between the actual bottom shear stress and the critical value for incipient motion τ_c [Pa] (Bagnold, 1956):

$$P = (\tau_b - \tau_c)\bar{u}_b, \tag{1}$$

where $\bar{u}_b$ is the flow velocity near the bottom [m·s^{-1}]. This assumption, referred to as the Bagnold hypothesis, has often been used in subsequent models of bedload transport. In his later papers, Bagnold put this idea aside without further justification. He merely assumed that P and ω were related to each other through an efficiency factor $e_b \leq 1$ (reminiscent of machine efficiency) (Bagnold, 1966):

$$P = e_b \omega. \tag{2}$$

Let us now look at how Bagnold modeled energy transfers between the discrete (particles) and continuous (water) phases. Bagnold (1954) observed that when sheared at sufficiently high rates, particles experience collisional interactions and, as a consequence, the effective normal and shear stresses, σ_p and τ_p [Pa], scale as the square shear rate $\dot{\gamma}$ [s^{-1}] and particle diameter d [m]:

$$\sigma_p \propto \varrho_p d^2 \dot{\gamma}^2 \quad \text{and} \quad \tau_p \propto \varrho_p d^2 \dot{\gamma}^2,$$

where ϱ_p is the particle density [kg·m^{-3}]. These expressions are often referred to as the Bagnold law (Campbell, 1990; Andreotti et al., 2013), and Bagnold referred to the normal stress σ_p experienced by particles as the dispersive stress. Bagnold's law implies that the ratio $\mu_b = \sigma_p/\tau_p$ is roughly constant for a certain range of shear rates and particle concentrations, and it can thus be interpreted as a dynamic friction coefficient. If bedload takes the form of a particle layer of thickness h [m] and concentration $c(y)$, where y [m] denotes the coordinate normal to the streambed, and moving at the velocity u_p [m·s^{-1}], then Bagnold's assumption implies that, under steady-state conditions, water supplies power to this carpet:

$$\begin{aligned} P &= \int_0^h \tau_p \frac{\mathrm{d}u_p}{\mathrm{d}y}\mathrm{d}y \\ &= \int_0^h \mu_b \sigma_p \frac{\mathrm{d}u_p}{\mathrm{d}y}\mathrm{d}y = -\int_0^h u_p \frac{\mathrm{d}}{\mathrm{d}y}\left(\mu_b \sigma_p\right)\mathrm{d}y \\ &= \mu \bar{\sigma}_p \bar{u}_p = \mu\left(\varrho_p - \varrho\right) g h_s \cos\theta \bar{u}_s, \end{aligned} \tag{3}$$

where $\sigma_p = c\left(\varrho_p - \varrho\right) g (h - y)\cos\theta$ [Pa] is the effective normal stress distribution (the normal stress borne by the particle phase) across the flow depth, μ is Bagnold's bulk friction coefficient, and $\bar{\sigma}_p = \left(\varrho_p - \varrho\right) g h_s \cos\theta$ is the effective normal stress [Pa] experienced by the particle layer. The mean values μ, $\bar{u}_s$ [m·s^{-1}] (mean bedload velocity), and h_s [m] (effective bedload layer thickness) are defined by virtue of the mean value theorem such that the integrals above can be replaced by a simpler algebraic expression (for instance, $\int_0^h c u_p \mathrm{d}y = \bar{c} h \bar{u}_s = h_s \bar{u}_s$, where $\bar{c}$ denotes the depth-averaged bedload concentration and $h_s = \bar{c} h$ an effective bedload layer thickness).

By considering that the power supplied P_s is equal to the power dissipated by the water stream $P = e_b \omega$, and by defining the bedload transport rate per unit width as $q_s = h_s \bar{u}_s$ [m^2· s^{-1}], Bagnold obtained $\mu \Delta\varrho g q_s \cos\theta = e_b \tau_b \bar{u}$ or, equivalently,

$$q_s = \frac{e_b}{\mu\cos\theta}\frac{\omega}{g\Delta\varrho} = \frac{e_b}{\mu\cos\theta}\frac{\bar{u}\tau_b}{g\Delta\varrho}, \tag{4}$$

where $\Delta\varrho = \varrho_p - \varrho$ [kg·m^{-3}].

2.1.2. Alternative formulation

If we take Bagnold's developments one step further, we can derive a scaling law for the bedload transport rate q_s by relating it to flow resistance. To that end, we use the Darcy–Weisbach relationship to express the mean flow velocity as a function of the bottom shear stress:

$$\bar{u} = \sqrt{\frac{8}{f}}\sqrt{\frac{\tau_b}{\varrho}}, \tag{5}$$

where f denotes the Darcy–Weisbach friction factor. Substituting this equation into Eq. (4) provides

$$\mu \Delta\varrho g q_s \cos\theta = e_b \tau_b^{3/2}\sqrt{\frac{8}{f}}\varrho^{-1/2}. \tag{6}$$

We define the dimensionless shear stress and bedload transport rate

$$\tau^* = \frac{\tau_b}{\Delta \varrho g d} \text{ and } \Phi = \frac{q_s}{\sqrt{sgd^3}}, \tag{7}$$

where $s = \Delta\varrho/\varrho$. The dimensionless shear stress is also referred to as the *Shields number* or stress. With this notation, we can recast Eq. (4) into the dimensionless form of

$$\Phi = \frac{e_b}{\mu \cos\theta}\sqrt{\frac{8}{f}}\tau^{*3/2}, \tag{8}$$

which leads to the asymptotic scaling $\Phi \propto \tau^{*3/2}$ when assuming that the friction factor f, the efficiency factor e_b, and friction angle μ tend to constant values in the limit of $\tau^* \to \infty$. The link between dimensionless bedload transport rate, flow resistance, and Shields stress was made explicitly by Parker et al. (1982) and Ferguson (2012) (among other authors).

2.1.3. A first critical look at Bagnold's assumptions

Here we review some assumptions used explicitly or implicitly by Bagnold (1966). Some of them require more attention and development, and they will be addressed in § 2.2–2.4.

One key assumption in Bagnold's model derivation is that the flow carrying bedload reaches a steady state. This implies, in particular, that sediment is fully available. Implicitly, Bagnold also assumed that the sediment had a representative diameter d, which implies that either this sediment is well-sorted or there is no significant size effect on the transport rate. Ignoring any dependence of bedload transport rates on particle size distribution, Bagnold did not differentiate between particles that were transported and those that lay on the bed surface or in the subsurface.

Bagnold gave no clear indication about bedload transport's alignment with the main flow direction. His first assumption in Eq. (1) has often been interpreted as the collinearity between bedload transport and shear stress directions, and it was criticized as such by Seminara et al. (2002) when they generalized bedload transport equations for flows over irregular topography. His second assumption in Eq. (2) involved stream power, an algebraic quantity with no preferential direction.

Although Bagnold (1966) considered the existence of a mobile bed as a crucial element to his model's validity, he did not try to relate particle exchanges to the bed and particle transport (as, for instance, Einstein (1950) did by studying entrainment and deposition rates). He stated that his theory could not apply to fixed beds. Nothing in his theoretical developments, however, justifies excluding fixed bottoms.

Bagnold assumed that he could calculate bedload transport in isolation from the fluid dynamics (turbulence, form drag, flow resistance). For him, knowing the tractive force exerted by the flow on the carpet was sufficient to calculate bedload transport rates. The alternative formulation presented in § 2.1.2 shows that it is possible to account for flow resistance in his bedload equation if the driving variable is the Shield stress τ^* instead of stream power.

Bagnold (1966) assumed that the mean bedload concentration could be fixed at a maximum value ($\bar{c} = 0.53$) much lower than the static bed's concentration ($\bar{c}_0 = 0.65$). This assumption is dubious, but probably not critical because Bagnold encoded varying bedload concentration's effect on flow dynamics into the dynamic friction coefficient μ_b (Bagnold, 1956, 1966). His definition of the bulk friction angle μ (see § 2.6) may thus compensate, to some extent, for the error made by assuming a constant bedload concentration.

Bagnold's assumption of $\tau_p = \mu_b \sigma_p$, used in Eq. (3), can be compared with Terzaghi's principle, used in geomechanics (Davis and Sevladurai, 2002). According to this principle, the base of a saturated cohesionless layer undergoes a normal effective stress σ_y' defined as the difference between the total normal stress $\sigma_y = \big((1-\zeta)\varrho_p + \zeta\varrho\big) g h_s \cos\theta$ and the interstitial fluid pressure p [Pa]: $\sigma_y' = \sigma_y - p$ [Pa], where $\zeta = 1 - c$ is the porosity (*i.e.*, ratio of the void volume to the total volume). In geomechanics, the granular layer is seen as a two-phase continuum. If the fluid pressure is assumed to be hydrostatic (*i.e.*, $p = \varrho g(h-y)\cos\theta$), then the effective normal stress matches Bagnold's dispersive stress σ_p: $\sigma_y' = (1-\zeta)(\varrho_p - \varrho) g h_s \cos\theta = \sigma_p$. Note that numerous authors have questioned the approximation of hydrostatic pressure (Iverson, 1997; Pailha and Pouliquen, 2009; Iverson and George, 2014; Bouchut et al., 2016; Guazzelli and Pouliquen, 2018) in their two-phase models of saturated granular flows because the fluid pressure fluctuations created by the rapid contraction and dilation of pores during shearing are non-negligible relative to hydrostatic pressure.

Bedload transport can be perceived differently depending on the timescale of observation. When looking at flume or river flows over timescales ranging from seconds to hours, bedload transport can be defined as the water-induced displacement of particles, and in this case, it makes sense to seek a dependence of bedload transport rates q_s on instantaneous water discharge q or water stream ω, as Bagnold did: $q_s = f(q)$ or $q_s = f(\omega)$. Over longer timescales, let us say months or years, bedload transport reflects spatial and temporal bed variations, and its rate can be related to bedform displacement (Nicholas et al., 1995; Vericat et al., 2017). When the bed profile is regarded as the linear superposition of bedforms with wavelength λ [m], amplitude $A(\lambda)$ [m] and propagation speed $C(\lambda)$ [m·s^{-1}] (typically for sand dunes), then the bedload transport rate can be defined as

$$q_s = (1-\zeta)\int A(k)C(k)\mathrm{d}k$$

where k is the Fourier mode (Simons et al., 1965; Nikora, 1984; Guala et al., 2014; Lee et al., 2023). We know of no generalization to other bedforms, but this lack of a generalized bedload transport model has been filled by the development of landscape evolution models, in which bed variations are modeled using cellular automata, nonlinear diffusion or advection-diffusion equations (Willgoose, 2005; Coulthard and Van De Wiel, 2012; Chen et al., 2014; Williams et al., 2016). Formally, the sediment volume transported over long periods could be computed by the time-integration of instantaneous bedload transport equations in the form $q_s = f(q)$ or $q_s = f(\omega)$. However, in practice this procedure may lead to inaccurate estimates of the sediment budget, particularly in the gravel-bed rivers for which Shield stresses remain close to the threshold of incipient motion (to within a factor of 2). Although Bagnold (1966) made no mention of the timescale for which his model holds, his derivation leads us to think that it is only valid when estimating instantaneous bedload transport rates.

2.2. Local and non-local transport

A caveat is in order at this stage. When expressing Bagnold's bedload equation in the form (8) and assuming that the parameters f, e_b, and μ are constant, we end up with the scaling of $\Phi \propto \tau^{*3/2}$, which does not differ from empirical equations like the Meyer-Peter–Müller equation (Meyer-Peter and Müller, 1948). Likewise, Bagnold's moving carpet concept was not so different from the sliding layers imagined by Paul du Boys (1879) and subsequent authors, who expressed bedload transport rates as a function of the water stream's driving force. There is a possibility of confusion here that we have to eliminate.

Models involving bottom shear stress assume that bedload transport is a local process: particle flux adjusts instantaneously to the bottom shear stress that the water flow exerts on the streambed. Bedload transport corresponds to the everyday experience of exerting friction to displace an object. By contrast, Bagnold's model implies that bedload transport is a non-local process: the energy dissipated by the particle carpet is part of the total energy dissipated by the water column. Calculating bedload transport rates involves determining all the

dissipative processes at play in a given flow region.

Bagnold's report and autobiography provided further grounds for using stream power (Bagnold, 1966, 1990). In real-world rivers, hydraulic conditions and bedload transport can exhibit substantial variations over short distances. Thus, they cannot be conveniently described using standard flow resistance equations based on bottom shear stress τ_b. This difficulty is alleviated if, instead of τ_b, one uses an effective cross-section (statistically representative of all sections in a given area), and stream power ω as the driving variable of bedload transport rates q_s. From this perspective, Bagnold's postulate is tantamount to stating that bedload transport rates can only be estimated on average and over sufficiently large spatial scales (typically, the cross-section). In practical applications to real-world cases, it is also far easier to estimate or measure the water discharge Q across a given cross-section, and deduce stream power ϱgQi than it is to measure the flow depth and velocity across that cross-section, and infer the bottom shear stress distribution.

Although this was never explicitly stated by Bagnold or subsequent authors using stream power (Ackers and White, 1973; Yang, 1984; Molinas and Wu, 2001; Abrahams and Gao, 2006; Ferguson, 2005; Parker et al., 2011; Gao, 2012; Ferguson, 2012; Lammers and Bledsoe, 2018), the point is not whether the main variable is stream power or bottom shear stress, but whether bedload transport is a local or non-local process. Indeed, in fluid dynamics, when thermodynamic processes (*e.g.*, heat dissipation, entropy) are not considered, governing equations based on power and dissipation are strictly equivalent to balance equations involving stress and momentum: the dissipated power is derived from the stresses by multiplying them by the velocity field. In this respect, working with bottom shear stress or with stream power relies on the same principle of momentum conservation. Claiming that bedload transport is a non-local process implies that it is an adjustment variable that depends on what happens macroscopically in a certain flow region. Bagnold assumed that the flow depth was the right length scale for this flow region and that energy was more appropriate than stress for taking stock of the different processes and their interplay in a simple manner. Bagnold did not comment much on this crucial assumption, but one can find detailed justifications in Yang (1992).

2.3. Bedload as a one-phase continuum at equilibrium

Although Bagnold worked on a microstructural theory of granular suspensions—the antecedent of kinetic theory for granular gases (Haff, 1983; Campbell, 1990; Hunt et al., 2002)—and the dynamics of saltating particles (Bagnold, 1954, 1973), he had preferred to work at a macroscopic scale when developing his bedload transport equation. In his pioneering paper (Bagnold, 1956, 1966), Bagnold viewed bedload transport as a one-phase continuum. Focusing on steady-state conditions, he assumed that the bedload layer (called the carpet) was at equilibrium, that is, "the forces acting on every layer of solids must be in statistical equilibrium." The bedload layer is then entirely characterized by its mean velocity $\bar{u}_s$ [m·s^{-1}], thickness h_s [m], and mean concentration $\bar{c}$. He defined the (volumetric) bedload transport rate as

$$q_s = \int_0^\infty c(y)u_p(y)\mathrm{d}y = \bar{c}h\bar{u}_s = h_s\bar{u}_s, \tag{9}$$

where c is the local particle concentration and u_p denotes the local sediment velocity [m·s^{-1}]. These assumptions about the nature of bedload transport have several important consequences.

First, particle size does not appear explicitly in the definition (9) of the bedload transport rate, and thus his theory was not tailored to sediments with a wide grain-size distribution in which, depending on their size, some grains may move, while others remain at rest. Bagnold thus ignored a number of the physical processes at work in sediment transport (partial mobility and transport, grain sorting, downstream fining, bed coarsening). The inclusion of the grain-size distribution in bedload transport equations has mostly been achieved empirically by hypothesizing equal mobility and hiding effects (Powell, 1998; Parker and Toro-Escobar, 2002; Wilcock and Crowe, 2003; Recking, 2010). Recently, however, the analogy with particle segregation in granular flows has led to advection-diffusive equations being proposed for predicting the time variations in the grain concentration (Ferdowsi et al., 2017; Rousseau et al., 2021).

Second, interstitial fluid plays no role other than having a buoyancy effect on sediment. Like many authors after him, this assumption had led Bagnold to consider that, as a first approximation, it was possible to distinguish between suspended and unsuspended (bedload) sediments. Dade and Friend (1998) showed that there was no clear separation between suspended load and bedload: for $0.3 \leq w_s/u^* \leq 3$, sediment transport involves mixed loads, that is, mixtures of suspended load and bedload. The assumption in Bagnold's theory that the sediment phase is fully subordinate to the fluid phase is also implicit. This assumption was consistent with Bagnold's statement that the efficiency factor should be low, typically in the 0.11–0.15 range (Bagnold, 1966). As will be shown later (see § 2.6), much higher values are observed in flume and pipe experiments, which may mean that a large part of the water stream's energy is dissipated, not only through turbulence and bed resistance to flow, but also through momentum exchanges with the bedload. Under these circumstances, the assumption of a fully subordinate sediment phase is questionable.

Third, in Bagnold's theory, equilibrium refers to the balance of forces (or stresses) in the direction normal to the bed. His definition is quite restrictive and differs from those used elsewhere. Gilbert (1914) seldom used the word "equilibrium"; instead, he wrote:

> "Whenever and wherever a stream's capacity is overtaxed by the supply of debris brought from points above, a deposit is made, building up the bed. If the supply is less than the capacity, and if the bed is of debris, erosion results."

We can deduce that equilibrium refers to the mass balance of the bed: flow is in equilibrium if neither erosion nor deposition occurs in a given reach or, in other words, the amount of sediment that leaves the reach matches the amount that is deposited there. Continuing along the same lines as Gilbert, Einstein (1950) defined flow equilibrium as the bed's mass balance over a given area (whose typical length scale is 100 grain diameters). In case of a mismatch between erosion and deposition, sediment transport is considered to be in a non-equilibrium state (Wu and Wang, 2007; Charru et al., 2013). Although both Einstein and Gilbert referred to equilibrium in terms of bed mass balance, their length scales differed, and thus their definitions did not overlap completely. When streambeds exhibit forms, mass can be conserved at a certain bed-length scale, whereas locally, some areas are preferentially subject to erosion or deposition; and even under steady-state flow conditions, sediment transport rates may exhibit huge temporal fluctuations due to sudden changes in the bed configuration (*e.g.*, bank failure) (Dhont and Ancey, 2018). In this respect, rivers are closer to punctuated equilibrium systems: phases of rapid changes—during which the bed self-adjusts in response to local changes in the bed configuration or to a varying sediment input—alternate with long periods of weak transport (Ancey, 2020b). More recently, when referring to weak sediment transport under steady-state conditions, the emphasis has been put on statistical equilibrium (Furbish et al., 2012; Ancey and Heyman, 2014; Furbish et al., 2017): the bedload transport rate is handled as a random variable whose variations are fully characterized by its probability density functions and power spectrum under bed equilibrium conditions. Said differently, the river attains an equilibrium state if the probability distribution of its flow variables (*e.g.*, the bedload transport rate, the cross-section) remains stationary. In stochastic theories of bedload transport, the ensemble-averaged transport rate $\langle q_s \rangle$ involves a diffusive contribution and is thus entirely controlled by the local flow conditions:

$$\langle q_s \rangle = \langle \gamma \rangle \langle \bar{u}_s \rangle + \frac{\partial}{\partial x}\left(D_r \langle \gamma \rangle\right) \tag{10}$$

where γ denotes the particle activity [m] (volume of moving particles per unit streambed area), $\bar{u}_s$ is the mean sediment velocity [m·s^{-1}], D_r is the particle diffusivity [m^2·s^{-1}], and the angle brackets $\langle\cdot\rangle$ are used to denote an ensemble-averaged quantity (Furbish et al., 2012; Ancey and Heyman, 2014; Furbish et al., 2017). Some fully deterministic models have also introduced diffusion. For instance, based on empirical evidence of space and time variations in the bedload transport rate, Charru et al. (2004) suggested a differential form for defining the local transport rate:

$$q_s = q_{eq} - T_s\frac{\partial}{\partial t}q_s - L_s\frac{\partial}{\partial_x}q_s, \tag{11}$$

where L_s [m] and T_s [s] are the length and time scales, called the saturation length and saturation time, representing the typical length and times needed to reach the equilibrium transport rate q_{eq} [m^2·s^{-1}] that is observed for a flat bed under steady-state conditions. As Wainwright et al. (2015) highlighted, the notion of bed equilibrium and transport capacity varies between authors.

Although based on force balance rather than mass balance, Bagnold's definition of equilibrium is not necessarily incompatible with Einstein's or Gilbert's definition. Indeed, as the kinematic wave approximation to the shallow water equations illustrates (Hunt, 1984; Singh, 2001), unsteady flows can be close to a dynamic equilibrium state while showing significant but slow time variations in their mass. By contrast, compared with more recent definitions involving a diffusive part, Bagnold's definition is unable to account for the possible modulation of bedload transport rates when the particle activity γ is non-uniformly distributed along the bed. The only way to account for this diffusive process would be to make the efficiency factor e_b dependent on sediment transport upstream, a possibility that Bagnold did not contemplate in his writings.

2.4. Link with variational principles

In their analogy between thermodynamic and geomorphic systems, Leopold and Langbein (1962) advocated using entropy to calculate a river's most probable state, *i.e.*, its longitudinal profile, its optimal cross-section, and the structure of its drainage networks. The most probable state is the one for which entropy is maximum or the entropy production rate is minimum. The equivalent of internal energy was the potential energy (Bagnold, 1966). Leopold and Langbein's seminal paper gave rise to abundant literature based on the premise that geomorphic equilibrium can be determined using variational principles such as the principle of least action or maximum entropy (Yang et al., 1981; Yang, 1996; Molnár and Ramirez, 1998; Yalin and Ferreira Da Silva, 1999, 2000; Huang and Nanson, 2000; Huang and Chang, 2006; Singh et al., 2003; Millar, 2005; Nanson and Huang, 2008; Xu et al., 2016; Joshi et al., 2018; Nanson and Huang, 2018; Tranmer et al., 2020). For instance, assuming that flow resistance can be estimated using the Manning–Strickler equation, Huang (2010) found that the bedload transport rate should vary as $\Phi = 6.09(\tau^* - 0.0474)^{5/3}$, with a 5/3 exponent, higher than the 3/2 exponent used in the original Meyer-Peter–Müller equation.

Among the various entropy-based approaches to bedload transport, Chih Ted Yang's model was based on Prigogine's and Gyarmati's principles to postulate that rivers are open dissipative systems, whose equilibrium corresponds to the state with the minimum entropy-production rate (Yang, 1971; Yang and Molinas, 1982; Yang, 1994, 1996). According to Yang (1996), bed equilibrium is reached when the total energy dissipation of $\mathscr{P}$ [W·m^{-2}] is minimum, where

$$\mathscr{P} = \varrho_s g q_s i + \varrho g q i, \tag{12}$$

and $\varrho_s = c\varrho_p + (1-c)\varrho$ is the bulk density. In spite of the theoretical and experimental evidence provided by Chih Ted Yang and coauthors, some researchers like Parker (1977) considered the principle of the minimum entropy-production rate to have been "pulled out of a hat." Indeed, in fluid mechanics, the only minimum dissipation principle commonly accepted is the Helmholtz–Korteweg theorem, which states that for incompressible Newtonian fluids, the solution to the Stokes equations minimizes the rate of energy dissipation (Keller et al., 1967; Batchelor, 1970). For inertial flows, no extremum principle exists. Gray and Ghidaoui (2009) and Gray et al. (2018) derived depth-averaged balance equations (including internal energy and entropy) for one-directional flows and found that regardless of the flow regime (steady or unsteady), the entropy production rate is:

$$\Lambda = \frac{\mathscr{P}}{T} = \frac{1}{T}(\varrho_s g q_s i + \varrho g q i), \tag{13}$$

where T denotes absolute temperature [K]. Gray et al. (2018) found that the entropy production rate Λ is not a convex function of the flow depth (there is, therefore, no minimum of $\Lambda(h)$ apart from the trivial solution $h = 0$). As a consequence, they concluded that "the use of an energy minimization principle with open channel flow is not physically warranted" (Gray et al., 2018). More generally, the idea that geomorphic systems can be studied using extremum principles taken from the thermodynamics of irreversible processes has long been debated, and the consensus leans towards the irrelevance of thermodynamics concepts (Davy and Davies, 1979; Davies and Sutherland, 1983; Griffiths, 1984; Thorn and Welford, 1994). From this perspective, there is little hope that Bagnold's assumption about stream power (as the main driving variable) could be justified *a posteriori* using variational principles.

2.5. Bedload transport regimes

Bagnold (1966) did not explicitly refer to transport regimes (his writings never employed the word "regime" but rather "stage"). Without abandoning the meaning that Bagnold (1966) wished to convey, we can consider there to be three distinct bedload regimes:

- When $\tau^* < \tau_c^*$: there is no bedload transport when the dimensionless shear stress is below the threshold of incipient motion τ_c^*, hereafter called *critical shear stress*. Most models of bedload transport assume the existence of a threshold of incipient motion, but its existence has been brought into question by some observations at low shear stress (see § 3.1 for further information).
- When $\tau_c^* < \tau^* < \tau_x^*$: bedload transport takes the form of saltating and rolling particles that move intermittently along the bed. Bagnold highlighted how difficult it was to predict bedload transport rates in this regime, which he referred to as the *transitional regime*. He referred to τ_x^* as the *critical bedload stage*. According to Bagnold (1966), it ranges from 0.25 (when $d \geq 2$ mm) to 0.5 (when $d \leq 0.3$ mm).
- When $\tau^* > \tau_x^*$: bedload transport occurs in the form of a particle carpet, in which particles experience collisions and friction. Bedforms disappear or, at least, cease to create appreciable form drag. Bagnold called this regime the *high transport stage*, but it is more commonly referred to as the *sheet-flow regime* in contemporary hydraulic literature, and we use this term hereafter.

Fig. 1 shows the Shields diagram in the (R, τ^*) space. For the critical shear stress τ_c^*, we used the parametrization proposed by da Silva and Bolisetti (2000), who defined it as a function of the particle Reynolds number R (see Appendix A):

$$R = \frac{\sqrt{sgd^3}}{\nu}, \tag{14}$$

where ν is the kinematic viscosity of water [m^2·s^{-1}].

Suspension occurs when turbulent velocity fluctuations are able to counterbalance the settling velocity w_s [m·s^{-1}] imposed by the particle's

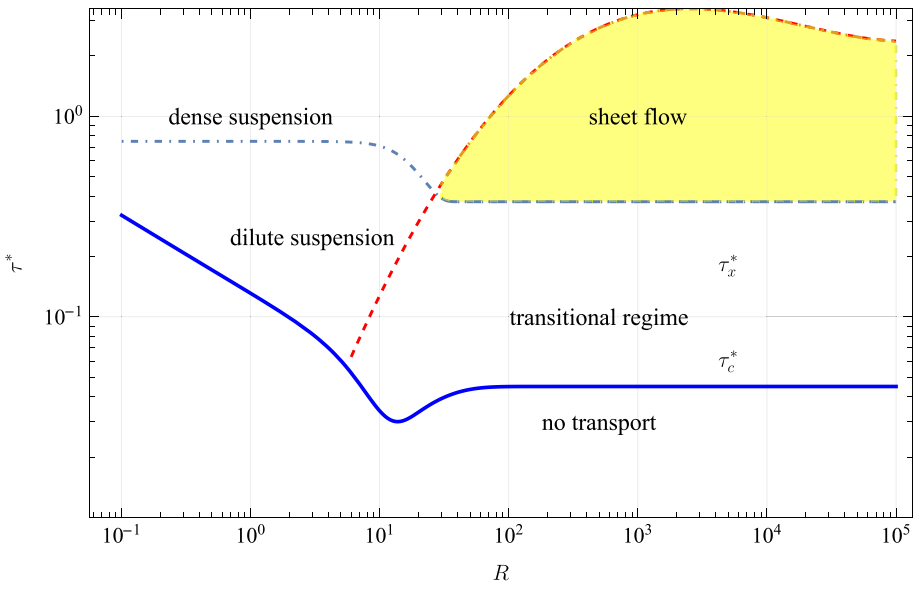

Fig. 1. Shields curve in the (R, τ^*) coordinate system, where R and τ^* denote the particle Reynolds number (14) and the Shields stress (7), respectively. The threshold of incipient motion τ_c^* is the empirical parametrization (A.1). The threshold for suspension $w_s = u^*$ is given by the dimensionless eq. (A.5). The critical stage τ_x^* is given by the dimensionless form of Eq. (16).

immersed weight. Bagnold (1966) assumed that the threshold for suspension was reached when $w_s = 1.25u^*$, where u^* [m·s^{-1}] denotes the friction velocity, which we simplify into

$$w_s = u^*. \tag{15}$$

Fig. 1 shows the dimensionless formulation (A.5) of this equation. Bagnold also considered the critical stage for carpet formation to be:

$$\tau_x = c_0 \varrho g d \tan\alpha, \tag{16}$$

where $c_0 = 1 - \zeta_0 = 0.65$ denotes the bed's static volume concentration. In a dimensionless form, the critical stage is thus $\tau_x^* = c_0 \tan\alpha$. Anticipating the results in Section 2.6, which specifies $\tan\alpha$'s dependence on flow conditions (see Eq. (18) below), we can plot the critical stage τ_x^* in Fig. 1. Four areas are bounded by the curves $w_s = u^*$, τ_x^*, and τ_c^*. The regime studied by Bagnold (1966) is the sheet-flow domain, colored in yellow. We define three additional regimes: Bagnold's transitional regime, which he did not investigate, but which we will characterize in more detail in the following section, and two regimes for suspended load (when $u^* > w_s$), which we will not study in this review paper: the dilute and dense suspension regimes.

2.6. Model calibration

Bagnold's model (8) involves three parameters: the dynamic friction coefficient μ, the efficiency factor e_b, and the Darcy–Weisbach friction coefficient f. These parameters cannot be determined theoretically using conservation principles in a simple manner, and we thus used empirical closure equations to relate these parameters to the flow variables. Here we provide the main results and refer the reader to the Supplementary Material for the detail.

2.6.1. Dynamic friction coefficient μ

For the friction coefficient μ, Bagnold (1956) found that the local Coulomb friction factor $\mu_b = \tau_p/\sigma_p$ was dependent on shear rate and particle concentration. Assuming a constant bedload concentration $c = 0.53$, he derived an expression for the bulk friction coefficient $\mu = \tan\alpha$ where α is the generalized internal friction angle ("generalized" means that this definition holds for stationary or creeping layers of grains, and we extend it to situations in which flow is more intense), with a dependence on the dimensionless number that came to bear this name:

$$G^2 = \frac{\varrho_p \tau_b d^2}{14\eta^2} = \frac{\varrho_p}{\varrho}\frac{\tau^*}{14}R^2, \tag{17}$$

where $\eta = \varrho\nu$ is the water's dynamic viscosity [kg·m^{-1}·s^{-1}]. Using Bagnold's (1956) data, we found that the dependence of the friction angle $\mu = \tan\alpha$ on the dimensionless number G can be approximated by the empirical equation:

$$\mu = \tan\alpha = \tan\alpha_{max} - \tan\alpha_{min}\tanh\frac{G^{1.8}}{1000}, \tag{18}$$

where $\tan\alpha_{max} = 0.75$ and $\tan\alpha_{\min} = 0.375$ are the upper and lower limits of the μ variation. As explained in § 2.1, this bulk friction coefficient μ represents the average Bagnold friction factor μ_b over the bedload layer thickness.

2.6.2. Efficiency factor e_b

For the efficiency factor e_b, Bagnold (1966) stated that the efficiency factor's upper bound was 0.15. Later, Bagnold (1977) abandoned the idea of calculating the efficiency factor and instead used empirical evidence to provide the following scaling law:

$$e_b = 1.6\sqrt{\frac{\omega - \omega_c}{\omega_c}}\left(\frac{h}{d}\right)^{-2/3}, \tag{19}$$

where ω_c denotes the threshold stream power (related to sediment's incipient motion) [W·m^{-2}], which was estimated using the Shields criterion and Keulegan's law

$$\omega_c = \tau_c u_{*c} = \varrho\left(sgd_p\right)^{3/2} 5.75\log\frac{12h_c}{d_p} = 2860 d_p^{3/2}\log\frac{12h_c}{d_p}, \tag{20}$$

where $\tau_c^* = 0.04$ is the critical Shields number, s is set to 1.6, $u_c^* = \sqrt{gh_c i}$ [m·s^{-1}] is the friction velocity for the depth h_c [m] related to incipient motion, and d_p [m] is the peak value (mode) of the grain size distribution. This definition raised criticisms as to its practical relevance given how difficult it is to determine the depth h_c. Further studies have suggested that the critical stream power varies as $d^{3/2}$ (Petit et al., 2005; Ferguson, 2005; Parker et al., 2011; Eaton and Church, 2011; Ferguson, 2012):

$$\omega_c = \varrho(sgd)^{3/2}\omega_c^*, \tag{21}$$

with $\omega_c^* \sim 0.1$—Ferguson (2012) found that ω_c^* depends on the bed slope and sediment gradation d_{84}/d_{50}, but overall, it lies in the 0.05–0.15 range.

Later, (Bagnold, 1980) corrected Eq. (19) and proposed a new scaling:

$$e_b \propto (\omega - \omega_c)^{1/2} d^{-1/2} h^{-2/3}. \tag{22}$$

Although Bagnold (1980, 1986) reported a good agreement between this scaling and bedload transport rate data (from laboratory flumes and field surveys), Martin and Church (2000) noted that Bagnold selected just a few datasets from among the many available at that time, and discarded others without providing any justification for doing so. They also found an inconsistency in the scaling, which led them to reconsider the dependence of e_b on flow parameters. Proceeding by trial and error, they found that the scaling of

$$e_b \propto (\omega - \omega_c)^{1/2} d^{1/4} h^{-1} \varrho^{-1/2} g^{-9/4} \tag{23}$$

provided the best fit with the data. As dimensionless forms are often preferable to monomial products (with no clear physical interpretation), we recast Martin and Church's suggestion in the form of a product of the following dimensionless groups: the scaled stream power $\Omega = \omega/(\nu g \rho)$, the particle Reynolds number R, the relative submergence $\xi = h/d$, and the density ratio s. Eq. (23) then reads,

$$e_b \propto \Omega^{1/2} \xi^{-1} s^{-1/4} R^{-1/2}, \tag{24}$$

which implies that the dimensionless bedload transport rate varies as $\Omega^{3/2}$:

$$\Phi \propto \Omega^{3/2} \xi^{-1} s^{-5/4} R^{-3/2}. \tag{25}$$

To further test this scaling, we defined the dimensionless number $\Pi = \Omega^{a_1} \xi^{a_2} R^{a_3} s^{a_4}$, where the exponents a_1 to a_4 were free parameters to be adjusted from data. We used the data recapped in Table 1 to set these exponents using a Markov chain Monte Carlo algorithm. We found $a_1 = 0.50 \pm 0.04$, $a_2 = -0.49 \pm 0.08$, $a_3 = -0.66 \pm 0.05$, and $a_4 = -0.83 \pm 0.08$. By setting, $a_1 = 1/2$, $a_2 = -1/2$, $a_3 = -2/3$, and $a_4 = -4/5$, we found that $e_b \propto \Pi$. We eventually ended up with the following scalings:

$$\begin{aligned} &e_b = 1.2\Pi \quad \text{with} \quad \Pi = \Omega^{1/2} \xi^{-1/2} R^{-2/3} s^{-4/5} \quad \text{and} \\ &\Phi = 4M \quad \text{with} \quad M = \Omega^{3/2} \xi^{-1/2} R^{-5/3} s^{-9/5}, \end{aligned} \tag{26}$$

which performs slightly better than Eq. (24) for the dataset used here—the coefficient of determination and the Bayesian information criterion were 0.61 and 1368, respectively, for Eq. (26), whereas they were 0.56 and 1416 for Eq. (24). The dimensionless number $M = \Omega^{3/2} \xi^{-1/2} R^{-5/3} s^{-9/5}$ has been labeled in reference to Yvonne Martin's contribution. As it was obtained by statistical adjustment, it has no special physical meaning. Note that we did not need to use a critical stream power to fit the power-law function (26) to the data. We refer the reader to the Supplementary Material (see § S4.1) to see how power-law functions with and without critical stream power compare with the data. In particular, we show that the form

$$\Phi \propto \omega^* - \omega_c^* \text{ with } \omega^* = \frac{\omega}{\varrho(sgd)^{3/2}}$$

suggested by Rob Feruguson (personal communucation), is a valuable alternative for fitting dimensionless transport rates, but it does not lead to a convenient expression of the efficiency factor e_b.

Expressing the efficiency factor e_b as a function of Π raises two issues. First, the number Π has no clear physical meaning. Second, Bagnold used the dimensionless shear stress τ^* in his flow regime classification, and the stream power ω as the driving variable in his bedload transport rate equation. It may be more efficient to seek a dependence of the efficiency factor e_b on τ^*. We used the data recapped in Table 1 and estimated the efficiency factor by using Eq. (4), where the friction factor μ was estimated using Bagnold's eq. (18) and the stream power was computed as $\omega = \varrho g q i = \tau_b \bar{u}$. With these assumptions, we can estimate e_b from laboratory data: $e_b = q_s \mu \cos\theta g \Delta\varrho/\omega$. When plotting the efficiency factor e_b with the Shields number τ^* (see Fig. S3 in the Supplementary Material), we find two experimental trends that are consistent with Bagnold's partitioning into bedload transport regimes:

- For the transitional regime ($\tau^* \leq \tau_x^*$ with $\tau_x^* \sim 0.5$), the efficiency factor e_b increases with increasing Shields numbers τ^*:

$$e_b = 2\tau^{*3/2}. \tag{27}$$

- For the sheet-flow regime ($\tau^* > \tau_x^*$), the efficiency factor e_b shows weak dependence on τ^*: $e_b = 0.4\tau^{*1/5}$. As a first approximation, we can consider that it reaches a constant value, but there is no unique plateau value. The asymptotic value ranges from 0.2 to 1. Not all data follow this trend. When sediment is made up of light, fine particles (see the data obtained by Matoušek et al. (2013) and Pugh and Wilson (1999) in Fig. S3 in the Supplementary Material), turbulence maintains those particles in suspension and the efficiency factor does not tend to a constant value.

2.6.3. Flow resistance factor f

The last parameter involved in Bagnold's bedload transport rate eq. (8) is the Darcy–Weisbach friction coefficient f, which represents resistance to flow. This coefficient f depends on dimensionless numbers such as the Reynolds and Froude numbers ($Re = \bar{u}h/\nu$ and $\mathrm{Fr} = \bar{u}/\sqrt{gh}$, respectively) and on the relative submergence ξ (defined as $\xi = h/k_s$, where k_s is the bed roughness size [m]): $f = f(Re, \mathrm{Fr}, \xi, \ldots)$ (Rouse, 1965;

Table 1
Experimental data used for calibrating the efficiency factor (see also Figs. S2 and S3 in the Supplementary Material). We report the type of experimental facility (flume with a free-surface flow or pressurized rectangular/cylindrical pipes), the ratio of the settling velocity w_s to the friction velocity u^*, the median particle diameter d_{50}, its density ratio $s = \varrho_p/\varrho - 1$, the range of flume/pipe slopes, and the range of Shields numbers. Wilson (1966) provided only partial information about his experiments (the data used here were obtained by digitizing his Fig. 2).

Authors	Device	w_s/u^*	d_{50} (mm)	s	i (%)	τ^*
Wilson (1966)	rect. Pipe	1.2–4.8	0.7	1.67	–	0.5–7.3
Aziz and Scott (1989)	flume	0.5–4.6	0.3–1	1.65	3–10	0.1–0.9
Nnadi and Wilson (1992)	rect. Pipe	0.4–1.4	0.7–4	0.14–1.67	1.7–7	0.1–0.9
Pugh and Wilson (1999)	cyl. Pipe	0.1–0.7	0.3–1	0.53–1.65	2–12	2–18
Gao (2008)	flume	1.2–6.9	1–7	1.65	2.5–3.3	0.07–1.2
Capart and Fraccarollo (2011)	flume	1.0–2.6	3.35	0.51	1–8	0.4–2.5
Matoušek (2009)	cyl. Pipe	0.1–0.8	0.37	1.65	2–16	0.7–23
Matoušek et al. (2013)	rect. Pipe	0.1–0.5	0.18	0.45	1–6.5	0.5–6
Matoušek et al. (2016)	flume	1.0–2.8	0.32	0.36	0.5–6	0.4–22
Rebai et al. (2022)	flume	1.4–3.4	3.6–6.4	0.4	1.2–5.9	0.3–1.3

Colosimo et al., 1988). This functional dependence is rather well-known when the bed is plane. It is a situation that is often met in gravel-bed rivers (i) when their slope lies in the 1%–3% range (Montgomery and Buffington, 1997), (ii) when water flows over antidunes under supercritical flow conditions (the free surface is then in phase with bed undulations) (Recking et al., 2009a; Cartigny et al., 2014; Pascal et al., 2021), or (iii) when all bedforms have been destroyed during floods (flow conditions referred to as the upper regime) (Kennedy, 1969; Julien and Raslan, 1998).

In other circumstances, bedload transport usually causes the formation of bedforms (step, pool, bar, dune, etc.) that make the determination of flow resistance far more complicated and uncertain. We refer the reader to the Supplementary Material, which includes further information on how bedforms and bedload transport affect flow resistance:

- When beds develop bedforms, more energy is dissipated by turbulence due to stronger vorticity and/or surface waves. This dissipation process is often called form friction (van Rijn, 1984b).
- Sediment transport also causes higher energy dissipation, except under certain flow conditions where sediment deposition between bedforms smooths out bed irregularities and thereby reduces form friction (Omid et al., 2010; Hohermuth and Weitbrecht, 2018).

Given how diversely bedforms can affect the velocity field, there is no all-purpose treatment for the additional energy dissipation they create, but many bespoke methods have been developed for particular types of bedforms. The common assumption is that energy dissipation at the grain and bedform scales is additive—which means that total friction can be broken down into skin and form frictions, respectively, and each contribution can be evaluated separately. As bedforms usually imply sediment transport, form friction also includes energy transfers from the water to the sediment. For dunes, several methods have been proposed for estimating energy dissipation as a function of their dimensions (Einstein, 1950; Engelund, 1966; Alam and Kennedy, 1969; van Rijn, 1984b). Field surveys reveal that these methods explain part of the variance in the f variations (de Lange et al., 2021). For other bedforms, determining flow resistance is far more complicated. For this reason, we mainly focus on the simplest case —the plane bed. It should, nevertheless, be remembered that bedforms such as alternate bars can increase flow resistance by a factor of 3 to 50 (see Fig. S5 in the Supplementary Material) and thus reduce bedload transport rates by a factor of 2 to 7 if $\Phi \propto f^{-1/2}$, as predicted by Bagnold's model (8).

For sufficiently deep flows over fixed-plane gravel beds, Keulegan (1938) showed that over most of the flow height, the velocity profile was consistent with the logarithmic profile provided by Prandtl's parametrization of the turbulent viscosity for turbulent flows near a solid boundary, and thus the depth-averaged velocity $\bar{u}$ can be expressed as a function of the friction velocity u^* and relative submergence ξ:

$$\frac{\bar{u}}{u^*} = \sqrt{\frac{8}{f}} = 6.25 + 5.75\log\frac{h}{k_s}. \tag{28}$$

This shows that the friction factor depends on relative submergence alone:

$$f = 8\left(\frac{u^*}{\bar{u}}\right)^2 = 8\left(6.25 + 5.75\log\frac{h}{k_s}\right)^{-2} = \left(2.03\log\frac{12.2h}{k_s}\right)^{-2}. \tag{29}$$

For shallow flows (typically when $\xi < 10$), it becomes more difficult to define the level at which the velocity drops to zero (Nikora et al., 2001)—the level that serves to locate the stream/bed interface. Furthermore, when the instantaneous velocity field shows significant time and space variations, especially near the bed, Prandtl's model is no longer valid and must be replaced with more sophisticated parameterizations of wall turbulence (Nikora et al., 2004, 2007; Manes et al., 2007; Lamb et al., 2017; Nikora et al., 2019; Rousseau and Ancey, 2022; Deal, 2022). To avoid using refined parametrization, we followed Recking et al. (2008b) and considered that under low submergence conditions, bed roughness was increased by a factor

$$\alpha_{rl} = 4\xi^{-0.43} \text{ subject to } 1 \le \alpha_{rl} \le 4. \tag{30}$$

We rewrote Keulegan's eq. (28) in the form (see § S1.3 in the Supplementary Material):

$$\sqrt{\frac{8}{f}} = \frac{\bar{u}}{u^*} = 6.25 + 5.75\log\frac{h}{\alpha_{rl}k_s}. \tag{31}$$

Recking et al. (2008b) also recommended using the characteristic diameter d_{84}, corresponding to the coarsest grain fraction, but they also mentioned that the median diameter d_{50} worked equally well. There is no consensus in the literature about the optimal value of the bed roughness size k_s: for gravel-bed rivers, $k_s = 2d_{90}$ (Kamphuis, 1974), $k_s = 3.5d_{84}$ (Hey, 1979), $k_s = 3d_{84}$ (Pitlick, 1992), $k_s = 5.9d_{50}$ (Millar, 1999), or $k_s = 2.4d_{90}$ (López and Barragán, 2008). Other empirical flow resistance equations have been proposed and can substitute for Eq. (31) (Thompson and Campbell, 1979; Ferguson, 2007; Lamb et al., 2017); the reader is referred to § S1.3 in the Supplementary Material.

Sediment transport's effect on flow resistance has been evaluated from laboratory experiments. Most authors consider that the Darcy–Weisbach coefficient f, derived from Keulegan's eq. (29), remains valid insofar as the roughness size k_s is reevaluated. For sand beds, k_s is often found to depend on the median particle diameter and the Shields number (Wilson, 1989; Camenen et al., 2006). For gravel beds with a slope $i \ge 1\%$, Recking et al. (2008b) found that k_s was a multiple of the coarse grain size d_{84}:

$$k_s = \alpha_b(\xi, i)d_{84}, \tag{32}$$

where the multiplying factor α_b is a function of the relative submergence $\xi = h/d_{84}$ and bed slope i (see § S2.1 in the Supplementary Material for the exact equation):

$$\alpha_b(\xi, i) \approx 7i^{0.85}\xi, \tag{33}$$

subject to $1 \le \alpha_b \le 2.6$. A consequence of this dependence on h/d_{84} is that flow resistance is constant over a certain range of flow depths corresponding to incipient and weak sediment transport (see Fig. S6 in the Supplementary Material).

In summary, when dealing with plane beds, we can assume that flow resistance in Bagnold's eq. (8) is properly described using Keulegan's eq. (29), where the roughness size k_s has been extended to account for additional dissipation due to (possible) flow shallowness and sediment transport: $k_s = \alpha_{rl}\alpha_b d_{84}$, where the coefficients α_{rl} and α_b are given by Eqs. (30) and (33), respectively.

2.7. Tentative summary

Here we summarize Bagnold's model of bedload transport by providing transport rate equations for the two regimes that he identified. Table 2 shows how Bagnold's model is broken down into different

Table 2
This table summarizes the main expressions for bedload transport rates under both regimes: flow resistance equations in the absence of bedforms, dimensionless bedload transport rate equations Φ, and trends (that is, how Φ scales with τ^*).

	Transitional regime	Sheet-flow regime
Flow resistance	$f = \left(2.03\log\frac{1.75}{i^{0.85}}\right)^{-2}$	$f = (2.03\log(4.2\xi))^{-2}$
Transport rate	$\Phi = \frac{2}{\mu\cos\theta}\sqrt{\frac{8}{f}}\tau^{*3}$	$\Phi = 7.4\frac{e_{b\infty}}{\mu\cos\theta}\left(\frac{s}{i}\right)^{1/6}\tau^{*5/3}$
Trend	$\Phi = 40\tau^{*3}$	$\Phi = 12\tau^{*5/3}$

expressions for each regime, and we provide further justifications below.

In Bagnold's model, scaled bedload transport depends on the dimensionless shear stress τ^*, bed slope i, Darcy–Weisbach friction coefficient f, relative density ratio s, and Bagnold number G: $\Phi = \Phi(\tau^*, i, f, s, G)$. In most cases, τ^* is the key parameter controlling the Φ variations with flow conditions; other dimensionless numbers play a less significant part. It would be useful to obtain a single equation that we could refer to as *Bagnold's master equation* and that would express Φ as a function of τ_* solely. Towards the end of his life, Bagnold was still seeking a correlation between transport rates and stream power. Thus, we also propose such a correlation in the form of a monomial product of dimensionless groups $\Phi(\Omega, \xi, s, R)$ that we will refer to as *Bagnold's scaling*.

2.7.1. Transitional regime

For $\tau_c^* < \tau^* < \tau_x^*$, where the critical transport stage is $\tau_x^* \sim 0.5$ for sand and $\tau_x^* \sim 0.25$ for gravel, sediment transport occurs intermittently.

When sediment transport involves weakly dissipative bedforms (*e.g.*, plane bed or antidunes for supercritical flows), flow resistance is roughly constant for a given slope. The Darcy–Weisbach friction coefficient f is given by Keulegan's Eq. (29) and roughness k_s is computed using Recking's eq. (32):

$$f_c(i) = \left(2.03\log\frac{12.2h}{\alpha_b\alpha_{rl}d_{84}}\right)^{-2} = \left(2.03\log\frac{12.2}{7\alpha_{rl}i^{0.85}}\right)^{-2}, \tag{34}$$

where the correcting factors α_b and α_{rl} are given by Eqs. (33) and (30), respectively. The Darcy–Weisbach friction factor f becomes independent of ξ for plane beds given the α_{rl} dependence on ξ. The efficiency factor e_b varies as:

$$e_b = 2\tau^{*3/2}. \tag{35}$$

As a result, the scaled sediment transport rate varies as τ^{*3}:

$$\Phi = \frac{e_b}{\mu\cos\theta}\sqrt{\frac{8}{f}}\tau^{*3/2} = \frac{2}{\mu\cos\theta}\sqrt{\frac{8}{f_c(\tan\theta)}}\tau^{*3}. \tag{36}$$

Let us provide a simple quantification. This equation provides the trend of $\Phi = 40\tau^{*3}$ reported in Fig. 2, where we set $f_c \sim 0.15$ and $\mu\cos\theta \sim 0.37$. This scaling is consistent with the pipe-flow data presented in Table 1.

When sediment transport is associated with bedforms (which is true in most cases), flow resistance is usually much higher than Keulegan's Eq. (29) predicts (as illustrated by Fig. S5). For regular bedforms, such as dunes, empirical equations can be used to determine flow resistance (van Rijn, 1984b; Van Rijn, 1993; Dey, 2014; Powell, 2014). As Bagnold's eq. (8) predicts that $\Phi \propto f^{-1/2}$, any increase in flow resistance involves a decrease in the bedload transport rate.

2.7.2. Sheet-flow regime

For $\tau^* \geq \tau_x^*$, sediment transport occurs in granular layers carried by the water flow.

At sufficiently high shear stresses, most longitudinal bedforms for this regime are smoothed out, and the flow involves the upper flow regime. In these circumstances, flow resistance varies with relative submergence ξ, with f given by Eq. (29) and k_s given by Eq. (32) (with $\alpha_b \to 2.9$ and $\alpha_{rl} \to 1$ for $\xi > 17$):

$$f(\xi) = \left(2.03\ \log\frac{12.2h}{\alpha_{rl}\alpha_b d_{84}}\right)^{-2} = (2.03\ \log(4.2\xi))^{-2}. \tag{37}$$

It is difficult to arrive at a scaling law for Φ when using a Keulegan-like expression for flow resistance. If we use the equivalence between the Darcy–Weisbach and Manning–Strickler equations, then we can write:

$$\sqrt{\frac{8}{f}} = \frac{Kd_{84}^{1/6}}{\sqrt{g}}\xi^{1/6} = 7.4\xi^{1/6} = 7.4\left(\frac{s\tau^*}{i}\right)^{1/6}, \tag{38}$$

where we use the relationship between the Strickler friction coefficient K and grain size d_{84} proposed by Jäggi (1984): $K = 23.2d_{84}^{-1/6}$ [$\mathrm{m^{1/3}\cdot s^{-1}}$]. As a first approximation, the efficiency factor is assumed to be constant: $e_b = e_{b\infty}$ where $e_{b\infty}$ lies in the 0.2–1 range. As a result, the scaled sediment transport rate varies as $\tau^{*5/3}$ if μ remains constant:

$$\Phi = 7.4\frac{e_{b\infty}}{\mu\cos\theta}\left(\frac{s}{i}\right)^{1/6}\tau^{*5/3}. \tag{39}$$

When we quantify this equation, it provides the trend of $\Phi = 12\tau^{*5/3}$ reported in Fig. 2 when we set $i \sim 0.1\%$, $s \sim 1.7$, $e_b \sim 0.2$ and $\mu\cos\theta \sim 0.4$ as a first approximation.

2.7.3. Bagnold's master equation and scaling

Using Guo (2002)'s method, we can derive a single equation that smoothly connects the two former trends of $\Phi = 12\tau^{*5/3}$ ($\tau^* \gg 1$) and $\Phi = 40\tau^{*3}$ ($\tau^* \ll 1$):

$$\Phi = 40\tau^{*3}\left(1 + \left(\frac{\tau^*}{\tau_1^*}\right)^{3/2}\right)^{-8/9}, \tag{40}$$

where $\tau_1^* = 0.40$ represents the upper limit of Bagnold's transitional regime and is fixed for all slopes i. We refer to this equation as *Bagnold's master equation*. Fig. 2(a) compares Bagnold's master eq. (40) with the same pipe-flow data used for model calibration.

In his last papers, Bagnold sought to express Φ's dependence on flow variables using regression. We have updated his analysis by using the pipe-flow data summarized in Table 1. We found that the dimensionless transport rate was a linear function of Martin's dimensionless number M:

$$\Phi = 4M \ \text{ with } \ M = \Omega^{3/2}\xi^{-1/2}s^{-9/5}R^{-5/3}, \tag{41}$$

where $\Omega = \omega/(\nu g\varrho)$ is the scaled stream power. This equation will be referred to as *Bagnold's scaling equation* throughout the rest of this review. Fig. 2(b) shows that this equation fits the pipe-flow data well over five orders of magnitude of M, from 10^{-2} to 10^3. The only data not represented by this equation involve small, lightweight particles (transported as suspended load rather than bedload). These data are roughly captured using the trend of $\Phi = 32M$, which would mean that the scaling does not change for suspended load, although the proportionality factor does. A curious behavior can be visualized in Fig. 2: for lightweight particles used by Nnadi and Wilson (1992), Matoušek et al. (2016), and Capart and Fraccarollo (2011), bedload transport rates behaved like $\Phi \propto \tau^*$ (for $\tau^* > 1$), and therefore, the points did not fall on the mean trend $\Phi = 12\tau^{*5/3}$. One possible explanation is that stress generation differs for fine and coarse lightweight particles at high shear stresses. Indeed, the strength of the momentum exchanges induced by particle collisions depends on the coefficient of restitution e, which is found to be an increasing number function of the Stokes number (Simeonov and Calantoni, 2012)

$$\mathrm{St} = \frac{2}{9}\frac{\varrho_p}{\varrho}\frac{d^2\dot{\gamma}}{\nu}.$$

In the experiments conducted by Capart and Fraccarollo (2011), we have $\varrho_p/\varrho = 1.5$, $d = 3.3$ mm, and $\dot{\gamma} \sim 40\ \mathrm{s^{-1}}$, which leads to $\mathrm{St} \sim 160$, and thus $e \sim 0.8$ (Simeonov and Calantoni, 2012). In this case, collisional interaction can be generated and dissipate energy (Jenkins and Hanes, 1998). However, taking a lower diameter, such as $d = 0.3$ mm, leads to $\mathrm{St} \sim 1.6$, and thus $e \sim 0.1$ (Simeonov and Calantoni, 2012), and in this case, turbulent drag and lubrication forces prevail in stress generation (Schmeeckle, 2014).

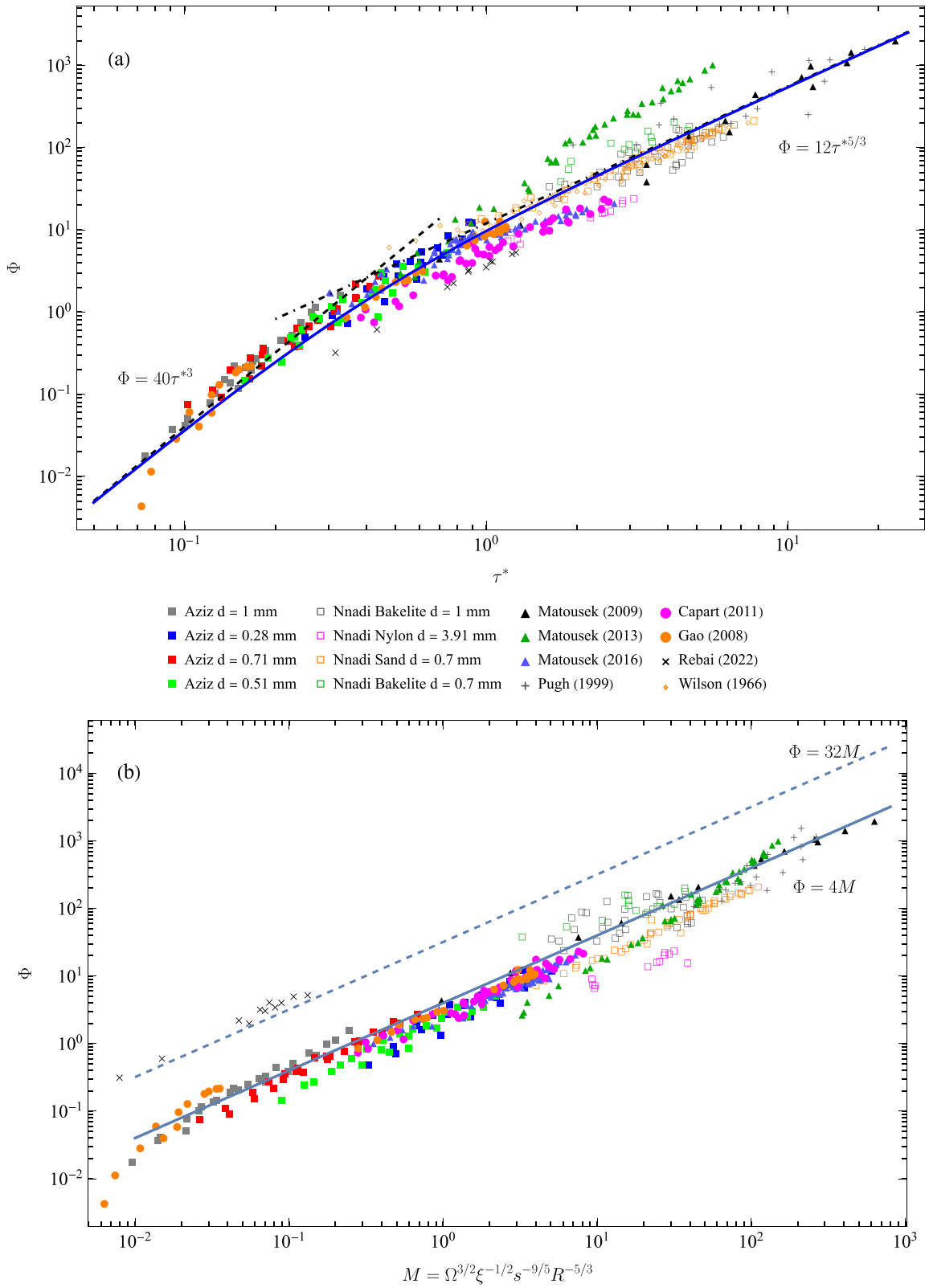

Fig. 2. (a) Variation in the dimensionless bedload transport rate Φ with scaled shear stress τ^*. The flume data come from the sources listed in Table 1. We also report two trends: $\Phi = 40\tau^{*3}$ (dashed line) for the transitional regime and $\Phi = 12\tau^{*5/3}$ (dot-dashed line) for the sheet-flow regime. The solid line shows Bagnold's master eq. (40). (b) Variation in the dimensionless bedload transport rate Φ with the monomial product M. The solid line shows Bagnold's scaling (41).

3. Applications to laboratory flumes and rivers

To further test Bagnold's model as summarized in § 2.7, we now compare its predictions with data collected in the laboratory and in the field, that is, with data that were not used to calibrate the model's parameters. We first consider flume experiments examining bedload transport from a variety of sources. Table 3 recaps these experiments' main features. Williams (1970) collected a large amount of experimental data under various flow conditions; here, we distinguish between data related to plane beds and data associated with bedforms. For all other authors except Cao (1985), the information about bedforms was missing.

Fig. 3(a) shows how the scaled bedload transport rate Φ varies with the dimensionless shear stress τ^*, while Fig. 3(b) shows the variation in the efficiency factor e_b with τ^*. Figs. 3(a) and (b) confirm the partitioning into three transport regimes.

3.1. Bagnold's no transport regime

For $\tau^* < 0.078$ (see Fig. S14 in the Supplementary Material for a close-up view), Fig. 3(a) shows a strong increase in bedload transport rate with increasing bottom shear stress: the mean trend fitted to the data is $\Phi = (10\tau^*)^{16}$, which is in close agreement with what Paintal (1971) obtained ($\Phi = (15\tau^*)^{16}$ for $\tau^* < 0.05$), and with what Pazis (1976) observed in his flume ($\Phi = (10\tau^*)^{8.28}$ for $\tau^* < 0.05$). The transport rates remain very low, with $\Phi < 0.02$. These low Φ values explain why this regime continues to be referred to as the no-transport regime.

This regime was not observed when studying efficiency factor e_b and calibrating it from pipe-flow data in § 2.6 since there were no experimental data corresponding to $\tau^* < 0.078$. Fig. 3(b) shows that efficiency factor e_b increases much more sharply in the no-transport regime ($e_b \propto \tau^{*10}$) than in the transitional regime ($e_b \propto \tau^{*3/2}$), but it does not exceed 0.05. Flow resistance is not changed to any significant degree when very few particles move.

Observing non-zero transport rates in the no-transport regime remains something of a stubborn paradox. For Paintal (1971), the threshold of incipient motion is an engineering reality insofar as engineers find the concept of critical shear stress very useful as it allows them to distinguish between stable and unstable beds. However, in nature, this threshold does not exist:

> "At a very low shear value, one has to wait for a longer time to see the movement, as the probability of movement becomes very small. But this probability is never zero except in still water."

Paintal's viewpoint is supported by strong experimental evidence (Graf and Pazis, 1977; Lavelle and Mofjeld, 1987; Van Rijn, 1993; Salevan et al., 2017; Dey and Ali, 2019), but Pähtz et al. (2020) pointed out that "a threshold must exist because the size of turbulent flow eddies is limited by the system dimensions." Recent analyses suggest that the initiation of particle movement is better described using criteria based on energy or impulse than on bottom shear stress (Diplas et al., 2008; Valyrakis et al., 2013; Pähtz et al., 2020). Gaeuman et al. (2015) and Shih and Diplas (2018) found that Φ's strong dependence on τ^* reflected the intermittency of bedload transport—long periods with no bedload transport are punctuated with short periods of activity—and it is because transport rates are averaged over time that the $\Phi \propto \tau^{*16}$ scaling emerges. For the moment, we can postpone a decision about the nature of the no-transport regime and merely assume its existence while conceding that although transport rates are non-zero, they remain vanishingly small.

Regardless of the existence of a critical shear stress for incipient motion, this regime exhibits specific features that make it difficult to study. Let us address some of them. At low bottom shear stresses, particles move along preferential paths, with just a few paths carrying most of the particles (Aussillous et al., 2016). The probability of entrainment depends crucially on bed slope and particle size gradation (Parker and Klingeman, 1982; Mueller et al., 2005; Lamb et al., 2008; Mao et al., 2008; Recking, 2009; Parker et al., 2011; Comiti and Mao, 2012; Prancevic and Lamb, 2015; Dey and Ali, 2019; Hassan et al., 2020). The bed slope's effect on incipient motion explains why Pazis (1976), who had investigated bedload transport on shallow slopes ($i \leq 1.4$), was able to observe bedload transport rates as low as 10^{-5} at $\tau^* = 0.02$, whereas Smart and Jaeggi (1983) and Rickenmann (1992), who worked with steep slopes ($i \geq 3\%$), observed such values at $\tau^* = 0.06$.

These features lead to strong spatial heterogeneity in the local particle flux. Furthermore, particles move intermittently, with a probability distribution of arrival times that closely follows an exponential distribution when the bed has developed no bedform (Ancey et al., 2008; Radice, 2009; Singh et al., 2009; Roseberry et al., 2012; Heyman et al., 2013; Campagnol et al., 2015; Furbish et al., 2017; Ancey and Pascal, 2020; Ashley et al., 2021; Benavides et al., 2022). Spatial and temporal fluctuations in bedload transport rates explain why the Φ data span four orders of magnitude for a given dimensionless stress (see Fig. 3(a)).

3.2. Bagnold's transitional regime

For $0.078 < \tau^* < 0.40$ (the transitional regime), Fig. 3(a) confirms that bedload transport rates scale as $\Phi = 40\tau^{*3}$, which was the trend fitted to pipe-flow data (see Fig. 2). The data scatter around the mean trend remains significant (about one order of magnitude) but is far less pronounced than for the no-transport regime. The experiments conducted by Williams (1970) showed that bed transport rates for flows associated with bedforms were noisier than for flows with no bedform. Bedform's effect on sediment transport is particularly visible in Fig. 3(b): for some runs, the efficiency factor was two orders of magnitude lower when bedforms were present. According to Bagnold's eq. (8), the dimensionless bedload transport rate scales as $f^{-1/2}$, and thus an increase in flow resistance induces a reduction in the transport rate. If the flow resistance increase is in the order of 10 times bigger (see Fig. S14 in the Supplementary Material), then the relative reduction in Φ is three times larger. This reduction may explain why the flume data are slightly below Bagnold's master curve and the pipe-flow data shown in Fig. 2(a).

Table 3
Experimental data considered in Fig. 3. We report flume width, median particle diameter d_{50}, particle density ϱ_p, the range of flume/pipe slopes, and the range of Shields numbers. (a) See also Graf and Pazis, 1977. (b) See also Smart (1984). (c) See also Graf and Suszka (1987).

Authors	W (mm)	d_{50} (mm)	ϱ_p (kg/m^3)	i (%)	τ^*
Williams (1970)	76–310	1.3	2650	0.1–3.6	0.04–2
Paintal (1971)	914	2.5–22	1450	0.1–1.0	0.03–0.09
Pazis (1976)[a]	500	0.5–3	1410–2650	0.01–0.14	0.017–0.052
Smart and Jaeggi (1983)[b]	200	2–10	2650	3–20	0.03–2.3
Ikeda (1983)	4000	6.5	2650	0.2–1.0	0.03–0.22
Cao (1985)	600	11–44	2650	0.5–9	0.04–0.2
Suszka (1987)[c]	600	12–23	2726	0.5–2.5	0.04–0.09
Wilcock (1990)	600	1.86	2650	0.01–0.05	0.035–0.019
Rickenmann (1992)	200	10	2650	7–20	0.23–0.73
Recking et al. (2008a)	100–250	2–12	2650	1–9	0.09–0.28
Deal et al. (2023)	10.5	4–10	2400–2800	3–11	0.05–0.20

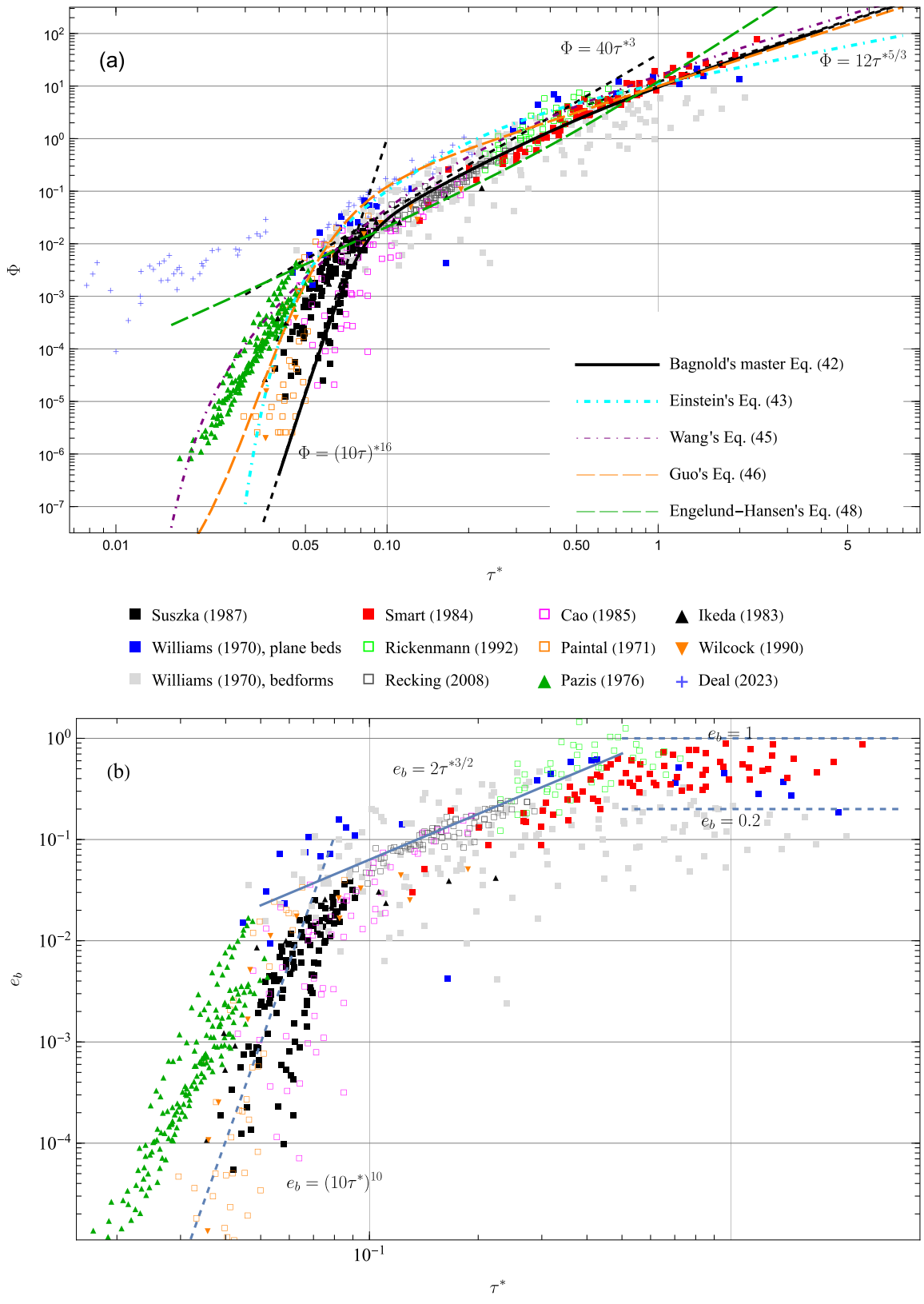

Fig. 3. (a) Variation in the dimensionless bedload transport rate Φ with the dimensionless shear stress τ^*. The dashed lines show the trends of $\Phi = (10\tau)^{*16}$, with $\Phi = 40\tau^{*3}$ coming from transitional regime Eq. (36) and $\Phi = 12\tau^{*5/3}$ coming from sheet-flow regime Eq. (39). The solid line shows Bagnold's master eq. (42) combining all three trends. We also plot Einstein's bedload eq. (43), Guo's eq. (46), Wang's eq. (45), and Engelund–Hansen's eq. (48) (evaluated using Jäggi's parametrization of friction (38), $i = 1\%$ and $s = 1.65$). (b) Variation in efficiency factor e_b with dimensionless shear stress τ^*. We also plot two experimental trends, $e_b = (10\tau^*)^{10}$ (no-transport regime) and $e_b = 2\tau^{*3/2}$ (transitional regime), and the boundaries $e_b = 0.2$ and $e_b = 1$ (sheet-flow regime).

Comparing the e_b variations with τ^* in Figs. 2(b) and 3(b) suggests that bedform's primary effect on factor efficiency is to increase the variability of e_b.

3.3. Bagnold's sheet-flow regime

For $\tau^* > 0.40$ (sheet-flow regime), flume data support scaling in the form of $\Phi = 12\tau^{*5/3}$, which is close to empirical equations like the Meyer-Peter–Müller equation: $\Phi = 8(\tau^* - 0.047)^{3/2}$ (Meyer-Peter and Müller, 1948). By reworking Meyer-Peter's data and taking sidewall effects into account, Wong and Parker (2006) arrived at a slightly different form of $\Phi = 4.93(\tau^* - 0.047)^{1.6}$, whose exponent was even closer to the 5/3 value presented here. Ribberink (1998) found that the scaling of $\Phi = 11(\tau^* - 0.055)^{1.65}$ properly described sediment transport rates for the full range of Shields values under both oscillatory and non-oscillatory flow conditions.

As there are few flume datasets available at high shear stresses, it is difficult to decide between Bagnold's updated model ($\Phi \propto \tau^{*5/3}$) and the Meyer-Peter–Müller equation ($\Phi \propto \tau^{*3/2}$). The element in favor of Bagnold's scaling is that it is more consistent with the pipe-flow data shown in Fig. 2. The efficiency factor e_b tends to a constant that ranges from 0.2 to 1. When bedforms are present, e_b can take values as low as 0.05. The highest e_b values corresponded to flows down steep slopes (typically the slopes above 10% studied by Smart and Jaeggi (1983) and Rickenmann (1992)). As highlighted in § 2.3, high e_b values question Bagnold's implicit assumption that the sediment phase is fully subordinate to the water phase and extracts only a small fraction of the power imparted to the water by the gravitational forces. One possible explanation for these anomalously high e_b values is that, from a mechanical standpoint, the intense bedload transport down steep slopes behaves differently from sediment transport on shallower slopes. When Takahashi (2007) wrote that "immature particles do not disperse in the entire depth, but they flow concentrated in a lower layer," he was referring to immature debris flows. We will return to this point later (see § 4.1).

3.4. Scaling with M

Fig. 4 shows how Φ varies with Martin's number, $M = \Omega^{3/2}R^{-5/3}\xi^{-1/2}s^{-9/5}$. At sufficiently high bedload transport rates ($\Phi > 10^{-2}$), the trend of $\Phi = 4M$ fitted to the pipe-flow data captured the flume data equally well over nearly three orders of magnitude in M ($4 \times 10^{-3} \leq M \leq 15$).

The data obtained by Rickenmann (1992) lay above this trend, but as indicated in § 3.3, those data pertained to steep slopes and might have been more representative of immature debris flows than of bedload transport. For $\Phi < 10^{-2}$ or $M < 4 \times 10^{-3}$, flume data deviate from the mean trend of $\Phi = 4M$. These data belong to the no-transport domain identified in § 3.1.

3.5. Comparison with bedload transport equations

As highlighted in § 2.7.3, in practical applications, a single equation is often preferred over a piecewise continuous equation. There is a price to pay for this, however: the only independent variable is the dimensionless shear stress τ^*, and the effects of other variables (bed slope i, flow resistance f, density ratio s) are ignored. Using Guo's (2002) method, we merged the three trends of $\Phi = (10\tau^*)^{16}$ ($\tau^* \leq 0.078$), $\Phi = 40\tau^{*3}$ ($0.078 \leq \tau^* \leq 0.40$), and $\Phi = 12\tau^{*5/3}$ ($0.40 \leq \tau^*$) to propose a

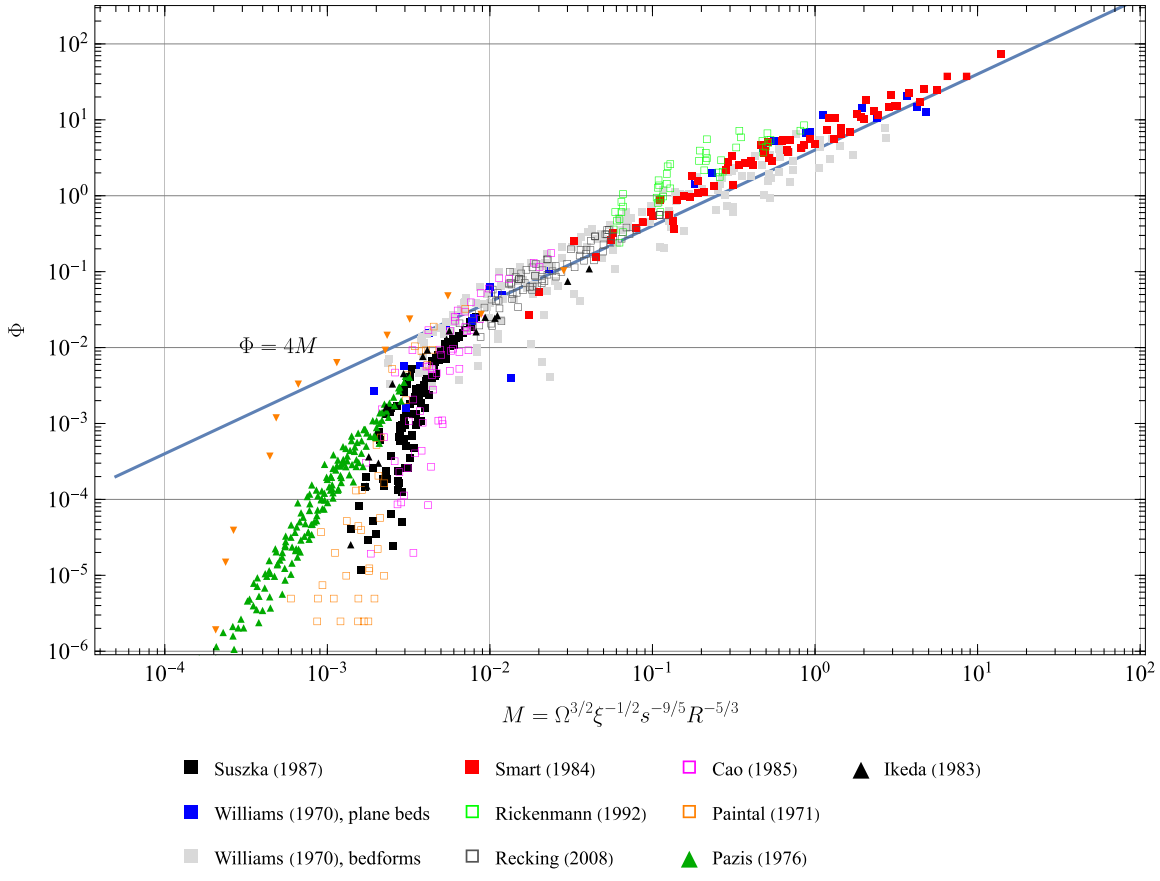

Fig. 4. Variation in the dimensionless bedload transport rate Φ with the dimensionless number $M = \Omega^{3/2}R^{-5/3}\xi^{-1/2}s^{-9/5}$. The straight line in the log–log representation shows the linear trend for $\Phi = 4M$.

single equation for the Bagnold model:

$$\Phi = (10\tau^*)^{16}\left(1+\left(\frac{\tau^*}{\tau_1^*}\right)^{3/2}\right)^{-8/9}\left(1+\left(\frac{\tau^*}{\tau_0^*}\right)^{8}\right)^{-13/8}, \tag{42}$$

where $\tau_0^* = 0.078$ and $\tau_1^* = 0.40$ are the lower and upper limits of Bagnold's transitional regime. Compared with Bagnold's first master eq. (40) fitted to pipe-flow data, here we consider that bedload transport rates decay strongly with τ^* when $\tau^* < \tau_0$, but they do not drop to 0.

Einstein (1950) is credited with one of the first theoretical models of bedload transport. His model involves the probability p of particle entrainment, which can be related to the scaled bedload transport rate Φ:

$$\Phi = \frac{\alpha p}{1-p} \text{ with } p = 1 - \frac{1}{\sqrt{\pi}}\int_{-a_1/\tau^* - a_2}^{a_1/\tau^* - a_2} e^{-x^2}\mathrm{d}x, \tag{43}$$

where Einstein (1942) fitted the parameters a_1, a_2, and α to the flume data collected by Gilbert (1914) and Meyer-Peter et al. (1934): $a_1 = 0.156$, $a_2 = 2.0$, and $\alpha = 1/27$. Einstein (1942) also proposed an empirical equation for moderate transport rates ($\Phi < 0.40$):

$$\Phi = \frac{1}{0.465}\exp\left(\frac{-0.391}{\tau^*}\right). \tag{44}$$

Cheng (2002) provided a variant of this equation that connects smoothly with Eq. (43) at high shear stresses: $\Phi = 13\tau^{*3/2}\exp(-0.05\tau^{*-3/2})$. Wang et al. (2008) modified Einstein's equation so that it is consistent with the scaling of $\Phi \propto \tau^{*3/2}$ at high shear stresses:

$$\Phi = \frac{\alpha p}{1-p}\frac{\tau^{*3/2}}{20} \text{ with } p = 1 - \frac{1}{\sqrt{\pi}}\int_{-a_1/\tau^* - a_2}^{\infty} e^{-x^2}\mathrm{d}x, \tag{45}$$

with $a_1 = 0.07$ and $a_2 = 2.0$. Guo (2021) adjusted Einstein's equation so that it becomes consistent with the scalings of $\Phi \propto \tau^{*16}$ found by Paintal (1971) when $\tau^* \ll 1$ and of $\Phi \propto \tau^{*5/3}$ found by Huang (2010) when $\tau^* \gg 1$:

$$\Phi = 10\tau_*^{5/3}\exp\left(-\frac{16}{1+(30\tau_*)^3}\right). \tag{46}$$

Engelund and Hansen (1967) developed a simple model of bedload transport over dunes. By using Bagnold's assumption (1) on energy dissipation, they obtained the following equation:

$$\Phi = 0.077\frac{4}{f}\sqrt{\tau^{*2}+0.15}\tau^{*2}. \tag{47}$$

If we use Jäggi's parametrisation (38) of flow resistance (see § 2.7), then

$$\Phi = 2.1\left(\frac{s}{i}\right)^{1/3}\sqrt{\tau^{*2}+0.15}\tau^{*7/3}. \tag{48}$$

Fig. 3(a) (see also Fig. S14 in the Supplementary Material for a close-up view) shows that the four models provide similar results for $\tau^* > 0.08$ when plotted in a log–log representation. At a low Shields stress ($\tau^* < 0.08$), the deviation between model predictions can be as large as one order of magnitude, but as the data scatter is huge (three orders of magnitude at $\tau^* = 0.05$), all of them are consistent with the existing data.

3.6. Influence of bedforms in natural rivers

Figs. 5 (a) and (b) show the variation in the dimensionless bedload transport Φ with the Shields stress τ^* and Martin number $M = \Omega^{3/2}R^{-5/3}\xi^{-1/2}s^{-9/5}$, for natural rivers, where the relative submergence ξ was computed from the hydraulic radius R_h rather than the depth: $\xi = R_h/d_{50}$. The reader is referred to Tables S2 to S4 in the Supplementary Material for details of the sources used for plotting Fig. 5. We only employed data from rivers that had been sufficiently documented (*i.e.*, with sufficient information about grain size distribution, cross-section profile, and hydraulic conditions). The data (10,496 data in all, corresponding to 81 sites) were categorized by bedform type and summarized in Table 4. As the data scatter is considerable (spanning two to nine orders of magnitude for the same dimensionless shear stress), we also ran a quantile regression analysis to determine how some quantiles varied with τ^* or M (Koenker et al., 2017). We considered the median bedload transport rate ($\Phi_{0.5}$ associated with the probability $p = 0.5$) and the quantiles of $\Phi_{0.9}$ and $\Phi_{0.1}$ associated with probabilities 0.9 and 0.1, respectively. There are two main reasons why the data scatter is considerable.

The first reason is related to the wide spectrum of physical processes involved. Laboratory experiments make it possible to study physical processes in isolation or jointly. In field surveys, however, it is rarely possible to disentangle the respective influences of the various processes involved in sediment transport. Under similar flow conditions, bedload transport can vary significantly because of.

- variations in sediment supply (Warburton, 1992; Nicholas et al., 1995; Recking, 2012; Dean et al., 2015; Piton and Recking, 2017; East et al., 2018),
- partial mobility (Wilcock and McArdell, 1997), grain shape (Dudill et al., 2020; Cassel et al., 2021; Deal et al., 2023),
- grain sorting and the pavement formation (Gomez, 1983; Iseya and Ikeda, 1987; Dietrich et al., 1989; Parker et al., 1982; Parker and Klingeman, 1982; Frey and Church, 2009; Ferdowsi et al., 2017; Recking et al., 2023),
- increased mobility as fine sediment is added (Venditti et al., 2010; Dudill et al., 2018),
- bedform migration (Gomez et al., 1989; Recking et al., 2009b; Guala et al., 2014; Strick et al., 2019; Terwisscha van Scheltinga et al., 2021),
- local changes in sediment storage (Hoey, 1992; Lisle and Church, 2002; Hassan et al., 2008),
- cross-section narrowing or widening (Surian and Cisotto, 2007; Mao and Surian, 2010; Nelson et al., 2015; Recking et al., 2016),
- flow confinement (Garcia Lugo et al., 2015; Carbonari et al., 2020),
- the features (magnitude, duration) of flood hydrographs (Hassan et al., 2006; Mao, 2012; Papangelakis and Hassan, 2016; Wang et al., 2019; Ravazzolo et al., 2022),
- the spatial distribution of shear stress (Powell et al., 1999; Yager et al., 2018, 2019; Monsalve et al., 2020),
- history dependence (Turowski et al., 2011; Mao, 2018; Masteller et al., 2019),
- the influence of bed and riparian vegetation (Tal and Paola, 2010; Comiti et al., 2011; Yager and Schmeeckle, 2013), and
- large pieces of wood (Ruiz-Villanueva et al., 2016; Wohl and Scott, 2017)

The second reason for data scatter is related to measurement uncertainties, errors, and bias. Field conditions exacerbate the difficulties of measuring bedload transport rates. First, measurements in the field are more prone to uncertainties than are laboratory measurements: techniques that involve collecting sediment in traps or baskets may provide inconsistent measurements (Childers, 1999; Ryan and Porth, 1999; Sterling and Church, 2002; Vericat et al., 2006; Bunte et al., 2008). For instance, when testing in the same river with the same flow conditions, Bunte et al. (2008) found that Helley-Smith samplers yielded transport rate values two to four orders of magnitude higher than sediment traps (owing to the fine mesh used in the Helley-Smith samplers). Furthermore, differences as high as a factor of five were observed when increasing the sampling duration of Helley-Smith samplers from 2 min to 60 min (Bunte and Abt, 2005); theoretical studies have revealed

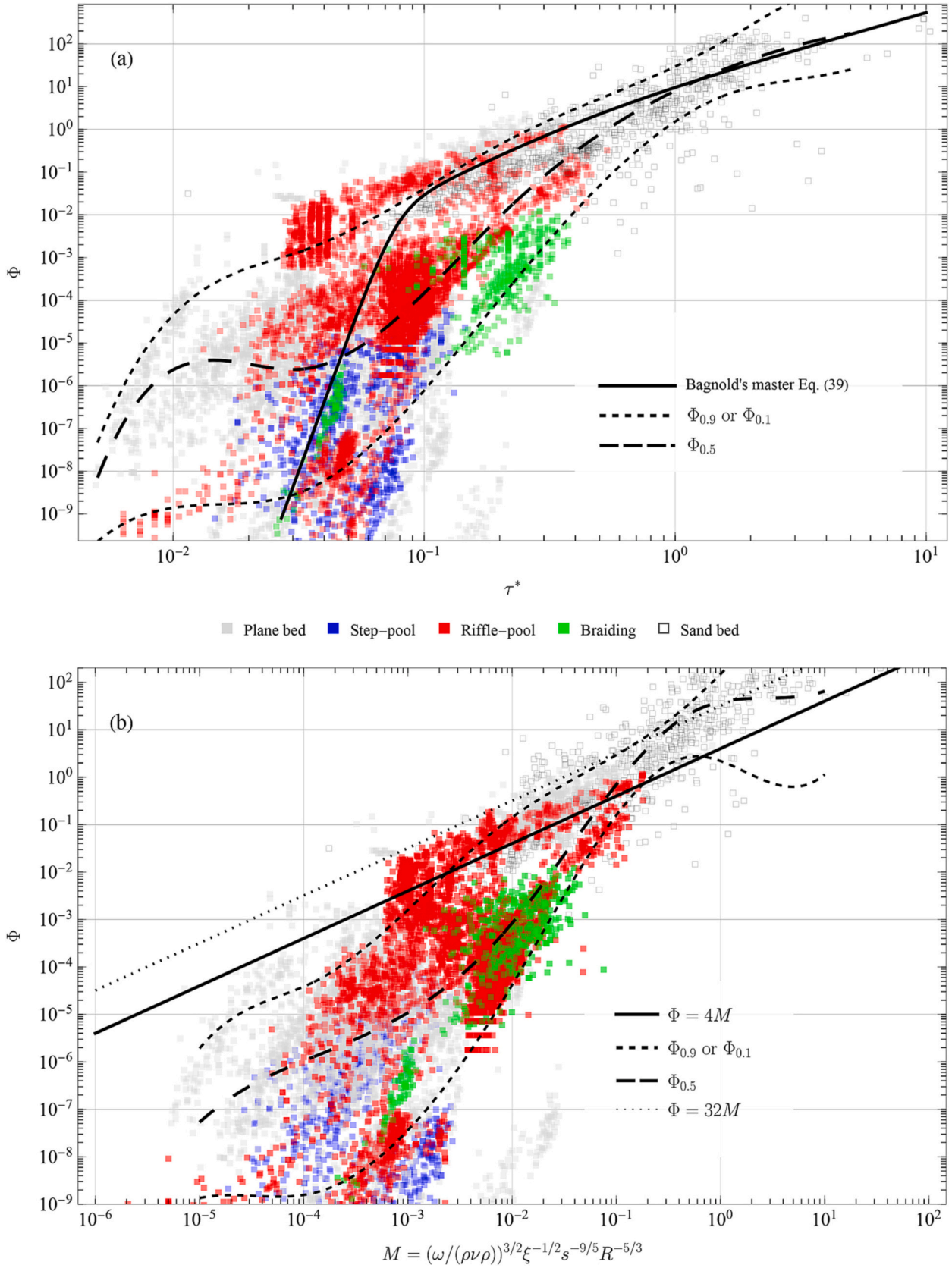

Fig. 5. (a) Variation in Φ with τ^* for gravel-bed rivers depending on the main types of bedforms at the monitoring station. (b) Variation of Φ with M. The data sources are indicated in Tables S2 to S4 in the Supplementary Material. See also Fig. S9 to S12 in the Supplementary Material, which shows how changing the characteristic diameter in the τ^* and Φ definitions modifies the data scatter; Fig. S15 for a selection of sites for which Bagnold's model provide good Φ estimates; and Fig. S16 for the variation in the efficiency factor e_b with τ^* for different types of bedform.

Table 4
Main features of the sites used in Fig. 5. See Tables S2 to S4 in the Supplementary Material for the detail (including the sources).

Morphology	Slope range (%)	Median size range (mm)	Number of sites	Sample size
Plane bed	0.028–4.5	4.0–210	46	4263
Riffle-pool	0.070–3.2	1.0–5	19	4093
Step-pool	2.070–5.1	40–207	7	683
Braiding	0.800–2.5	20–50	3	495
Sand	0.001–3.1	0.1–11	5	824

that under steady-state-flow and weak-transport conditions, the variance of time-averaged transport rates varies as the inverse of the integration time, and thus accurate measurements require long sampling durations, a condition that is hardly ever met in the field (Ancey and Pascal, 2020) (or, at the very least, long sampling durations are seldom compatible with steady water discharge). In Fig. 5, sampling durations ranged from seconds to one day, making it difficult to compare time-averaged rate measurements with one another. Moreover, bedload samplers usually only provide point measurements of transport rates, and deducing totals over the cross-section is also subject to sampling errors. Other techniques are based on acoustic or seismic sensors (*e.g.*, hydrophones, geophones, impact pipes) (Gray et al., 2010). The main difficulty then becomes correlating recorded signals and transport rates, which implies the calibration of every sensor. In their study of geophones and other acoustic methods, Rickenmann and his colleagues found that calibration was sensitive to site-specific features such as flow velocity and bed roughness, with calibration factors varying by a factor of 20 between samples (Rickenmann and Fritschi, 2017; Rickenmann et al., 2022; Nicollier et al., 2022). Uncertainties concern not only bedload transport rates but also hydraulic variables (*e.g.*, flow depth and water discharge) and bed configuration (surface and subsurface grain size distribution, bed slope).

Although the trend in Fig. 5(a) is less clear than in Fig. 3(a) reporting laboratory data, there is a noticeable change in Φ's dependence on τ^* when τ^* is in the 0.07–0.30 range. For $\tau < 0.1$, transport rates Φ vary sharply with increasing Shield stress τ^*, and variability is enormous (up to six orders of magnitude). For $\tau^* > 0.3$, Φ's dependence on τ^* is less marked, roughly consistent with Bagnold's master eq. (42). Variability is also less pronounced. For gravel-bed rivers, this change in behavior has often been attributed to the breakup of the pavement layer, the transition from partial transport to equal-mobility transport, or the part played by sediment supply relative to the transport capacity (Emmett and Wolman, 2001; Ryan et al., 2002; Barry et al., 2004; Ryan et al., 2005). However, it should be noted that this change is also visible in Fig. 3(a) for laboratory flume data, that is, for flow conditions where geomorphological processes (such as pavement or limited sediment supply) were not occurring. This point suggests that the change in behavior for $\tau^* \sim 0.1$ (where the $\sim$ symbol means "is of the order of") may be the result of geomorphological processes, but may also reflect the occurrence of Bagnold's transitional regime.

Figs. 5(a) and (b) also show that, on average, bedload transport rates in rivers are one to three orders of magnitude lower than those predicted by Bagnold's master equation or scaling and, in this respect, Bagnold's model performs no better than other models when applied to real-world rivers (Herbertson, 1969; van Rijn, 1984a; Gomez and Church, 1989; Barry et al., 2008; Recking, 2010; Hinton et al., 2018; Armijos et al., 2021). In contrast to this trend, we also observe that lots of data lie above Bagnold's master curve and scaling, especially those related to sand-bed rivers at high Shields stresses. It is often argued that bedload transport equations fitted to laboratory data can deliver the flow's transport capacity, usually defined as the maximum amount of sediment that a river can carry (Wainwright et al., 2015), and thus those equations represent the upper bound of Φ variations with τ^*. Fig. 5(a) shows that for gravel-bed rivers, the $\phi_{0.9}$ curve is fairly close to Bagnold's master eq. (42) for $\tau > 0.09$, but is far above it for $\tau^* < 0.09$. For sand-bed rivers, meanwhile, at a Shields stress exceeding 1, Bagnold's master eq. (42) captures the median curve $\phi_{0.5}$. One tentative explanation for the difference between gravel-bed and sand-bed rivers relates to the grain size distribution's influence on transport rates. For sand-bed rivers, this distribution is usually narrow, all particle sizes are mobile, and the determination of the median grain size required by the definition of the scale transport rate (7) is fairly accurate, which may explain why Bagnold's master eq. (42) closely matches the median trend of $\phi_{0.5}$. Gravel-bed rivers usually exhibit a much wider grain size distribution than sand-bed rivers. At low Shields stresses ($\tau^* < 0.09$), only the finer grains are mobile, which explains why Bagnold's master eq. (42), based on the surface median grain size d_{50}, underestimates bedload transport rates. The presence or absence of fine patches might explain some of the substantial scatter in Fig. 5(a). At higher Shields stresses ($\tau^* > 0.09$), Bagnold's master eq. (42) predicts transport rates Φ of the right order for some riffle-pool rivers (see below), but it usually tends to overestimate Φ by a factor 4 to 300. Braiding and step-pool rivers experience low transport rates, and in Fig. 5(a) their behavior is captured by the $\phi_{0.1}$ curve. Note that the lack of data on high transport rates in step-pool and braided rivers does not mean that it is not possible to achieve high transport rates in these streams, but simply that it is particularly difficult to measure bedload transport there.

Similar comments can be made when looking at Bagnold's scaling in Fig. 5(b). There is a marked difference between gravel-bed and sand-bed rivers. For $M > 0.01$, data related to sand-bed rivers follow the trend of $\Phi = 32M$ that was reported as the trend for a suspended load in Fig. 2 (b). As shown by the comparison of Bagnold's master equation and scaling in Fig. 2 with field data, the proportionality factor of Bagnold's scaling seems sensitive to the mode of transportation, and if this trend were confirmed, then this scaling could provide a rapid test for discriminating between bedload and suspended load. Some riffle-pool rivers exhibit a behavior close to that of sand-bed rivers, with many transport rates falling between the two trends of $\Phi = 4M$ and $\Phi = 32M$. For other rivers, Bagnold's scaling (41) provides the upper bound of dimensionless transport rates.

What is not seen in Figs. 5(a) and (b) is that taken individually, some sites (17 out of 81) yielded bedload transport rate data that Bagnold's equation managed to describe very closely (see Figs. S13(a) and (b) in the Supplementary Material). However, for the majority of sites (48/81), the correlation between the data and Bagnold's eq. (42) was only moderately good (see below). For the remaining sites (16/81), there was no correlation between the data and Bagnold's master equation.

For the majority of sites (48/81) with a partial agreement between the data and Bagnold's eq. (42), the trend of $\Phi(\tau^*)$ was correct in the log–log plot, in that the slope for the $\Phi(\tau^*)$ data in the log-plot was close to 3, as predicted by Bagnold's equation for the transitional regime, but shifted away from the data. This shift could mean that the sediment size scale used to define the Shields stress (7) was not the right one. It may indicate (i) an improper definition of the dimensionless shear stress τ^* and/or (ii) an incorrect scale for the dimensionless transport rate Φ. Regarding the first alternative, a number of authors have argued that using a reach-averaged dimensionless shear stress τ^* is not representative of the actual stress borne by mobile particles. They have, therefore, suggested using shear stress partitioning to modulate the stress effectively imparted to the mobile fraction (Parker et al., 1982; Diplas, 1987; Wilcock and Crowe, 2003; Yager et al., 2007; Recking, 2013; Schneider et al., 2015; Yager et al., 2018, 2019). Regarding the second alternative, authors such as Parker et al. (1982), Whiting and King (2003), and Pitlick et al. (2008) have noted that the bedload size distribution is usually closer to the observed subsurface distribution than to the distribution on the bed surface. Thus, in this respect, when defining the dimensionless transport rate (7), it makes more sense to use the subsurface median particle size than the surface median particle size. We do not enter into a more in-depth exploration of these alternatives here.

4. Insight from recent research

Over the decades since Bagnold's last papers, a great deal of work has been accomplished on bedload transport and granular flows, and it is thus interesting to examine the extent to which our current understanding of bedload transport confirms or disproves Bagnold's views. Bagnold's seminal work, in particular, inspired later generations of researchers and gave birth to the kinetic theory of granular flows (Campbell, 1990; Hunt et al., 2002) that has since been applied to bedload transport. We will review the various paths explored to date below.

We begin by recasting Bagnold's partitioning into transport regimes, specifying them in more detail, adding a fourth regime (hyperconcentrated flow), and addressing the part that bed slope plays in a regime's occurrence (see § 4.1). This partitioning is essentially based on the macroscopic features exhibited by different transport regimes, but we can propose another partitioning by making a finer-scale examination of how particle contact controls the overall dynamics of bedload transport (see § 4.2). In recent years, many microstructural models of bedload transport have been proposed, and it is interesting to note what they can add to our understanding of bedload transport, particularly the scaling behavior of transport rates (see § 4.3).

4.1. Bedload transport regimes

One particularly important point in Bagnold's theory concerns the partitioning of sediment transport into three regimes (see § 2.5): the no transport regime, the transitional regime, and the high-transport stage that we now refer to as the sheet-flow regime. As discussed in § 3.1, labeling the first regime as "no transport" is misleading in the sense that weak bedload transport continues to be observed when the Shields stress τ^* drops below the threshold of incipient motion, τ_c^*. Furthermore, Bagnold stated that predicting bedload transport in the transitional regime was difficult, if not impossible. Admittedly, laboratory and field measurements show that the variability in bedload transport rates is considerable, giving the impression that bedload transport is a noise-driven process in this regime. However, when time-averaged, these measurements lead to consistent power-law relationships, $\Phi \propto \tau^{*3}$, which suggests that there is some determinism hidden behind the variability in Φ. Lastly, bedload transport experiments at steep slopes have been associated with high values of efficiency factor e_b (see § 3.3), which calls into question Bagnold's central assumption that the bedload extracts a small amount of energy from the water stream. There is a transport regime in which bedload transport is intense and takes the form of "immature debris flow" (Takahashi, 1981) or "hyperconcentrated flow" (Rickenmann, 1992). This regime is observed with steep slopes when the bed is subject to intense erosion or failure. All in all, therefore, there are five sediment transport regimes: suspended load, hyperconcentrated flow, and the three bedload transport regimes identified by Bagnold. Table 5 attempts to reshape Bagnold's regime classification, shown in § 2.5, and specifies the regimes in terms of particle interactions, displacement modes, and coupling with the stream. We also suggest renaming the regimes as follows.

The *Rarefied transport regime* corresponds to weak sediment transport ($\Phi < 0.02$). It occurs when the Shields stress drops below a critical threshold of τ_r^*, located just above the threshold of incipient motion τ_c^*, which may not be unique and may vary with time, bed slope, and grain size (among other parameters) (Buffington and Montgomery, 1997; Yager et al., 2018; Pähtz et al., 2020; Benavides et al., 2022). Indeed, there is some consensus on τ_c^* (with field and laboratory studies giving τ_c^* values in the 0.04–0.10 range), but much less is known about τ_r^*; we will return to its value in Eq. (50), below. As summarized by Furbish et al. (2017),

> "sediment particle motions are mostly patchy, intermittent, and rarefied (...). This is particularly relevant to coarse-sediment rivers in which sediment transport predominantly occurs as bedload close to threshold (...); that is, where rarefied conditions likely are the norm."

In this regime, particles move erratically, mostly individually, and thus experience only fluid forces and frictional–collisional contact forces with the bed. On initially plane beds, microforms (*e.g.*, ripples) are created, initiating a slight bed instability (Coleman and Melville, 1994). Finer grains are more prone to transport than coarse grains. Moreover, bedload transport rates show enormous fluctuations due to the high variability in the number of moving particles per unit stream bed area—a variable called particle activity γ (Ancey et al., 2008; Singh et al., 2009; Roseberry et al., 2012). Theoretically, this regime has often been investigated using stochastic models of particle advection and diffusion (Furbish et al., 2017; Ancey, 2020a, 2020b). In gravel-bed rivers, where sediment mobility is poor, a recent approach implemented by Recking (2010) gave interesting results by associating this regime with the mobility of the bulk's coarse fraction (considered through its d_{84} value), which in turn was used as a proxy for the fine fraction's mobility (see Figs. S9 to S12 in the Supplementary Material).

The kinetic regime refers to the regime in which moving particles start to interact with each other. Ashley et al. (2021) suggested that this

Table 5
Summary of sediment transport characteristics for the three regimes defined by Bagnold (1966), which we have renamed the rarefied transport regime, the kinetic regime, and the sheet-flow regime.

	Rarefied (dilute) transport	Kinetic regime	Sheet flow
	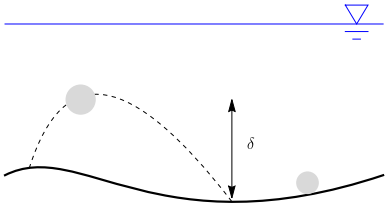	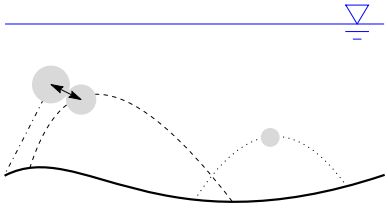	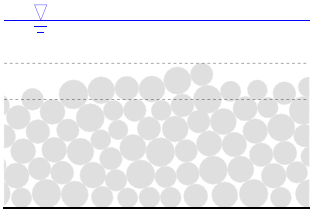
Shields range	$\tau_c^* \le \tau^* < \tau_r^*$	$\tau_r^* \le \tau^* < \tau_x^*$	$\tau^* \ge \tau_x^*$
Interactions	grain to bed	collision + grain to bed	grain–grain
Movement	rolling, saltation (patchy)	rolling, saltation (more regular)	dense flow
Bedforms	microform	mesoscale structure (*e.g.*, dune)	upper regime (plane bed)
Thickness δ	$\delta \sim 1 - 3d$	$\delta \sim 3d$	$\delta \sim 10d$
Flow resistance	mostly skin friction ($k_s \sim d_{90}$)	skin + form friction +bedload	$k_s/d = 2 + 6\tau_c^{*5/2}$
Mobility	partial	partial	full
Intermittency	highly fluctuating q_s	granular gas	continuous flow
Control variable(s)	particle activity	particle activity and velocity	bedload velocity and depth

regime was achieved when the collision number $\Theta = 2d_{50}\bar{u}_s\gamma^2/E$ (where E is particle entrainment, and $\bar{u}_s$ is mean particle velocity) exceeds unity. Recking et al. (2008b) identified this regime (that they called Domain 2, see also § S2.1 in the Supplementary Material where these domains are defined) by noticing that flow resistance was increased by bedload transport. Because of the particle collisions in this regime, bedload transport is akin to granular gases, and this analogy has been used to develop theoretical models. The challenge is considerable because there is no clear separation between particle and flow-length scales, which makes any attempt to derive continuum models almost impossible (Tan and Goldhirsch, 1998; Goldhirsch, 1999). The stochastic approach is also fraught with difficulties because of correlated motion (Aussillous et al., 2016; Ancey and Pascal, 2020). Both particle activity and velocity experience significant spatial and temporal variations, which leads to q_s fluctuations that cover several orders of magnitude (Dhont and Ancey, 2018; Ancey, 2020b). The flow thickness ranges from $2d$ to $3.5d$ (van Rijn, 1984a).

The sheet-flow regime corresponds to the bedload transport that occurs under intense flow conditions in the form of a particle carpet or bedload sheet. Flow is so intense that bedforms are usually destroyed, and the streambed is covered by a granular flow whose thickness is typically $10d$. This regime is, therefore, often associated with the upper-regime plane-bed condition. On steeper slopes (typically over 20%), beds may become unstable and yield to form mature debris flows (Takahashi, 1981; Tognacca, 1997; Gregoretti, 2000; Armanini et al., 2005; Prancevic et al., 2014; Lanzoni et al., 2017). The authors who addressed the transition to a sheet-flow regime arrived at several different conclusions. Nnadi and Wilson (1995) observed that for sand transported in a pressure-driven flow, bedforms were destroyed when $\tau^* > 1$, whereas van Rijn (1984a) indicated that the plane-bed condition was met when the transport stage $T = \tau_b/\tau_c - 1 > 25$, but Julien and Raslan (1998) found that under low submergence conditions ($\xi < 100$), the condition was met when $T > 4$. Gao (2008) suggested that the transition between the kinetic and sheet-flow regimes occurred when the proportion of mobile grains, $P_g = \tau^*\left(1 - \tau_c^*/\tau^*\right)^3$, equalled unity, namely for τ^* in the 0.50–0.55 range. These values are slightly higher than the $\tau_0 = 0.40$ threshold defined in § 2.7.3 as the upper threshold found for the transitional regime. Growing knowledge of granular flows and suspensions has opened the possibility of developing a continuum model of intense bedload transport (Forterre and Pouliquen, 2008; Guazzelli and Pouliquen, 2018). Section 4.3 will provide a few examples of these models.

Bedload can transform into suspended load when fluid drag and turbulence are sufficient to break particle contacts within the bedload layer. Sheet flows can be fluidized when most particles are held in suspension by turbulence or contacts between grains are lubricated by viscous forces. Sumer et al. (1996) observed no suspension for $w/u^* < 1$. This condition is close to the one used by Bagnold (1966) and the subsequent propositions for defining the transition from bedload to suspended load (van Rijn, 1984a; Celik and Rodi, 1991; Cheng and Chiew, 1999; García, 2007; Ma et al., 2020), even though most recent formulations have preferred to express the threshold of transition probabilistically (Cheng and Chiew, 1999; Dey et al., 2018). We return to the problem of bedload fluidization in § 4.2.1.

Bagnold focused on shallow bed slopes and, as a consequence, the regime diagram shown in Fig. 1 is ill-adapted to steep slopes. Sloping beds induce two major changes. First, the threshold of incipient motion increases as slopes steepen (Tsujimoto, 1991; Recking et al., 2008b; Lamb et al., 2008). Then, on slopes steeper than 20%, if the flow is sufficiently intense, the bed may fail suddenly and release large amounts of sediment. The water–sediment mixture then forms immature debris flows (also called hyperconcentrated flows) or mature debris flows. Prancevic et al. (2014) suggested including an upper bound in the Shields diagram related to bed failure. Based on Takahashi's work (Takahashi, 1981), they proposed an equation for predicting bed failure:

$$\tau_k^* = (1-\zeta)(\tan\phi - \tan\theta) - \frac{\varrho}{\Delta\varrho}\tan\theta, \tag{49}$$

where ζ denotes bed porosity and ϕ is the internal friction angle. Recking et al. (2008b) observed different behaviors depending on slope and relative submergence (see § S2.1 in the Supplementary Material). In particular, they found that flow resistance depended on the sediment transport strength, and they distinguished between intermittent and continuous bedload transport regimes (called Domains 2 and 3, respectively). Their definition of the critical relative submergence, ξ_{23}, delineating Domains 2 and 3, leads to a potential candidate for the definition of the critical threshold, τ_r^*, for observing the transition from the rarefied transport regime to the kinetic regime:

$$\tau_r^* = \frac{i}{s}\xi_{23} = 0.3i^{0.25}. \tag{50}$$

We know of no study investigating the dependence of Bagnold's critical bedload stage τ_x^* on slope i. Without any information, we assume that τ_x^* is constant and set it to the value of $\tau_1^* = 0.40$ found by deriving Bagnold's master equation from the respective expressions of Bagnold's model in § 2.7.3.

Fig. 6 shows the different regimes depending on bed slope. The regime studied in detail by Bagnold (1966) was the sheet-flow (or carpet) domain, colored yellow. Overall, it extends over the 0.4–0.9 range in terms of Shields numbers, and it is observed for slopes shallower than approximately 20%, which is consistent with laboratory observations of bed failure (Tognacca, 1997; Prancevic et al., 2014). This figure is useful to set the stage by defining and delineating distinct regimes of bedload transport, but there is much speculation behind it: first, the curves plotted in Fig. 6 rely on a limited number of experimental investigations; second, we only consider the simplest scenario of straight channels in which the material is of a unique size and is fully available. To the best of our knowledge, how a wider grain-size distribution and a limited supply of bedload material might affect the transport regime identified by Bagnold has not attracted any attention.

4.2. Regime partitioning depending on particle contact type

4.2.1. From the frictional to the viscous regime

In his pioneering experiments, Bagnold (1954) used neutrally buoyant particles, and thus in his study of the bulk friction coefficient μ (see § 2.6), he considered only two types of particle contact: viscous contact at low G values and collisional contact at high G values. Yet, real-world rivers involve negatively buoyant particles, and thus particles can undergo sustained frictional contact. We need to determine the type of particle contact depending on flow conditions because particle contact greatly influences how energy imparted by the fluid to the particles is dissipated through contact.

At rest, negatively buoyant particles settle and experience only frictional contacts. When they are sheared at a sufficiently high rate $\dot{\gamma}$, contacts are lubricated by the interstitial fluid, and, thus, there is a sudden change in particle stress generation (and energy dissipation). Ancey and Coussot (1999) and Ancey (2001) found that this transition could be predicted using a dimensionless number (that they called the Leighton number) related to the ratio of the lubrication force to the frictional force experienced by particles: $\mathrm{Le} = \varrho\nu\dot{\gamma}/\left(\Delta\varrho g h_s\right)$, where h_s is the bedload layer thickness and $\dot{\gamma}$ denotes the shear rate. A similar number, $I_v = \eta\dot{\gamma}/\sigma_y'$, was introduced later by Courrech du Pont et al. (2003) and Cassar et al. (2005) in their studies of underwater granular avalanches, and this has proved to be the main dimensionless number controlling the rheological behavior of granular suspensions (Boyer et al., 2011; Guazzelli and Pouliquen, 2018).

By assuming that $\dot{\gamma} \propto u^*/h_s$ and $h_s = O(10d)$ (with d as the mean particle diameter), then we can recast the Leighton number as $\mathrm{Le} = \tau^{*1/2}/(10R)$. Ancey and Coussot (1999) observed that the transition

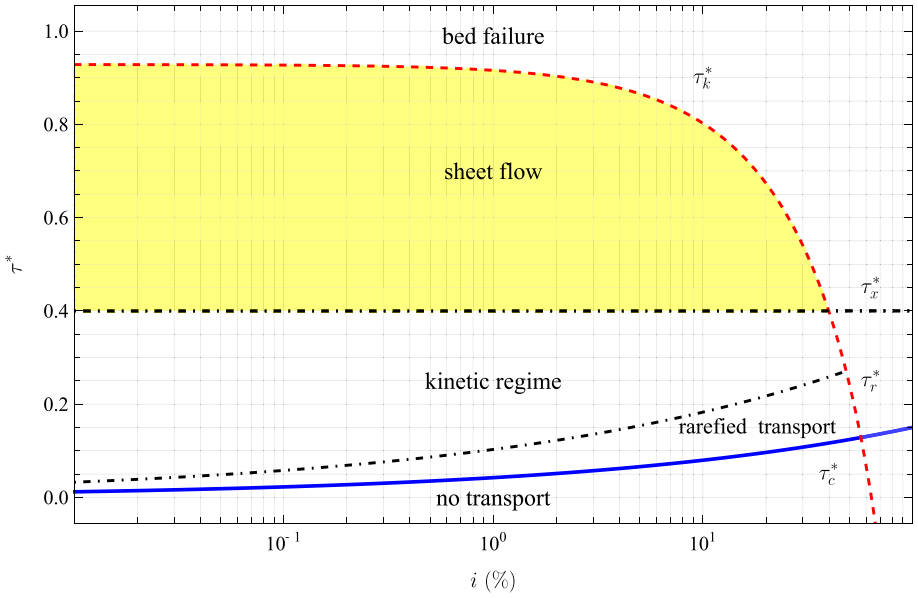

Fig. 6. Shields curve in the (i, τ^*) coordinate systems. The threshold of incipient motion, τ_c^*, is the empirical equation proposed by Recking et al. (2008b): $\tau_c^* = 0.15i^{0.275}$. The critical stage of $\tau_x^* = 0.40$ is also reported. The bed failure condition is given by Takahashi's eq. (49) (with $\phi = 55^\circ$ and $\zeta = 0.35$). The separation, $\tau_r^*(i)$, between the rarefied transport and kinetic regimes, is evaluated using eq. (50), as proposed by Recking et al. (2008b).

from the frictional to the lubricated contact regime occurred at $\mathrm{Le} \sim 10^{-1}$. This leads to the following critical (dimensionless) stress related to this transition:

$$\tau_{fv}^* = R^2. \tag{51}$$

Put differently, when $\tau^* \ll \tau_{fv}^*$, sediment transport takes the form of a particle carpet with sustained frictional contacts between particles, whereas when $\tau^* \gg \tau_{fv}^*$, the moving granular layer is fluidized, with lubricated contacts between particles. We thus expect a significant change in behavior when $\tau^* = O\left(\tau_{fv}^*\right)$. Although dense granular suspensions do not change appearance at the macroscopic scale during the transition from the frictional to the lubricated regime, their microscopic behavior changes significantly because lubricated contacts usually dissipate much less energy than frictional contacts. This sudden change in energy dissipation explains why densely particle-laden currents halt when they transition from a lubricated to a frictional regime (Hallworth and Huppert, 1998; Amy et al., 2005).

In their study of fine sediment transport, Ma et al. (2020) also observed an abrupt change in the sediment transport rate: fine sediment was carried at much higher rates than Engelund and Hansen (1967) had predicted, but above a critical threshold of shear stress, observations were consistent with Engelund and Hansen's model. Ma et al. (2020) suggested that the threshold was given by

$$\frac{u^*}{w_s} = 9, \tag{52}$$

where w_s and u^* denote the settling and friction velocities, respectively. When $u^* > 9w_s$, sediment is carried as suspended load at the rate of $\Phi = 0.72\tau^{*5/3}/f$, whereas for $u^* < 9w_s$, sediment is carried as bedload at the rate of $\Phi = 0.4\tau^{*5/2}/f$. Using the analytical approximation (A.3) of the settling velocity and Eq. (52), we can express the threshold for the frictional to viscous transition as

$$\tau_{fv}^* = 81\left(\frac{F(R^2)}{R}\right)^{2/3}. \tag{53}$$

For very fine sediment ($R < 10$), the settling velocity can be determined using Stokes drag force, and one then obtains $F = R^4/5832$ (Dietrich, 1982). In this case, Eq. (53) simplifies into

$$\tau_{fv}^* = \frac{1}{4}R^2. \tag{54}$$

Although criteria (51) and (53) (or its approximation (54)) do not match exactly, they convey the same order of magnitude. Ma et al. (2020) found that the transition from high to low transport rates occurred for a particle diameter close to 100 μm, that is, for a particle Reynolds number around $R \sim 4$. Eq. (53) predicts that the transition from a viscous to a frictional regime occurs at $\tau_{fv}^* = 2.5$, a value that is consistent with what Ma et al. (2020) observed for the Yellow River. We also note that when f is set to 0.05 (a reasonable value for a sand-bed river involving dunes), the scalings found by Ma et al. (2020) were close to what Bagnold's master eq. (42) predicts.

4.2.2. *From the frictional to the collisional regime*

If the interstitial fluid plays a minor role in stress generation, then granular bulks experience frictional and collisional contacts when they are sheared at a rate of $\dot{\gamma}$. The respective contributions of friction and collision to the total stress depend on the shear rate $\dot{\gamma}$. Ancey and Evesque (2000) defined a dimensionless number, which they called the Coulomb number, but which was subsequently renamed the "inertial number" (GdR-MiDi, 2004):

$$I = \frac{\varrho_p d^2 \dot{\gamma}^2}{\sigma_y'}, \tag{55}$$

where σ_y' is the effective normal stress experienced by the particles ($\sigma_y' = \sigma_y - p$ where σ_y and p denote the total normal stress and the fluid pressure, respectively). If we assume $\sigma_y' \propto \Delta\varrho g d$ and $\dot{\gamma} \propto u^*/d$, then

$$I = \frac{\varrho_p}{\varrho}\tau^*. \tag{56}$$

The bulk behaves like a frictional material when $I \ll 1$, and, conversely, it fluidizes and behaves like a Bagnold fluid when $I \gg 1$. It has been shown that it is possible to relate the shear and normal stresses within the bulk using this inertial number (Ancey and Evesque, 2000; GdR-MiDi, 2004; Jop et al., 2006; Forterre and Pouliquen, 2008):

$$\tau = \mu_g(I)\sigma_y^{'}, \tag{57}$$

where μ_g is a generalized Coulomb friction. To plot the transition from the frictional to the collisional regime, we arbitrarily set the inertial number to unity and, thus, in terms of Shields number, the transition is observed at

$$\tau_{fc}^* = \frac{\varrho}{\varrho_p} \sim 0.4. \tag{58}$$

This value is close to the threshold value of $\tau_0 = 0.40$ defined in Bagnold's master equation (see § 2.7.3), marking the limit between the transitional and sheet-flow regimes. This proximity suggests that the change in the exponent in the scaling law (from $\Phi \propto \tau^{*3}$ to $\Phi \propto \tau^{*5/3}$) is associated with a change in the prevalent type of contact (from frictional to frictional–collisional) within the bedload layer.

Armanini et al. (2005) used the rheological model proposed by Bagnold (1954) to compute the collisional stresses in rapidly flowing granular suspensions. They used the Bagnold number to differentiate the so-called macro-viscous (viscous contact) and grain-inertia (collisional contact) regimes. Bagnold used neutrally buoyant particles, which thus underwent no frictional contact, only viscous forces. In their experiments, Armanini et al. (2005) assumed that viscous contact was replaced by frictional contact. If we translate the criterion based on the Bagnold number, as proposed by Armanini et al. (2005), into one based on the Shields number (see § S3 in the Supplementary Material), we find that the transition from the frictional to the collisional regime should occur at Shields value

$$\tau_{fc}^* = \frac{200}{R^2}. \tag{59}$$

Armanini et al. (2005) also introduced the Stokes number,

$$\mathrm{St} = \frac{1}{18}\frac{\varrho_p}{\varrho}\frac{d^2\dot{\gamma}}{\nu}, \tag{60}$$

which is often interpreted as a reflection of the strength of coupling between the solid and fluid phases (Batchelor, 1989). Armanini et al. (2005) found that the transition between the frictional and collisional regime occurs for $\mathrm{St} \sim 7.5$. If we estimate the shear rate of $\dot{\gamma}$ as $\dot{\gamma} = u^*/h_s$, with the bedload layer thickness of $h_s = O(10d)$, we can then recast the criterion based on the Stokes number into one based on the Shields number:

$$\tau_{fc}^* = \frac{500}{R^2}. \tag{61}$$

Criteria (59) and (61) are equivalent to each other to within a multiplicative factor, but, as shown in Fig. 7, they are not consistent with the criterion (58) based on the inertial number.

4.2.3. Summary: contact diagram

Eqs. (53) and (58) are plotted in Fig. 7 in order to more easily locate the frictional, collisional, and viscous regimes in the (R, τ^*) diagram. Although the positions of these regimes are somewhat arbitrary (because they depend on the threshold value for each transition), they help to present and delineate four distinct domains. In most circumstances, particles interact with each other through frictional contacts. At high shear stresses ($\tau^* > 0.4$), coarse particles (for $R > 2$) also undergo collisional interactions. Finer particles ($R < 2$) experience viscous and frictional forces at low shear stresses, whereas at high shear stresses ($\tau^* > 0.4$), their contacts are predominantly viscous and collisional. There is a reasonably good match between Fig. 7, based on particle contact, and Bagnold's partitioning in Fig. 1.

4.3. Microstructural approaches to intense bedload transport

A great deal of work has been done to investigate intense sediment transport. An exhaustive review of these past studies is beyond the scope of the present paper. Here, we focus on sufficiently coarse particles. Typically, with $d = 1$ mm and $d = 1$ cm, we get $R = 127$ and $R = 4023$, respectively. Table 6 recaps the significant contributions to bedload-sheet theory, specifying the features of the flow domains they investigated and the scaling laws $\Phi(\tau^*)$ they obtained. Additional control parameters, such as interstitial fluid properties (temperature, density, viscosity) and bed features (mainly their angle θ) could be important,

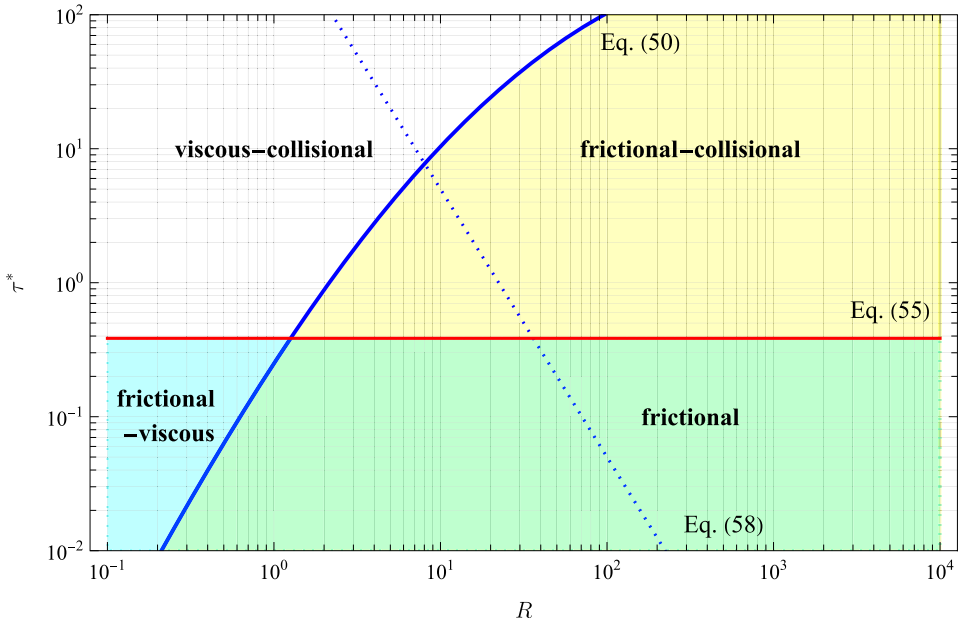

Fig. 7. Contact types in the R, τ^* diagram. The solid blue line shows the transition from the frictional to the lubricated contact regime, as predicted by eq. (53). The solid red line shows the transition from the frictional to the collisional contact regime, as predicted by eq. (58). The dotted line is criterion (61), as proposed by Armanini et al. (2005), initially based on the Stokes number. (For interpretation of the references to colour in this figure legend, the reader is referred to the web version of this article.)

but their effects are as yet poorly documented.

One particular difficulty with these models is that they involve parameters whose values are difficult to adjust from independent experiments. Authors may then be tempted to set parameters such that their model's outcomes match well-known bedload transport equations, such as the Meyer-Peter–Müller equation. This explains why some authors ended up with the same scaling law as the Meyer-Peter–Müller equation. Overall, the models best suited to coarse bedload include those of Berzi and Fraccarollo (2013) (who obtained $\Phi \approx 4\tau^{1.8}$ in the 0.3–3 range of the Shields number) and of Maurin et al. (2018) (who ended up with $\Phi \approx 0.79\left(\widehat{\tau}^{*} - \widehat{\tau}_c^{*}\right)^{1.6}$ in the 0.1–0.5 range of the Shields number τ^{*}, and in the 0.5–6 range for the modified Shields number $\widehat{\tau}^{*}$). Both models credited Bagnold's scaling law (8).

Apart from these two studies corroborating Bagnold's scaling, the other studies do not show results that are consistent with one another. For instance, for the frictional–collisional regime (for which $\Phi \propto \tau^{*5/3}$ if Bagnold's scaling is correct), studies lead to scalings of $\Phi \propto \tau^{*p}$, with p in the 1.5–2.5 range (see Fig. S17 in the Supplementary Material, where the p values are mapped).

5. Conclusions

The present paper has thoroughly examined bedload transport scaling behavior. We sought to know whether a power-law relationship

Table 6
Theoretical approaches to intense bedload transport. Where available, we show each author's contribution by specifying the flow types addressed, the Reynolds number range $R = \sqrt{sgd^3}/\nu$ ($s = \Delta\varrho/\varrho$), the Shields number range $\tau^{*} = u^{*2}/(sgd)$, and the ratio of the settling to shear velocities w_s/u^{*}. We summarize the model components of how the solid and fluid phases are modelled. KT is a shorthand notation for kinetic theory, $\mu(I)$ refers to the $\mu(I)$ rheology (GdR-MiDi, 2004; Forterre and Pouliquen, 2008), Coulomb means that the authors assume a Coulombian behaviour ($\tau = \sigma' \tan\alpha$). DEM means "discrete element methods." LBM refers to "Lattice Boltzmann Method." For turbulence in the fluid phase, authors used the $k-\varepsilon$ model, the mixing length ℓ_m approximation, or large eddy simulations (LES). Some authors considered a viscous shear stress rather than a turbulent one. The interplay between the solid and fluid phases was often modeled using a drag force. Some authors also assumed that particle collisions were mediated by viscous forces and, thus, assumed a viscous damping effect. Section S3 in the Supplementary Material provides further information about the results reported here.

Authors	flow type	R	τ^{*}	w_s/u^{*}	Solid phase	Fluid phase	Scaling
Amoudry et al. (2008)	two-phase suspension	20			KT	$k-\varepsilon$	
Armanini et al. (2005)	two-phase	520			KT, Coulomb		$Q_s = F(\theta)Q$ or $\Phi \propto \tau^{*3/2}$
Berzi and Jenkins (2008)	two-phase	520			$\mu(I)$ + KT	viscous drag	$\Phi \propto \tau^{*1/2}$
Berzi (2011)	layered flow	$50-200$	<1.25		KT	damping effect	$\Phi \approx \tau^{*3}$
Berzi and Fraccarollo (2013)	layered flow	1150	$0.3-3$		KT	damping effect	$\Phi \approx 4\tau^{1.8}$
Berzi (2013)	layered flow	46	$1-10$		KT		$\Phi \approx 10\tau^{1.6}$
Berzi and Fraccarollo (2016)	turbulent suspension	20	$0.5-10$	$0.55-1.1$	KT		$\Phi \approx 30\tau^{2}$
Capart and Fraccarollo (2011)	layered flow	430	$0.4-2.5$	$0.8-2.2$	$\mu(I)$ + KT		$\Phi \approx 0.4\tau^{2}$
Chauchat (2018)	two-phase flow	220	~ 0.5		$\mu(I)$	ℓ_m + drag	consistent with $\Phi = 11.8\tau^{*1.5}$
Cheng et al. (2018)	two-phase	220	~ 0.5		KT	LES	
Chiodi et al. (2014)	two-phase	3			$\mu(I)$		$\Phi \propto 6\left(\tau^{*} - \tau_c^{*}\right)^{3/2}$ with $\tau_c^{*} = 0.037$ for $\tau^{*} < 0.15$ $\Phi \propto \tau^{*5}$ for $\tau^{*} > 0.15$
Durán et al. (2014)	two-phase	10			DEM	ℓ_m + drag	$\Phi \approx 1.3\left(\tau^{*} - \tau_c^{*}\right)^{3/2}$ with $\tau_c^{*} = 0.004$
Gonzalez-Ondina et al. (2018)	two-phase	$15-450$	$0.4-5.5$	$0.3-1.7$	KT	$k-\varepsilon$	
Hanes and Inman (1985)	one-phase				Bagnold		$\Phi \approx 3.5\tau^{*5/2}$
Hsu et al. (2004)	two-phase	230	$0.3-3.5$		KT	$k-\varepsilon$ + drag	$\Phi \approx 20\left(\tau^{*} - \tau_c^{*}\right)^{1.8}$ with $\tau_c^{*} = 0.05$
Jenkins and Hanes (1998)	two-phase	150	$0.7-2.6$		KT	ℓ_m + drag	$\Phi \approx 9\sqrt{\rho_p/\rho}\left(\tau^{*} - \tau_c^{*}\right)^{1.53}$ with $\tau_c^{*} = 0.05$
Kaczmarek et al. (2019)	layered flow	$10-3200$	$0.7-2.6$		KT	ℓ_m + drag	$\Phi \approx 8\left(\tau^{*} - \tau_c^{*}\right)^{3/2}$ with $\tau_c^{*} = 0.05$
Lee et al. (2016)	two-phase	$16-235$	$1-2.3$		$\mu(I)$	$k-\varepsilon$ + drag	$\Phi \approx 3.5\tau^{*5/2}$
Longo (2005)	two-phase	$6-17$	$1.1-4$		KT	$k-\varepsilon$	$\Phi \approx 19.8\tau^{*1.83}$
Matoušek and Zrostlík (2020)	one-phase	$410-130$	$0.5-1.7$		KT		$\Phi \approx 8.6\tau^{*1.05}$
Maurin et al. (2016)	two-phase	$310-2900$	$0.2-0.7$		$\mu(I)$ or DEM	ℓ_m + drag	$\Phi \approx 8\tau^{*3/2}$
Maurin et al. (2018)	two-phase	$310-2900$	$0.1-0.5$		$\mu(I)$ or DEM	ℓ_m + drag	$\widetilde{\Phi} \approx 0.79\left(\widetilde{\tau}^{*} - \widetilde{\tau}_c^{*}\right)^{1.6}$ with $\widetilde{\tau}_c^{*} = 0.1$
Pähtz and Durán (2020)	two-phase	$50-100$	$0.1-0.5$		DEM	drag + viscous	$\widetilde{\Phi} \propto \widetilde{\tau}_c^{*2}$
Revil-Baudard and Chauchat (2013)	two-phase	$15-150$	$1.25-2.3$		DEM	drag + viscous	$\Phi \approx 20\tau^{*1.8}$
Schmeeckle (2014)	two-phase	45	$0.1-1.6$		DEM	LES	$\Phi \approx 5\tau^{*2.5}$ for $\tau^{*} > 0.8$
Zhang et al. (2022)	two-phase	$1700-3400$	$0.046-0.14$		DEM	LBM	$\Phi \approx 8(\tau^{*} - 0.033)^{3/2}$

of $\Phi \propto \tau^{*n}$, relating the bedload transport rate Φ to the Shield stress τ^*, could properly describe both laboratory and field data and, if so, what value the exponent n might take. Many papers have addressed this question, and the fact that they have reached no consensus about that value may mean that finding a universal law of bedload transport is a pipe dream. One solution to this conundrum could be that there simply is no unique value for the exponent n but that the scaling law is defined piecewise, implying that n changes value depending on τ^*. Exploring this idea by defining distinct bedload transport regimes and directly adjusting n from the data related to each regime could prove to be a perilous fitting exercise in the sense that bedload transport rates are noisy and infinite solutions could be found. An alternative would be to constrain the form of the bedload transport rate equation using physical principles.

Ralph Bagnold voiced a similar idea nearly 60 years ago (Bagnold, 1966), and we were curious to see how Bagnold's model might assist us in finding a constrained form for bedload transport rates. In § 2.1, we showed that his 1966 model could be cast in the following dimensionless form:

$$\Phi = \frac{e_b}{\mu \cos\theta} \sqrt{\frac{8}{f}} \tau^{*3/2}. \tag{62}$$

This form differs from the more usual one in which the driving variable is the dimensionless stream power (per unit width), $\Omega = \omega/(\varrho g \nu)$, instead of the Shield stress, τ^*:

$$\Phi = \frac{e_b}{\mu \cos\theta} \frac{\Omega}{sR}. \tag{63}$$

Admittedly, the main reason for using Eq. (62) is that Bagnold used ω as the driving variable of bedload transport; however, he also used the Shields stress τ^* to partition bedload transport into three distinct regimes. For the sake of consistency, we have mainly used τ^* as the driving variable. In Eq. (62), we assumed that the friction factor μ is given by Bagnold's model (18) fitted to his rheometric data, and we calibrated the efficiency factor e_b and the Darcy–Weisbach flow resistance coefficient f from independent sets of pipe and flume data related to plane-bed flow conditions. The extension to more complicated bed structures remains a challenge.

When applied to laboratory flumes, Eq. (62) properly describes bedload transport rates over two orders of magnitude of the Shields stress τ^* (see § 3). We also proposed a simplified variant of Eq. (62), which retains only Φ's dependence on τ^*, and that we referred to as Bagnold's master equation:

$$\Phi = (10\tau^*)^{16} \left(1 + \left(\frac{\tau^*}{\tau_1^*} \right)^{3/2} \right)^{-8/9} \left(1 + \left(\frac{\tau^*}{\tau_0^*} \right)^{8} \right)^{-13/8}, \tag{64}$$

where $\tau_0^* = 0.078$ and $\tau_1^* = 0.40$ are estimates of the lower and upper limits of the regime qualified as "transitional" by Bagnold (1966) and that we suggest naming the "kinetic regime." This equation summarizes three scalings: $\Phi \propto \tau^{*16}$ in the no-transport regime (or rarefied transport regime) for $\tau^* < \tau_0^*$; $\Phi \propto \tau^{*3}$ in the transitional regime (or kinetic regime) for $\tau_0^* \leq \tau^* < \tau_1^*$; and $\Phi \propto \tau^{*5/3}$ in the high-transport regime (or sheet-flow regime) for $\tau^* \geq \tau_1^*$. Incidentally, the term of *no-transport regime* may be confusing when working with mountain rivers (the situation is different with lowland rivers) since even during low-intensity floods (those whose peak discharge does not mobilize the pavement layer), the Shields number remains less than τ_0^*, and most bedload transport occurs under such conditions. Referring to this regime as the *rarefied transport regime* may be preferable, but this designation would also come with some risk of confusion, since transport is not necessarily so rarified.

When applied to field data, Eq. (64) provides the correct trend for the majority of rivers. However, for some rivers (about 20% of the sites studied in § 3.6), the data show little correlation between water discharge and bedload transport rates, and Eq. (63) is unable to capture the right order of magnitude of the observed transport rates.

In his final papers, Bagnold also used regression analysis to determine Φ's dependence on stream power, flow depth, and grain size (Bagnold, 1980, 1986). We updated his results by using a Markov chain Monte Carlo algorithm to determine this dependence. We found that for bedload transport, the transport rate scales as

$$\Phi = 4M, \tag{65}$$

where $M = \Omega^{3/2} \xi^{-3/2} s^{-9/5} R^{-5/3}$ is a dimensionless number that we have called the Martin number. When the bedload transforms into a suspended load, the exponent remains the same, but the proportionality factor increases to $\Phi = 32M$. When trialed on laboratory flume data, Eq. (65) correctly describes transport rates over five orders of magnitude in M. We refer to Eq. (65) as Bagnold's scaling equation.

Overall, Bagnold's approach has two interesting features. First, the partitioning of bedload transport types into three transport regimes is corroborated by a variety of laboratory experiments and, to some extent, by field surveys. The Shields stress has a markedly different influence on each of the three regimes' transport rates—Φ ($\Phi \propto \tau^{*16}$, $\Phi \propto \tau^{*3}$, and $\Phi \propto \tau^{*5/3}$)—whereas scaling behavior with the Martin number remains the same in each. Second, the predictive capacity of Bagnold's master eq. (64) and scaling (65) is good for laboratory flume experiments and satisfactory for real-world rivers. Many processes may explain why the model performs much worse with gravel-bed rivers. Typical examples of these processes include the intricate coupling between sediment transport and bedforms, the limited supply of bedload material, and grain sorting.

Bagnold's approach also raises several important issues that we have examined throughout this review paper without providing any definitive answers. First, Eqs. (62) and (63) use two different driving variables that are underpinned by two distinct views of what controls bedload transport. When using the Shield stress τ^*, we emphasize that bedload transport is a local process controlled by the shear stress exerted by the water stream on its bed. Using the stream power Ω amounts to postulating that bedload transport is controlled at the flow scale. Naturally, under steady-state uniform-flow conditions, eqs. (62) and (63) are exactly equivalent, but under time-dependent or non-uniform-flow conditions, this is no longer the case. A number of studies have pointed out the non-local character of bedload transport under non-uniform conditions (Charru et al., 2004; Lajeunesse et al., 2010; Furbish et al., 2012; Ancey et al., 2015; Furbish et al., 2017), using differential operators to account for the diffusive behavior of bedload transport. There are still many unanswered questions about which driving variable is most relevant (Ω or τ^*) when the flow is no longer under steady-state uniform-depth conditions.

A second issue is that Bagnold's approach assumed that the bedload was fully subordinate to the water stream, from which it extracts a small amount of energy to set it in motion and carry it. This assumption is consistent with the low values for the efficiency factor ($e_b < 0.2$) found by Bagnold (1966) and other authors (Gomez, 2022). However, it contrasts with the values reported in this review for both laboratory and field data (with values of e_b reaching and even exceeding unity). These high efficiency-factor values suggest that Bagnold's assumption breaks at high transport rates. Laboratory data showed no radical bedload transport rate variations with the Shields stress τ^*, which may explain why Bagnold's master eq. (62) performs well even though one of its working assumptions is no longer valid. Most of the theoretical and numerical models reported in Table 6 do not use this assumption and instead use a coupling of the solid and fluid phases through interstitial pressure and drag forces. Unfortunately, at this time, although these phases are better described, we do not have more information or more confidence about the scaling behavior of Φ.

A third issue, implicit in Bagnold's approach, is that the model provides the amount of sediment transported along "a length of channel

sufficient to include all repetitive irregularities of slope, cross-section, and boundary" (Bagnold, 1966). Bagnold's assumption implies that (i) the model only provides space-averaged estimates of bedload transport, and (ii) bedload transport is aligned with the main flow direction. There are thus two limitations to keep in mind. First, even when involving local Shields stress τ^*, the model is not supposed to provide the spatial distribution of bedload transport rates. The consequence is that its inclusion in morphodynamic models requires further assumptions about the cross-section's spatial evolution due to erosion and deposition (Cunge et al., 1980, see Chap. 7.2). Second, extending Bagnold's model to two-directional flows, as Seminara et al. (2002) tried to do, is problematic. The model is best suited to unidirectional flows.

A fourth issue raised by Bagnold's approach was his use of crude criteria, based on threshold values of the Shields stress, to delineate the transport regimes. Overall, experimental and field observations confirm these values, but this good agreement must be tempered by the fact that the data's large scatter makes an exact determination of these thresholds illusory. Authors have tried to provide other criteria based on steric considerations (*e.g.* Gao, 2008; Ashley et al., 2021), or on alternative dimensionless numbers (Maurin et al., 2016). In recent years, several studies have proposed dimensionless numbers to characterize flow regimes in granular suspensions (Savage, 1984; Ancey et al., 1999; Ancey and Evesque, 2000; Forterre and Pouliquen, 2008; Delannay et al., 2017). These numbers were often defined using characteristic times of interaction or relaxation between the solid and fluid phases. We found that they were not necessarily consistent with each other (see § 4.3). For instance, distinguishing between friction-dominated and collision-dominated regimes can be done using the Bagnold number (Armanini et al., 2005) or the inertial number (Ancey and Evesque, 2000; GdR-MiDi, 2004), but outputs are contradictory (see § 4.2). Further work is needed to elucidate the nature and limits of bedload transport regimes.

Lastly, applying Bagnold's approach to real-world rivers requires further work to determine how bedforms affect energy transfer and flow resistance (and thus how the efficiency factor and Darcy–Weisbach coefficients are changed). Apart from a few studies on material supply affects the value of e_b (Gomez, 2006;Gomez et al., 2022), there has been no investigation of how to update Bagnold's approach to account for bedform's influence on bedload transport. Bagnold's model (62) suggests that bedforms lead to reduced energy transfer (thus a reduction in e_b) and increased flow resistance (thus an increase in f). The next step should be a detailed comparison between Bagnold's model and laboratory or field data related to streams with bedforms, in which the efficiency factor e_b and friction factor are evaluated independently.

Returning to the initial question in this review paper's title, we can say that Bagnold's approach has some decisive advantages and raises some interesting questions (highlighted above) about the nature of bedload transport. Insofar as we have calibrated the model parameters from an independent dataset and tested Bagnold's equations to a wide range of flow conditions, we can state that Bagnold's ideas undoubtedly remain relevant. Bagnold's main result, $\Phi \propto \Omega^{3/2}$, remains valid for a wide range of flow conditions.

Declaration of Competing Interest

The authors declare that they have no known competing financial interests or personal relationships that could have appeared to influence the work reported in this paper.

Data availability

All the data related to natural rivers used in this paper can be downloaded from https://doi.org/10.5281/zenodo.7746863. The Supplementary Material provides the sources of these data and explains how the raw data were post-processed. It also provides additional information about the data analyzed in this review paper. The data related to laboratory experiments can be also obtained directly from the references cited in Tables 1 and 2. The authors also refer readers to www.bedloadweb.com, a website developed by Alain Recking, which compares bedload transport equations with field data.

Acknowledgments

The authors thank Jonathan Laronne and Kyle Stark for sharing their data on ephemeral streams. Christophe Ancey acknowledges the support of the Swiss National Science Foundation (grant No. 200020_204108). We are grateful to Prof. Basil Gomez, Prof. Rob Ferguson, Prof. Michael Church, and an anonymous reviewer for the numerous remarks that helped to improve this paper.

Appendix A. Shields diagram

da Silva and Bolisetti (2000) proposed an empirical equation for the Shields curve:

$$\tau_c^* = 0.13\xi^{-0.392}\exp\left(-0.015\xi^2\right) + 0.045\left(1-\exp\left(-0.068\xi\right)\right), \tag{A.1}$$

where

$$\xi = \left(\frac{\varrho_p}{\varrho}\frac{gd^3}{\nu^2}\right)^{1/3} = \left(\frac{\varrho_p}{\Delta\varrho}R^2\right)^{1/3}. \tag{A.2}$$

Dietrich (1982) developed an empirical equation that captures the settling velocity w_s of spherical particles:

$$w_s = \left(\frac{\Delta\varrho}{\varrho}g\nu\right)^{1/3}F^{1/3}(d^*) \quad \text{with } d^* = \frac{\Delta\varrho}{\varrho}\frac{gd^3}{\nu^2} = R^2, \tag{A.3}$$

and

$$10^5\log F = -376715 + 192944\log d^* - 9815\log^2 d^* - 575\log^3 d^* + 56\log^4 d^*, \tag{A.4}$$

where log gives the logarithm with base 10. The condition of $u^* = w_s$ can be cast in a dimensionless form by substituting w_s with eq. (68).

$$\tau^* = \frac{\varrho}{\Delta\varrho}\frac{1}{gd}\left(\frac{\Delta\varrho}{\varrho}g\nu\right)^{1/3}F^{2/3}(d^*) = R^{-2/3}F^{2/3}\left(R^2\right). \tag{A.5}$$

Appendix B. Nomenclature

Table B.7
Roman symbols.

Ba	–	Bagnold number
C	–	bedload concentration
$\bar{C}$	–	mean bedload concentration
d	m	particle diameter
d_{50}	m	mean particle diameter
d_{84}	m	particle diameter quantile related to frequency $p = 0.84$
e	–	coefficient of restitution
e_b	–	efficiency factor
f	–	Darcy–Weisbach friction
Fr	–	Froude number
g	m/s^2	gravitational acceleration
G	–	Bagnold number
h	m	flow depth
h_s	m	bedload layer thickness
i	–	bed slope
I	–	inertial number
k_s	m	bed roughness
ℓ_m	m	mixing length
L_s	m	saturation length
L	–	Leighton number
M	–	Martin's number
P	W/m^2	power per unit surface
q	m^2/s	flow rate per unit width
q_{eq}	m^2/s	equilibrium flow rate per unit width
q_s	m^2/s	bedload transport rate per unit width
R	–	particle Reynolds number
R_h	m	hydraulic radius
s	–	density ratio
St	–	Stokes number
T	K	temperature
T_s	s	saturation time
$\bar{u}$	m/s	depth-averaged velocity
u^*	m/s	friction velocity
$\bar{u}_s$	m/s	bedload velocity
w_s	m/s	settling velocity
x	m	streamwise coordinate
y	m	cross-stream coordinate

In this article, log refers to the decimal logarithm (with base 10) whereas ln is the natural logarithm (with base e).

Table B.8
Greek symbols.

α	–	friction angle
α_{rl}	–	correcting factor of roughness size accounting for roughness layer
α_b	–	correcting factor of roughness size accounting for bedload transport
$\Delta\varrho$	kg/m^3	density difference $\Delta\varrho = \varrho_p - \varrho$
η	Pa s	water dynamic viscosity
γ	m	particle activity
$\dot{\gamma}$	1/s	shear rate
κ	–	von Kármán's constant ($\kappa = 0.41$)
Λ	W/m^2/K	entropy production rate
μ	–	Bagnold's bulk friction coefficient
μ_b	–	Bagnold's local friction coefficient
ω	W/m^2	stream power per unit length
Ω	–	scaled stream power $\Omega = \omega/(g\nu\varrho)$
ω_c	W/m^2	critical stream power per unit length related to incipient motion
Φ	–	dimensionless bedload transport rate
Π	–	dimensionless number
σ'	Pa	effective normal stress
σ_g	–	gradation factor $\sigma_g = d_{84}/d_{50}$
σ_p	Pa	particle normal stress
τ^*	–	Shields number
τ_c^*	–	critical Shields number related to the onset of sediment motion
τ_{fv}^*	–	critical Shields number related to the transition from frictional to viscous regimes
τ_0^*	–	Shields stress related to the transition from the no-transport to transitional regimes
τ_1^*	–	Shields stress related to the transition from the transitional to sheet-flow regimes
τ_b	Pa	bottom shear stress
τ_k^*	–	dimensionless critical shear stress related to bed failure
τ_p	Pa	particle shear stress
τ_x	Pa	critical bedload stage

(*continued on next page*)

Table B.8 (*continued*)

τ_x^*	–	dimensionless critical bedload stage
θ	–	bed angle
ϱ	kg/m^3	water density
ϱ_p	kg/m^3	particle density
ϱ_s	kg/m^3	bulk sediment density
ξ	–	relative submergence
ξ_{12}	–	relative submergence at the transition between Recking's Domains 1 and 2 (see Supplementary Material)
ξ_{23}	–	relative submergence at the transition between Recking's Domains 2 and 3 (see Supplementary Material)
ζ	–	bed or bedload porosity

Appendix A. Supplementary data

Supplementary data to this article can be found online at https://doi.org/10.1016/j.earscirev.2023.104571.

References

Abrahams, A.D., Gao, P., 2006. A bed-load transport model for rough turbulent open-channel flows on plane beds. Earth Surf. Process. Landf. 31, 910–928.

Ackers, P., White, M.M., 1973. Sediment transport: new approach and analysis. J. Hydraul. Div. ASCE 99, 2041–2060.

Alam, A.M.Z., Kennedy, J.F., 1969. Friction factors for flow in sand-bed channels. J. Hydraul. Div. ASCE 95, 1973–1992.

Amoudry, L., Hsu, T.J., Liu, P.L.F., 2008. Two-phase model for sand transport in sheet flow regime. J. Geophys. Res. Oceans 113, C03011.

Amy, L.A., Hogg, A.J., Peakall, J., Talling, P.J., 2005. Abrupt transitions in gravity currents. J. Geophys. Res. 110, F03001.

Ancey, C., 2001. Role of lubricated contacts in concentrated polydisperse suspensions. J. Rheol. 45, 1421–1439.

Ancey, C., 2020a. Bedload transport: a walk between randomness and determinism. Part 1: State of the art. J. Hydraul. Res. 58, 1–17.

Ancey, C., 2020b. Bedload transport: a walk between randomness and determinism. Part 2: Challenges and prospects. J. Hydraul. Res. 58, 18–33.

Ancey, C., Coussot, P., 1999. Transition from frictional to viscous regime for granular suspensions. C. R. Acad. Sci. Paris sér. IIb 327, 515–522.

Ancey, C., Evesque, P., 2000. Frictional-collisional regime for granular suspension flows down an inclined channel. Phys. Rev. E 62, 8349–8360.

Ancey, C., Heyman, J., 2014. A microstructural approach to bed load transport: mean behaviour and fluctuations of particle transport rates. J. Fluid Mech. 744, 129–168.

Ancey, C., Pascal, I., 2020. Estimating mean bedload transport rates and their uncertainty. J. Geophys. Res. Earth Surf. 125 e2020JF005534.

Ancey, C., Coussot, P., Evesque, P., 1999. A theoretical framework for very concentrated granular suspensions in a steady simple shear flow. J. Rheol. 43, 1673–1699.

Ancey, C., Davison, A.C., Böhm, T., Jodeau, M., Frey, P., 2008. Entrainment and motion of coarse particles in a shallow water stream down a steep slope. J. Fluid Mech. 595, 83–114.

Ancey, C., Bohorquez, P., Heyman, J., 2015. Stochastic interpretation of the advection diffusion equation and its relevance to bed load transport. J. Geophys. Res. Earth Surf. 120, 2529–2551.

Andreotti, B., Forterre, Y., Pouliquen, O., 2013. Granular Media: Between Fluid and Solid. Cambridge University Press, Cambridge.

Armanini, A., Capart, H., Fraccarollo, L., Larcher, M., 2005. Rheological stratification in experimental free-surface flows of granular-liquid mixtures. J. Fluid Mech. 532, 269–319.

Armijos, E., Merten, G.H., Groten, J.T., Ellison, C.A., Lisiecki, L.U., 2021. Performance of bedload sediment transport formulas applied to the Lower Minnesota River. J. Hydrol. Eng. 26, 05021014.

Ashley, T.C., Naqshband, S., McElroy, B., 2021. Lower-stage plane bed topography is an outcome of rarefied, intermittent sediment transport. J. Geophys. Res. Earth Surf. 126 e2020JF005754.

Aussillous, P., Zou, Z., Guazzelli, E., Yan, L., Wyart, M., 2016. Scale-free channeling patterns near the onset of erosion of sheared granular beds. Proc. Natl. Acad. Sci. U. S. A. 113, 11788–11793.

Aziz, N.M., Scott, D.E., 1989. Experiments on sediment transport in shallow flows in high gradient channels. Hydrol. Sci. J. 34, 465–478.

Bagnold, R.A., 1954. Experiments on a gravity-free dispersion of large solid spheres in a Newtonian fluid under shear. Proc. R. Soc. Lond. 225, 49–63.

Bagnold, R.A., 1956. The flow of cohesionless grains in fluids. Proc. R. Soc. Lond. 249, 235–296.

Bagnold, R.A., 1966. An approach to the sediment transport problem from general physics. Professional paper 422-I. United States Geological Survey.

Bagnold, R.A., 1973. The nature of saltation and of 'bed load' transport in water. Proc. R. Soc. London Ser. A 332, 473–504.

Bagnold, R.A., 1977. Bed load transport by natural rivers. Water Resour. Res. 13, 303–312.

Bagnold, R.A., 1980. An empirical correlation of bedload transport rates in flumes and natural rivers. Proc. R. Soc. London Ser. A 372, 453–473.

Bagnold, R.A., 1986. Transport of solids by natural water flow: evidence for a worldwide correlation. Proc. R. Soc. London Ser. A 405, 369–374.

Bagnold, R.A., 1990. Sand, Wind, and War: Memoirs of a Desert Explorer. The University of Arizona Press, Tucson.

Bak, P., 1996. How Nature Works. Oxford University Press, Oxford.

Barenblatt, G.I., 2003. Scaling. Cambridge University Press, Cambridge.

Barry, J.J., Buffington, J.M., King, J.G., 2004. A general power equation for predicting bed load transport rates in gravel bed rivers. Water Resour. Res. 40, W10401.

Barry, J.J., Buffington, J.M., Goodwin, P., King, J.G., Emmett, W.W., 2008. Performance of bed-load transport equations relative to geomorphic significance: predicting effective discharge and its transport rate. J. Hydraul. Eng. 134, 601–615.

Batchelor, G.K., 1970. The stress system in a suspension of free-force particles. J. Fluid Mech. 41, 545–570.

Batchelor, G.K., 1989. A brief guide to two-phase flow. In: Germain, P., Piau, J.M., Caillerie, D. (Eds.), Theoretical and Applied Mechanics. Elsevier Science Publishers, North-Holland, pp. 27–41.

Benavides, S.J., Deal, E., Rushlow, M., Venditti, J.G., Zhang, Q., Kamrin, K., Perron, J.T., 2022. The impact of intermittency on bed load sediment transport. Geophys. Res. Lett. 49 e2021GL096088.

Berzi, D., 2011. Analytical solution of collisional sheet flows. J. Hydraul. Eng. 137, 1200–1207.

Berzi, D., 2013. Transport formula for collisional sheet flows with turbulent suspension. J. Hydraul. Eng. 139, 359–363.

Berzi, D., Fraccarollo, L., 2013. Inclined, collisional sediment transport. Phys. Fluids 25, 106601.

Berzi, D., Fraccarollo, L., 2016. Intense sediment transport: collisional to turbulent suspension. Phys. Fluids 28, 023302.

Berzi, D., Jenkins, J.T., 2008. A theoretical analysis of free-surface flows of granular-liquid mixtures. J. Fluid Mech. 608, 393–410.

Blondeaux, P., Colombini, M., Seminara, G., Vittori, G., 2018. Introduction to Morphodynamics of Sedimentary Patterns. Genova University Press, Genova, Italia.

Bouchut, F., Fernández-Nieto, E.D., Mangeney, A., Narbona-Reina, G., 2016. A two-phase two-layer model for fluidized granular flows with dilatancy effects. J. Fluid Mech. 801, 166–221.

Boyer, F., Guazzelli, E., Pouliquen, O., 2011. Unifying suspension and granular rheology. Phys. Rev. Lett. 107, 188301.

Buffington, J.M., Montgomery, D.R., 1997. A systematic analysis of eight decades of incipient motion studies, with special reference to gravel-bedded rivers. Water Resour. Res. 33, 1993–2029.

Bunte, K., Abt, S., 2005. Effect of sampling time on measured gravel bed load transport rates in a coarse-bedded stream. Water Resour. Res. 41, W11405.

Bunte, K., Abt, S.R., Potyondy, J.P., Swingle, K.W., 2008. A comparison of coarse bedload transport measured with bedload traps and Helley-Smith samplers. Geodin. Acta 21, 53–66.

Camenen, B., Bayram, A., Larson, M., 2006. Equivalent roughness height for plane bed under steady flow. J. Hydraul. Eng. 132, 1146–1158.

Campagnol, J., Radice, A., Ballio, F., Nikora, V., 2015. Particle motion and diffusion at weak bed load: accounting for unsteadiness effects of entrainment and disentrainment. J. Hydraul. Res. 63, 633–648.

Campbell, C.S., 1990. Rapid granular flows. Annu. Rev. Fluid Mech. 22, 57–92.

Cao, H.H., 1985. Résistance hydraulique d'un lit de gravier mobile à pente raide. Ph.D. thesis. Ecole Polytechnique Fédérale de Lausanne.

Capart, H., Fraccarollo, L., 2011. Transport layer structure in intense bed-load. Geophys. Res. Lett. 38, L20402.

Carbonari, C., Recking, A., Solari, L., 2020. Morphology, bedload and sorting process variability in response to lateral confinement: results from physical models of gravel-bed rivers. J. Geophys. Res. Earth Surf. 125 e2020JF005773.

Cartigny, M.J.B., Ventra, D., Postma, G., Den Berg, J.H., 2014. Morphodynamics and sedimentary structures of bedforms under supercritical-flow conditions: new insights from flume experiments. Sedimentology 61, 712–748.

Cassar, C., Nicolas, M., Pouliquen, O., 2005. Submarine granular flows down inclined planes. Phys. Fluids 17, 103301.

Cassel, M., Lavé, J., Recking, A., Malavoi, J.R., Piégay, H., 2021. Bedload transport in rivers, size matters but so does shape. Sci. Rep. 11, 1–11.

Celik, I., Rodi, W., 1991. Suspended sediment-transport capacity for open channel flow. J. Hydraul. Eng. 117, 191–204.

Charru, F., Mouilleron, H., Eiff, O., 2004. Erosion and deposition of particles on a bed sheared by a viscous flow. J. Fluid Mech. 519, 55–80.
Charru, F., Andreotti, B., Claudin, P., 2013. Sand ripples and dunes. Annu. Rev. Fluid Mech. 45, 469–493.
Chauchat, J., 2018. A comprehensive two-phase flow model for unidirectional sheet-flows. J. Hydraul. Res. 56, 15–28.
Chen, A., Darbon, J., Morel, J.M., 2014. Landscape evolution models: a review of their fundamental equations. Geomorphology 219, 68–86.
Cheng, N.S., 2002. Exponential formula for bedload transport. J. Hydraul. Eng. 128, 942–946.
Cheng, N.S., Chiew, Y.M., 1999. Analysis of initiation of sediment suspension from bed load. J. Hydraul. Eng. 125, 855–861.
Cheng, Z., Hsu, T.J., Chauchat, J., 2018. An Eulerian two-phase model for steady sheet flow using large-eddy simulation methodology. Adv. Water Resour. 111, 205–223.
Childers, D., 1999. Field comparisons of six pressure-difference bedload samplers in high-energy flow. Technical Report 92-4068. US Department of the Interior, US Geological Survey.
Chiodi, F., Claudin, P., Andreotti, B., 2014. A two-phase flow model of sediment transport: transition from bedload to suspended load. J. Fluid Mech. 755, 561–581.
Church, M., Ferguson, R.I., 2015. Morphodynamics: rivers beyond steady state. Water Resour. Res. 51, 1883–1897.
Cohen, H., Laronne, J.B., Reid, I., 2010. Simplicity and complexity of bed load response during flash floods in a gravel bed ephemeral river: a 10 year field study. Water Resour. Res. 46, W11542.
Coleman, S.E., Melville, B.W., 1994. Bed-form development. J. Hydraul. Eng. 120, 544–560.
Colosimo, C., Copertino, V.A., Veltri, M., 1988. Friction factor evaluation in gravel-bed rivers. J. Hydraul. Eng. 114, 861–876.
Comiti, F., Mao, L., 2012. Recent advances in the dynamics of steep channels. In: Church, M., Biron, M.P., Roy, A.G. (Eds.), Gravel-Bed Rivers: Processes, Tools, Environments. John Wiley & Sons, Chichester, pp. 351–377.
Comiti, F., Da Canal, M., Surian, N., Mao, L., Picco, L., Lenzi, M.A., 2011. Channel adjustments and vegetation cover dynamics in a large gravel bed river over the last 200 years. Geomorphology 125, 147–159.
Cook, H.L., 1935. Outline of the energetics of stream-transportation of solids. Trans. Am. Geophys. Union 16, 456–463.
Coulthard, T.J., Van De Wiel, M.J., 2012. Modelling river history and evolution. Phil. Trans. R. Soc. A 370, 2123–2142.
Courrech du Pont, S., Gondret, P., Perrin, B., Rabaud, M., 2003. Granular avalanches in fluids. Phys. Rev. Lett. 90, 044301.
Cunge, J.A., Holly, F.M., Verwey, A., 1980. Practical Aspects of Computational River Hydraulics. Pitman publishing, Boston.
da Silva, A.M.A.F., Bolisetti, T., 2000. A method for the formulation of Reynolds number functions. Can. J. Civ. Eng. 27, 829–833.
Dade, W.B., Friend, P.F., 1998. Grain-size, sediment-transport regime, and channel slope in alluvial rivers. J. Geol. 106, 661–676.
Davies, T.R.H., Sutherland, A.J., 1983. Extremal hypotheses for river behavior. Water Resour. Res. 19, 141–148.
Davis, R.O., Sevladurai, A.P.S., 2002. Plasticity and Geomechanics. Cambridge University Press, Cambridge.
Davy, B.W., Davies, T.R.H., 1979. Entropy concepts in fluvial geomorphology: a reevaluation. Water Resour. Res. 15, 103–106.
de Lange, S.I., Naqshband, S., Hoitink, A.J.F., 2021. Quantifying hydraulic roughness from field data: can dune morphology tell the whole story? Water Resour. Res. 57 e2021WR030329.
Deal, E., 2022. Flow resistance in very rough channels. Water Resour. Res. 58 e2021WR031790.
Deal, E., Venditti, J.G., Benavides, S.J., Bradley, R., Zhang, Q., Kamrin, K., Perron, J.T., 2023. Grain shape effects in bed load sediment transport. Nature 613, 298–302.
Dean, D.J., Topping, D.J., Schmidt, J.C., Griffiths, R.E., Sabol, T.A., 2015. Sediment supply versus local hydraulic controls on sediment transport and storage in a river with large sediment loads. J. Geophys. Res. Earth Surf. 121.
Delannay, R., Valance, A., Mangeney, A., Roche, O., Richard, P., 2017. Granular and particle-laden flows: from laboratory experiments to field observations. J. Phys. D. Appl. Phys. 50, 053001.
Dey, S., 2014. Fluvial Hydrodynamics: Hydrodynamic and Sediment Transport Phenomena. Springer, Berlin.
Dey, S., Ali, S.K., 2019. Bed sediment entrainment by streamflow: state of the science. Sedimentology 66, 1449–1485.
Dey, S., Ali, S.Z., Padhi, E., 2018. Advances in analytical modeling of suspended sediment transport. J. Hydro-Env. Res. 20, 110–126.
Dhont, B., Ancey, C., 2018. Are bedload transport pulses in gravel-bed rivers created by bar migration or sediment waves? Geophys. Res. Lett. 45, 5501–5508.
Dietrich, W.E., 1982. Settling velocity of natural particles. Water Resour. Res. 18, 1615–1626.
Dietrich, W.E., Kirchner, J.W., Ikeda, H., Iseya, F., 1989. Sediment supply and the development of the coarse surface layer in gravel-bedded rivers. Nature 340, 215–217.
Diplas, P., 1987. Bedload transport in gravel-bed streams. J. Hydraul. Eng. 113, 277–292.
Diplas, P., Dancey, C.L., Celik, A., Valyrakis, M., Greer, K., Akar, T., 2008. The role of impulse on the initiation of particle movement under turbulent flow conditions. Science 322, 717–720.
Dodds, P.S., Rothman, D.H., 2000. Scaling, universality, and geomorphology. Annu. Rev. Earth Planet. Sci. 28, 571–610.
Donat, J., 1929. Über Sohlangriff and Geschiebetrieb. Deutsche Wasserwirtschaft 26, 451–455.
du Boys, P., 1879. Le Rhône et les rivières à lit affouillable – Étude du régime du Rhône et de l'action exercée par les eaux sur un lit à fond de graviers indéfiniment affouillable. Annales des Ponts et Chaussées 49, 141–195.
Dudill, A., de Micheaux, H.L., Frey, P., Church, M., 2018. Introducing finer grains into bedload: the transition to a new equilibrium. J. Geophys. Res. Earth Surf. 123, 2602–2619.
Dudill, A., Venditti, J.G., Church, M., Frey, P., 2020. Comparing the behaviour of spherical beads and natural grains in bedload mixtures. Earth Surf. Process. Landf. 45, 831–840.
Durán, O., Andreotti, B., Claudin, P., 2014. Turbulent and viscous sediment transport—a numerical study. Adv. Geosci. 37, 73–80.
East, A.E., Logan, J.B., Mastin, M.C., Ritchie, A.C., Bountry, J.A., Magirl, C.S., Sankey, J. B., 2018. Geomorphic evolution of a gravel-bed river under sediment-starved vs. sediment-rich conditions: River response to the world's largest dam removal. J. Geophys. Res. Earth Surf. 123, 3338–3369.
Eaton, B.C., Church, M., 2011. A rational sediment transport scaling relation based on dimensionless stream power. Earth Surf. Process. Landf. 36, 901–910.
Einstein, H.A., 1937. Der Geschiebetrieb als Wahrscheinlichkeitproblem (Bedload transport as a probability problem). (english translation by W. W. Sayre). In: Sedimentation (Symposium to honor H. A. Einstein), edited by H. W. Shen, Fort Collins, Colorado, 1972, C1–C105. ETHZ.
Einstein, H.A., 1942. Formulas for the transportation of bed load. Trans. Am. Soc. Civ. Eng. 107, 561–597.
Einstein, H.A., 1950. The bed-load function for sediment transportation in open channel flows. Technical Report Technical Report No. 1026. United States Department of Agriculture.
Emmett, W.W., Wolman, M.G., 2001. Effective discharge and gravel-bed rivers. Earth Surf. Process. Landf. 26, 1369–1380.
Engelund, F., 1966. Hydraulic resistance of alluvial streams. J. Hydraul. Div. ASCE HY2 315–326.
Engelund, F., Hansen, E., 1967. A monograph on sediment transport in alluvial streams. Technical Report. Technical University of Denmark.
Ferdowsi, B., Ortiz, C.P., Houssais, M., Jerolmack, D.J., 2017. River-bed armouring as a granular segregation phenomenon. Nat. Commun. 8, 1–10.
Ferguson, R., 1986. Hydraulics and hydraulic geometry. Prog. Phys. Geogr. 10, 1–31.
Ferguson, R.I., 2005. Estimating critical stream power for bedload transport calculations in gravel-bed rivers. Geomorphology 70, 33–41.
Ferguson, R.I., 2007. Flow resistance equations for gravel- and boulder-bed streams. Water Resour. Res. 43, W05427.
Ferguson, R.I., 2012. River channel slope, flow resistance, and gravel entrainment thresholds. Water Resour. Res. 48, W05517.
Forchheimer, P., 1914. Hydraulik. Druck und Verlag von B. G. Teubner, Leipzig.
Forterre, Y., Pouliquen, O., 2008. Flows of dense granular media. Annu. Rev. Fluid Mech. 40, 1–24.
Frey, P., Church, M., 2009. How river beds move. Science 325, 1509–1510.
Furbish, D.J., Haff, P.K., Roseberry, J.C., Schmeeckle, M.W., 2012. A probabilistic description of the bed load sediment flux: 1. Theory. J. Geophys. Res. 117, F03031.
Furbish, D.J., Fathel, S.L., Schmeeckle, M.W., Jerolmack, D.J., Schumer, R., 2017. The elements and richness of particle diffusion during sediment transport at small timescales. Earth Surf. Process. Landf. 42, 214–237.
Gaeuman, D., Holt, C.R., Bunte, K., 2015. Maximum likelihood parameter estimation for fitting bedload rating curves. Water Resour. Res. 51, 281–301.
Gao, P., 2008. Transition between two bed-load transport regimes: Saltation and sheet flow. J. Hydraul. Eng. 134, 340–349.
Gao, P., 2012. Validation and implications of an energy-based bedload transport equation. Sedimentology 59, 1926–1935.
García, M.H., 2007. Sediment transport and morphodynamics. In: García, M.H. (Ed.), Sedimentation Engineering. American Society of Civil Engineers, Reston. volume ASCE Manuals and Reports on Engineering Practice 110, pp. 21–164.
Garcia Lugo, G.A., Bertoldi, W., Henshaw, A.J., Gurnell, A.M., 2015. The effect of lateral confinement on gravel bed river morphology. Water Resour. Res. 51, 7145–7158.
GdR-MiDi, 2004. On dense granular flows. Eur. Phys. J. E 14, 341–365.
Gilbert, G.K., 1914. The transportation of débris by running water. Technical Report. U. S. Geological Survey Professional Paper vol. 86.
Gleason, C.J., 2015. Hydraulic geometry of natural rivers: a review and future directions. Prog. Phys. Geogr. 39, 337–360.
Goldhirsch, I., 1999. Scales and kinetics of granular flows. Chaos 9, 659–672.
Gomez, B., 1983. Temporal variations in bedload transport rates: the effect of progressive bed armouring. Earth Surf. Process. Landf. 8, 41–54.
Gomez, B., 1991. Bedload transport. Earth-Sci. Rev. 31, 89–132.
Gomez, B., 2006. The potential rate of bed-load transport. Proc. Natl. Acad. Sci. U. S. A. 103, 17170–17173.
Gomez, B., 2022. The efficiency of the river machine. Geomorphology 410, 108271.
Gomez, B., Church, M., 1989. An assessment of bed load sediment transport formulae for gravel bed rivers. Water Resour. Res. 25, 1161–1186.
Gomez, B., Soar, P.J., 2022. Bedload transport: beyond intractability. R. Soc. Open Sci. 9, 211932.
Gomez, B., Naff, R.L., Hubbell, D.W., 1989. Temporal variations in bedload transport rates associated with the migration of bedforms. Earth Surf. Process. Landf. 14, 135–156.
Gomez, B., Soar, P.J., Downs, P.W., 2022. Good vibrations: big data impact bedload research. Earth Surf. Process. Landf. 47, 129–142.
Gonzalez-Ondina, J.M., Fraccarollo, L., Liu, P.L.F., 2018. Two-level, two-phase model for intense, turbulent sediment transport. J. Fluid Mech. 839, 198–238.
Graf, W.H., Pazis, G.C., 1977. Deposition and erosion in an alluvial channel. J. Hydraul. Res. 15, 151–166.

Graf, W.H., Suszka, L., 1987. Sediment transport in steep channels. J. Hydrosci. Hydraul. Eng. 5, 11–26.
Gray, W.G., Ghidaoui, M.S., 2009. Thermodynamic analysis of stream flow hydrodynamics. J. Hydraul. Res. 47, 403–417.
Gray, J.R., Laronne, J.B., Marr, J.D.G., 2010. Bedload-surrogate monitoring technologies. Technical Report 1411328485. US Department of the Interior, US Geological Survey.
Gray, W.G., Ghidaoui, M.S., Karney, B.W., 2018. Does the stream power theory have a physical foundation? J. Hydraul. Res. 56, 585–595.
Gregoretti, C., 2000. The initiation of debris flow at high slopes: experimental results. J. Hydraul. Res. 38, 83–88.
Griffiths, G.A., 1984. Extremal hypotheses for river regime: an illusion of progress. Water Resour. Res. 20, 113–118.
Guala, M., Singh, A., BadHeartBull, N., Foufoula-Georgiou, E., 2014. Spectral description of migrating bed forms and sediment transport. J. Geophys. Res. Earth Surf. 119, 123–137.
Guazzelli, E., Pouliquen, O., 2018. Rheology of dense granular suspensions. J. Fluid Mech. 852, P1.
Guo, J., 2002. Logarithmic matching and its applications in computational hydraulics and sediment transport. J. Hydraul. Res. 40, 555–565.
Guo, J., 2021. Generalized bed-load function based on empirical data. J. Hydraul. Eng. 147, 06021008.
Haff, P.K., 1983. Grain flow as a fluid-mechanical phenomenon. J. Fluid Mech. 134, 401–430.
Hallworth, M.A., Huppert, H.E., 1998. Abrupt transitions in high-concentrations, particle-driven gravity currents. Phys. Fluids 10, 1083–1087.
Hanes, D.M., Inman, D.L., 1985. Observations of rapidly flowing granular-fluid materials. J. Fluid Mech. 150, 357–380.
Hassan, M.A., Egozi, R., Parker, G., 2006. Experiments on the effect of hydrograph characteristics on vertical grain sorting in gravel bed rivers. Water Resour. Res. 42, 2005W09408.
Hassan, M.A., Smith, B.J., Hogan, D.L., Luzi, D.S., Zimmermann, A.E., Eaton, B.C., 2008. Sediment storage and transport in coarse bed streams: scale considerations. In: Habersack, H., Piégay, H., Rinaldi, M. (Eds.), Gravel-Bed Rivers VI: From Process Understanding to River Restoration, vol. 11. Elsevier, Amsterdam, pp. 473–496.
Hassan, M.A., Saletti, M., Johnson, J.P.L., Ferrer-Boix, C., Venditti, J.G., Church, M., 2020. Experimental insights into the threshold of motion in alluvial channels: sediment supply and streambed state. J. Geophys. Res. Earth Surf. 125 e2020JF005736.
Herbertson, J.G., 1969. A critical review of conventional bed load formulae. J. Hydrol. 8, 1–26.
Hey, R.D., 1979. Flow resistance in gravel-bed rivers. J. Hydraul. Div. ASCE 105, 365–379.
Heyman, J., Mettra, F., Ma, H.B., Ancey, C., 2013. Statistics of bedload transport over steep slopes: separation of time scales and collective motion. Geophys. Res. Lett. 40, 128–133.
Hinton, D., Hotchkiss, R.H., Cope, M., 2018. Comparison of calibrated empirical and semi-empirical methods for bedload transport rate prediction in gravel bed streams. J. Hydraul. Eng. 144, 04018038.
Hoey, T.B., 1992. Temporal variations in bedload transport rates and sediment storage in gravel-bed rivers. Prog. Phys. Geogr. 16, 319–338.
Hohermuth, B., Weitbrecht, V., 2018. Influence of bed-load transport on flow resistance of step-pool channels. Water Resour. Res. 54, 5567–5583.
Hsu, T.J., Jenkins, J.T., Liu, P.L.F., 2004. On two-phase sediment transport: sheet flows of massive particles. Proc. R. Soc. London Ser. A 460, 2223–2250.
Huang, H.Q., 2010. Reformulation of the bed load equation of Meyer-Peter and Müller in light of the linearity theory for alluvial channel flow. Water Resour. Res. 46, W09533.
Huang, H.Q., Chang, H.H., 2006. Scale independent linear behavior of alluvial channel flow. J. Hydraul. Eng. 132, 722–730.
Huang, H.Q., Nanson, G.C., 2000. Hydraulic geometry and maximum flow efficiency as products of the principle of least action. Earth Surf. Process. Landf. 25, 1–16.
Hunt, B., 1984. Dam-break solution. J. Hydraul. Eng. 110, 675–686.
Hunt, M.L., Zenit, R., Campbell, C.S., Brennen, C.E., 2002. Revisiting the 1954 suspension experiments of R. A. Bagnold. J. Fluid Mech. 452, 1–24.
Ikeda, H., 1983. Experiments on bedload transport, bed forms and sedimentary structures using fine gravel in the 4-metre wide flume. Technical Report Paper 2. Environmental Research Center. Tsukuba University.
Iseya, F., Ikeda, H., 1987. Pulsations in bedload transport rates induced by a longitudinal sediment sorting: A flume study using sand and gravel mixtures. Geogr. Annal. Ser. A 15–27.
Iverson, R.M., 1997. The physics of debris flows. Rev. Geophys. 35, 245–296.
Iverson, R.M., George, D.L., 2014. A depth-averaged debris-flow model that includes the effects of evolving dilatancy. I. Physical basis. Proc. R. Soc. London Ser. A 470, 20130819.
Jäggi, M., 1984. Der Geschiebetransport in Flüssen nach der VAW-Formel 1983. SIA 102, 940–943.
Jenkins, J.T., Hanes, H.M., 1998. Collisional sheet flows of sediment driven by a turbulent fluid. J. Fluid Mech. 370, 29–52.
Jop, P., Pouliquen, O., Forterre, Y., 2006. A constitutive law for dense granular flows. Nature 441, 727–730.
Joshi, I., Dai, W., Bilal, A., Upreti, A.R., He, Z., 2018. Evaluation and comparison of extremal hypothesis-based regime methods. Water 10, 271.
Julien, P.Y., Raslan, Y., 1998. Upper-regime plane bed. J. Hydraul. Eng. 124, 1086–1096.
Kaczmarek, L.M., Biegowski, J., Sobczak, A., 2019. Modeling of sediment transport in steady flow over mobile granular bed. J. Hydraul. Eng. 145, 04019009.
Kalinske, A.A., 1947. Movement of sediment as bed-load in rivers. Trans. Am. Geophys. Union 28, 615–662.
Kamphuis, J.W., 1974. Determination of sand roughness for fixed beds. J. Hydraul. Res. 12, 193–203.
Keller, J.B., Rubenfeld, L.A., Molyneux, J.E., 1967. Extremum principles for slow viscous flows with applications to suspensions. J. Fluid Mech. 30, 97–125.
Kennedy, J.F., 1969. The formation of sediment ripples, dunes, and antidunes. Annu. Rev. Fluid Mech. 1, 147–168.
Keulegan, G.H., 1938. Laws of turbulent flows in open channels. J. Res. Natl. Bur. Stand. 21, 707–741.
Koenker, R., Chernozhukov, V., He, X., Peng, L., 2017. Handbook of Quantile Regression. CRC Press, Boca Raton.
Kuhnle, R.A., Southard, J.B., 1988. Bed load transport fluctuations in a gravel bed laboratory channel. Water Resour. Res. 24, 247–260.
Lacey, G., 1930. Stable channels in alluvium. Min. Proc. I. Civil. Eng. 229, 259–292.
Lajeunesse, E., Malverti, L., Charru, F., 2010. Bed load transport in turbulent flow at the grain scale: Experiments and modeling. J. Geophys. Res. 115, F04001.
Lamb, M.P., Dietrich, W.E., Venditti, J.G., 2008. Is the critical Shields stress for incipient sediment motion dependent on channel-bed slope? J. Geophys. Res. 113, F02008.
Lamb, M.P., Brun, F., Fuller, B.M., 2017. Hydrodynamics of steep streams with planar coarse-grained beds: turbulence, flow resistance, and implications for sediment transport. Water Resour. Res. 53, 2240–2263.
Lammers, R.W., Bledsoe, B.P., 2018. Parsimonious sediment transport equations based on Bagnold's stream power approach. Earth Surf. Process. Landf. 43, 242–258.
Lanzoni, S., Gregoretti, C., Stancanelli, L.M., 2017. Coarse-grained debris flow dynamics on erodible beds. J. Geophys. Res. Earth Surf. 122, 592–614.
Lavelle, J.W., Mofjeld, H.O., 1987. Do critical stresses for incipient motion and erosion really exist? J. Hydraul. Eng. 113, 370–385.
Lee, C.H., Low, Y.M., Chiew, Y.M., 2016. Multi-dimensional rheology-based two-phase model for sediment transport and applications to sheet flow and pipeline scour. Phys. Fluids 28, 053305.
Lee, J., Singh, A., Guala, M., 2023. On the scaling and growth limit of fluvial dunes. J. Geophys. Res. Earth Surf. 128 e2022JF006955.
Leopold, L.B., Langbein, W.B., 1962. The concept of entropy in landscape evolution. Technical Report. United States Geological Survey.
Leopold, L.B., Maddock, T., 1953. The Hydraulic Geometry of Stream Channels and Some Physiographic Implications. Technical Report. US Geological Survey.
Li, C., Czapiga, M.J., Eke, E.C., Viparelli, E., Parker, G., 2015. Variable Shields number model for river bankfull geometry: bankfull shear velocity is viscosity-dependent but grain size-independent. J. Hydraul. Res. 53, 36–48.
Lisle, T.E., 1995. Particle size variations between bed load and bed material in natural gravel bed channels. Water Resour. Res. 31, 1107–1118.
Lisle, T.E., Church, M., 2002. Sediment transport-storage relations for degrading, gravel bed channels. Water Resour. Res. 38, 1219.
Longo, S., 2005. Two-phase flow modeling of sediment motion in sheet-flows above plane beds. J. Hydraul. Eng. 131, 366–379.
López, R., Barragán, J., 2008. Equivalent roughness of gravel-bed rivers. J. Hydraul. Eng. 134, 847–851.
Ma, H., Nittrouer, J.A., Wu, B., Lamb, M.P., Zhang, Y., Mohrig, D., Fu, X., Naito, K., Wang, Y., Moodie, A.J., 2020. Universal relation with regime transition for sediment transport in fine-grained rivers. Proc. Natl. Acad. Sci. U. S. A. 117, 171–176.
MacDougall, C.H., 1933. Bed-Sediment transportation in open channels. Trans. Am. Geophys. Union 14, 491–495.
Manes, C., Pokrajac, D., McEwan, I., 2007. Double-averaged open-channel flows with small relative submergence. J. Hydraul. Eng. 133, 896–904.
Mao, L., 2012. The effect of hydrographs on bed load transport and bed sediment spatial arrangement. J. Geophys. Res. 117, F03024.
Mao, L., 2018. The effects of flood history on sediment transport in gravel-bed rivers. Geomorphology 322, 196–205.
Mao, L., Surian, N., 2010. Observations on sediment mobility in a large gravel-bed river. Geomorphology 114, 326–337.
Mao, L., Uyttendaele, G.P., Iroumé, A., Lenzi, M.A., 2008. Field based analysis of sediment entrainment in two high gradient streams located in Alpine and Andine environments. Geomorphology 93, 368–383.
Martin, Y., Church, M., 2000. Re-examination of Bagnold's empirical bedload formulae. Earth Surf. Process. Landf. 25, 1011–1024.
Masteller, C.C., Finnegan, N.J., Turowski, J.M., Yager, E.M., Rickenmann, D., 2019. History-dependent threshold for motion revealed by continuous bedload transport measurements in a steep mountain stream. Geophys. Res. Lett. 46, 2018GL081325.
Matoušek, V., 2009. Concentration profiles and solids transport above stationary deposit in enclosed conduit. J. Hydraul. Eng. 135, 1101–1106.
Matoušek, V., Zrostlík, V., 2020. Collisional transport model for intense bed load. J. Hydrol. Hydromech. 68, 60–69.
Matoušek, V., Krupička, J., Picek, T., 2013. Validation of transport and friction formulae for upper plane bed by experiments in rectangular pipe. J. Hydrol. Hydromech. 61, 120–125.
Matoušek, V., Bareš, V., Krupička, J., Picek, T., Zrostlík, V., 2016. Experimental evaluation of bed friction and solids transport in steep flume. Can. J. Chem. Eng. 94, 1076–1083.
Maurin, R., Chauchat, J., Frey, P., 2016. Dense granular flow rheology in turbulent bedload transport. J. Fluid Mech. 804, 490–512.
Maurin, R., Chauchat, J., Frey, P., 2018. Revisiting slope influence in turbulent bedload transport: consequences for vertical flow structure and transport rate scaling. J. Fluid Mech. 839, 135–156.
Métivier, F., Lajeunesse, E., Devauchelle, O., 2017. Laboratory rivers: Lacey's law, threshold theory, and channel stability. Earth Surf. Dyn 5, 187–198.

Meyer-Peter, E., Müller, R., 1948. Formulas for bed load transport. IAHR (Ed.), 2nd meeting, Stockholm, Sweden, pp. 39–64.
Meyer-Peter, E., Favre, H., Einstein, H.A., 1934. Neure Versuchsresultate über den Geschiebetrieb. Schweizerische Bauzeitung 113, 147–150.
Millar, R.G., 1999. Grain and form resistance in gravel-bed rivers. J. Hydraul. Res. 37, 303–312.
Millar, R.G., 2005. Theoretical regime equations for mobile gravel-bed rivers with stable banks. Geomorphology 64, 207–220.
Molinas, A., Wu, B., 2001. Transport of sediment in large sand-bed rivers. J. Hydraul. Res. 39, 135–146.
Molnár, P., Ramirez, J.A., 1998. Energy dissipation theories and optimal channel characteristics of river networks. Water Resour. Res. 34, 1809–1818.
Monsalve, A., Segura, C., Hucke, N., Katz, S., 2020. A bed load transport equation based on the spatial distribution of shear stress—Oak Creek revisited. Earth Surf. Dyn 8, 825–839.
Montgomery, D.R., Buffington, J.M., 1997. Channel-reach morphology in mountain drainage basins. Geol. Soc. Am. Bull. 109, 596–611.
Mueller, E.R., Pitlick, J., Nelson, J.M., 2005. Variation in the reference Shields stress for bed load transport in gravel-bed streams and rivers. Water Resour. Res. 41, W04006.
Nanson, G.C., Huang, H.Q., 2008. Least action principle, equilibrium states, iterative adjustment and the stability of alluvial channels. Earth Surf. Process. Landf. 33, 923–942.
Nanson, G.C., Huang, H.Q., 2018. A philosophy of rivers: equilibrium states, channel evolution, teleomatic change and least action principle. Geomorphology 302, 3–19.
Nelson, P.A., Brew, A.K., Morgan, J.A., 2015. Morphodynamic response of a variable-width channel to changes in sediment supply. Water Resour. Res. 51, 5717–5734.
Nicholas, A.P., Ashworth, P.J., Kirkby, M.J., Macklin, M.G., Murray, T., 1995. Sediment slugs: large-scale fluctuations in fluvial sediment transport rates and storage volumes. Prog. Phys. Geogr. 19, 500–519.
Nicollier, T., Antoniazza, G., Ammann, L., Rickenmann, D., Kirchner, J.W., 2022. Toward a general calibration of the Swiss plate geophone system for fractional bedload transport. Earth Surf. Dyn 10, 929–951.
Nikora, V., 1984. The structure of turbulent flow and statistical characterisation of dune-covered river beds (with examples of field studies in rivers Turunchuk, Rioni, and Tsheniscali). Ph.D. thesis.
Nikora, V., Goring, D.G., McEwan, I., Griffiths, G., 2001. Spatially averaged open-channel flow over rough bed. J. Hydraul. Eng. 127, 123.
Nikora, V., Koll, K., McEwan, I., McLean, S., Dittrich, A., 2004. Velocity distribution in the roughness layer of rough-bed flows. J. Hydraul. Eng. 130, 1036–1042.
Nikora, V., McLean, S., Coleman, S., Pokrajac, D., McEwan, I., Campbell, L., Aberle, J., Clunie, D., Koll, K., 2007. Double-averaging concept for rough-bed open-channel and overland flows: Applications. J. Hydraul. Eng. 133, 873–883.
Nikora, V.I., Stoesser, T., Cameron, S.M., Stewart, M.T., Papadopoulos, K., Ouro, P., McSherry, R., Zampiron, A., Marusic, I., Falconer, R.A., 2019. Friction factor decomposition for rough-wall flows: theoretical background and application to open-channel flows. J. Fluid Mech. 872, 626–664.
Nnadi, F.N., Wilson, K.C., 1992. Motion of contact-load particles at high shear stress. J. Hydraul. Eng. 118, 1670–1684.
Nnadi, F.N., Wilson, K.C., 1995. Bed-load motion at high shear stress: dune washout and plane-bed flow. J. Hydraul. Eng. 121, 267–273.
Omid, M.H., Karbasi, M., Farhoudi, J., 2010. Effects of bed-load movement on flow resistance over bed forms. Sadhana 35, 681–691.
Pähtz, T., Durán, O., 2020. Unification of aeolian and fluvial sediment transport rate from granular physics. Phys. Rev. Lett. 124, 168001.
Pähtz, T., Clark, A.H., Valyrakis, M., Durán, O., 2020. The physics of sediment transport initiation, cessation, and entrainment across aeolian ansd fluvial environments. Rev. Geophys. 58 e2019RG000679.
Pailha, M., Pouliquen, O., 2009. A two-phase flow description of the initiation of underwater granular avalanches. J. Fluid Mech. 633, 115–135.
Paintal, A.S., 1971. Concept of critical shear stress in loose boundary open channel flows. J. Hydraul. Res. 9, 92–113.
Papangelakis, E., Hassan, M.A., 2016. The role of channel morphology on the mobility and dispersion of bed sediment in a small gravel-bed stream. Earth Surf. Process. Landf. 41, 2191–2206.
Parker, G., 1977. Discussion of "Minimum unit stream power and fluvial hydraulics". J. Hydraul. Div. ASCE 103, 811–816.
Parker, G., 1991. Selective sorting and abrasion of river gravel: I. Theory. J. Hydraul. Eng. 117, 131–149.
Parker, G., Klingeman, P.C., 1982. On why gravel bed streams are paved. Water Resour. Res. 18, 1409–1423.
Parker, G., Toro-Escobar, C.M., 2002. Equal mobility of gravel bed in streams: the remains of the day. Water Resour. Res. 38, 1264.
Parker, G., Klingeman, P.C., McLean, D.G., 1982. Bedload and size distribution in paved gravel-bed streams. J. Hydraul. Div. ASCE 108, 544–571.
Parker, C., Clifford, N.J., Thorne, C.R., 2011. Understanding the influence of slope on the threshold of coarse grain motion: revisiting critical stream power. Geomorphology 126, 51–65.
Pascal, I., Bohorquez, P., Ancey, C., 2021. The variability of antidune morphodynamics on steep slopes. Earth Surf. Process. Landf. 46, 1750–1765.
Pazis, G., 1976. Faible transport des sédiments par érosion et déposition dans les canaux alluvionnaires. Ph.D. thesis. École Polytechnique Fédérale de Lausanne.
Petit, F., Gob, F., Houbrechts, G., Assani, A.A., 2005. Critical specific stream power in gravel-bed rivers. Geomorphology 69, 92–101.
Phillips, C., Masteller, C.C., Slater, L.J., Dunne, K.B.J., Francalanci, S., Lanzoni, S., Merritts, D.J., Lajeunesse, E., Jerolmack, D.J., 2022. Threshold constraints on the size, shape and stability of alluvial rivers. Nat. Rev. Earth Environ. 3, 406–419.
Pitlick, J., 1992. Flow resistance under conditions of intense gravel transport. Water Resour. Res. 28, 891–903.
Pitlick, J., Mueller, E.R., Segura, C., Cress, R., Torizzo, M., 2008. Relation between flow, surface-layer armoring and sediment transport in gravel-bed rivers. Earth Surf. Process. Landf. 33, 1192–1209.
Piton, G., Recking, A., 2017. The concept of travelling bedload and its consequences for bedload computation in mountain streams. Earth Surf. Process. Landf. 42, 1505–1519.
Powell, D.M., 1998. Patterns and processes of sediment sorting in gravel-bed rivers. Prog. Phys. Geogr. 22, 1–32.
Powell, D.M., 2014. Flow resistance in gravel-bed rivers: progress in research. Earth-Sci. Rev. 136, 301–338.
Powell, D.M., Reid, I., Laronne, J.B., 1999. Hydraulic interpretation of cross-stream variations in bed-load transport. J. Hydraul. Eng. 125, 1243–1252.
Prancevic, J.P., Lamb, M.P., 2015. Unraveling bed slope from relative roughness in initial sediment motion. J. Geophys. Res. Earth Surf. 120, 474–489.
Prancevic, J.P., Lamb, M.P., Fuller, B.M., 2014. Incipient sediment motion across the river to debris-flow transition. Geology 42, 191–194.
Pugh, F.J., Wilson, K.C., 1999. Velocity and concentration distributions in sheet flow above plane beds. J. Hydraul. Eng. 125, 117–125.
Radice, A., 2009. Use of the Lorenz curve to quantify statistical nonuniformity of sediment transport rate. J. Hydraul. Eng. 135, 320–326.
Ravazzolo, D., Mao, L., Friedrich, H., 2022. Hydrograph shape impact on sand infiltration and sediment transport dynamics in gravel-bed rivers. Water Resour. Res. 58 e2021WR031362.
Rebai, D., Berzi, D., Ballio, F., Matousek, V., 2022. Experimental comparison of inclined flows with and without intense sediment transport: flow resistance and surface elevation. J. Hydraul. Eng. 148, 04022026.
Recking, A., 2009. Theoretical development on the effects of changing flow hydraulics on incipient bed load motion. Water Resour. Res. 45, W04401.
Recking, A., 2010. A comparison between flume and field bed load transport data and consequences for surface-based bed load transport prediction. Water Resour. Res. 46, W03518.
Recking, A., 2012. Influence of sediment supply on mountain streams bedload transport. Geomorphology 175-176, 139–150.
Recking, A., 2013. Simple method for calculating reach-averaged bed-load transport. J. Hydraul. Eng. 139, 70–75.
Recking, A., Frey, P., Paquier, A., Belleudy, P., Champagne, J.Y., 2008a. Bed-load transport flume experiments on steep slopes. J. Hydraul. Eng. 134, 1302–1310.
Recking, A., Frey, P., Paquier, A., Belleudy, P., Champagne, J.Y., 2008b. Feedback between bed load transport and flow resistance in gravel and cobble bed rivers. Water Resour. Res. 44, W05412.
Recking, A., Bacchi, V., Naaim, M., Frey, P., 2009a. Antidunes on steep slopes. J. Geophys. Res. 114, F04025.
Recking, A., Frey, P., Paquier, A., Belleudy, P., 2009b. An experimental investigation of mechanisms involved in bed load sheet production and migration. J. Geophys. Res. 114, F03010.
Recking, A., Liébault, F., Peteuil, C., Jolimet, T., 2012. Testing bedload transport equations with consideration of time scales. Earth Surf. Process. Landf. 37, 774–789.
Recking, A., Piton, G., Vazquez-Tarrio, D., Parker, G., 2016. Quantifying the morphological print of bedload transport. Earth Surf. Process. Landf. 41, 809–822.
Recking, A., Vázquez Tarro, D., Piton, G., 2023. The contribution of grain sorting to the dynamics of the bedload active layer. Earth Surf. Process. Landf. 48 https://doi.org/10.1002/esp.5530.
Revil-Baudard, T., Chauchat, J., 2013. A two-phase model for sheet flow regime based on dense granular flow rheology. J. Geophys. Res. Oceans 118, 2012JC008306.
Ribberink, J.S., 1998. Bed load transport for steady and unsteady oscillatory flows. Cost. Eng. 34, 59–82.
Richards, K.S., 1977. Channel and flow geometry: a geomorphological perspective. Prog. Phys. Geogr. 1, 65–102.
Rickenmann, D., 1992. Hyperconcentrated flow and sediment transport at steep slopes. J. Hydraul. Eng. 117, 1419–1439.
Rickenmann, D., Fritschi, B., 2017. Bedload transport measurements with impact plate geophones in two Austrian mountain streams (Fischbach and Ruetz): system calibration, grain size estimation, and environmental signal pick-up. Earth Surf. Dyn 5, 669–687.
Rickenmann, D., Ammann, L., Nicollier, T., Boss, S., Fritschi, B., Antoniazza, G., Steeb, N., Chen, Z., Wyss, C., Badoux, A., 2022. Comparison of calibration characteristics of different acoustic impact systems for measuring bedload transport in mountain streams. Earth Surf. Dyn 10, 1165–1183.
Roseberry, J.C., Schmeeckle, M.W., Furbish, D.J., 2012. A probabilistic description of the bed load sediment flux: 2. Particle activity and motions. J. Geophys. Res 117. F03032.
Rouse, H., 1965. Critical analysis of open-channel resistance. J. Hydraul. Div. ASCE 91, 1–23.
Rousseau, G., Ancey, C., 2022. An experimental investigation of turbulent free-surface flows over a steep permeable bed. J. Fluid Mech. 941, A51.
Rousseau, H., Chassagne, R., Chauchat, J., Maurin, R., Frey, P., 2021. Bridging the gap between particle-scale forces and continuum modelling of size segregation: application to bedload transport. J. Fluid Mech. 916, A26.
Ruiz-Villanueva, V., Piégay, H., Gurnell, A.M., Marston, R.A., Stoffel, M., 2016. Recent advances quantifying the large wood dynamics in river basins: new methods and remaining challenges. Rev. Geophys. 54, 611–652.
Ryan, S.E., Porth, L.S., 1999. A field comparison of three pressure-difference bedload samplers. Geomorphology 30, 307–322.

Ryan, S.E., Porth, L.S., Troendle, C.A., 2002. Defining phases of bedload transport using piecewise regression. Earth Surf. Process. Landf. 27, 971–990.
Ryan, S.E., Porth, L.S., Troendle, C.A., 2005. Coarse sediment transport in mountain streams in Colorado and Wyoming, USA. Earth Surf. Process. Landf. 30, 269–288.
Salevan, J.C., Clark, A.H., Shattuck, M.D., O'Hern, C.S., Ouellette, N.T., 2017. Determining the onset of hydrodynamic erosion in turbulent flow. Phys. Rev. Fluids 2, 114302.
Savage, S.B., 1984. The mechanics of rapid granular flows. Adv. Appl. Mech. 24, 289–366.
Schmeeckle, M.W., 2014. Numerical simulation of turbulence and sediment transport of medium sand. J. Geophys. Res. Earth Surf. 119, 2013JF002911.
Schneider, J.M., Rickenmann, D., Turowski, J.M., Bunte, K., Kirchner, J.W., 2015. Applicability of bed load transport models for mixed-size sediments in steep streams considering macro-roughness. Water Resour. Res. 51, 5260–5283.
Schoklitsch, A., 1934. Der Geschiebetrieb und die Geschiebefracht. Wasserkraft und Wasserwirtschaft 4, 1–7.
Schwindt, S., Negreiros, B., Mudiaga-Ojemu, B.O., Hassan, M.A., 2023. Meta-analysis of a large bedload transport rate dataset. Geomorphology 435, 108748.
Seddon, J.A., 1886. Some considerations of the relation of bedload to the variables in river hydraulics. J. Assoc. Eng. Soc. 5, 127–134.
Seminara, G., Solari, L., Parker, G., 2002. Bed load at low Shields stress on arbitrary sloping beds: failure of the Bagnold hypothesis. Water Resour. Res. 38, 1249.
Seshadri, R., Na, T.Y., 1985. Group Invariance in Engineering Boundary Value Problems. Springer, New York.
Shields, A., 1936. Anwendung der Aehnlichkeitsmechanik und der Turbulenzforschung auf die Geschiebebewegung. Technical Report. Mitteilungen der Preussischen Versuchsanstalt für Wasserbau und Schiffbau, Heft 26.
Shih, W., Diplas, P., 2018. A unified approach to bed load transport description over a wide range of flow conditions via the use of conditional data treatment. Water Resour. Res. 54, 3490–3509.
Simeonov, J.A., Calantoni, J., 2012. Modeling mechanical contact and lubrication in direct numerical simulations of colliding particles. Int. J. Multiphase Flow 46, 38–53.
Simons, D.B., Richardson, E.V., Nordin, C.F., 1965. Bedload equation for ripples and dunesv. U. S. Geological Survey.
Singh, V.P., 2001. Kinematic wave modelling in water resources:a historical perspective. Hydrol. Process. 15, 671–706.
Singh, A., Nott, P.R., 2003. Experimental measurements of the normal stresses in sheared Stokesian suspensions. J. Fluid Mech. 490, 293–320.
Singh, V.P., Yang, C.T., Deng, Z.Q., 2003. Downstream hydraulic geometry relations:1. Theoretical development. Water Resour. Res. 39, 1337.
Singh, A., Fienberg, K., Jerolmack, D.J., Marr, J., Foufoula-Georgiou, E., 2009. Experimental evidence for statistical scaling and intermittency in sediment transport rates. J. Geophys. Res. 114, 2007JF000963.
Smart, G.M., 1984. Sediment transport formula for steep channels. J. Hydraul. Eng. 110, 267–276.
Smart, G.M., Jaeggi, M.N.R., 1983. Sedimenttransport in steilen Gerinnen. Technical Report 64. Mitteilungen 64 der Versuchanstalt für Wasserbau, Hydrologie und Glaziologie.
Solé, R.V., Manrubia, S.C., Benton, M., Kauffman, S., Bak, P., 1999. Criticality and scaling in evolutionary ecology. Trends Ecol. Evol. 14, 156–160.
Sornette, D., 2000. Critical Phenomena in Natural Sciences. Springer, New York.
Sterling, S.M., Church, M., 2002. Sediment trapping characteristics of a pit trap and the Helley–Smith sampler in a cobble gravel bed river. Water Resour. Res. 38, 19–1–19–11.
Strick, R.J.P., Ashworth, P.J., Sambrook Smith, G.H., Nicholas, A.P., Best, J.L., Lane, S. N., Parsons, D.L.R., Simpson, C.J., Unsworth, C.A., Dale, J., 2019. Quantification of bedform dynamics and bedload sediment flux in sandy braided rivers from airborne and satellite imagery. Earth Surf. Process. Landf. 44, 953–972.
Sumer, B.M., Kozakiewicz, A., Fredsoe, J., Deigaard, R., 1996. Velocity and concentration profiles in sheet-flow layer of movable bed. J. Hydraul. Eng. 122, 549–558.
Surian, N., Cisotto, A., 2007. Channel adjustments, bedload transport and sediment sources in a gravel-bed river, Brenta River, Italy. Earth Surf. Process. Landf. 32, 1641–1656.
Suszka, L., 1987. Sediment transport at steady and unsteady flow: a laboratory study. Ph. D. thesis. Ecole Polytechnique Fédérale de Lausanne.
Takahashi, T., 1981. Debris flow. Annu. Rev. Fluid Mech. 13, 57–77.
Takahashi, T., 2007. Debris Flow: Mechanics, Prediction, and Countermeasures. Taylor and Francis, London.
Tal, M., Paola, C., 2010. Effects of vegetation on channel morphodynamics: results and insights from laboratory experiments. Earth Surf. Process. Landf. 35, 1014–1028.
Tan, M., Goldhirsch, I., 1998. Rapid granular flows as mesoscopic systems. Phys. Rev. Lett. 81, 3022.
Terwisscha van Scheltinga, R.C., Coco, G., Kleinhans, M.G., Friedrich, H., 2021. Sediment transport on a sand bed with dunes: deformation and translation fluxes. J. Geophys. Res. Earth Surf. 127 e2021JF006292.
Thompson, S.M., Campbell, P.L., 1979. Hydraulics of a large channel paved with boulders. J. Hydraul. Res. 17, 341–354.
Thompson, P.W., Tiffany, J.B., Bentzel, C.E., Schweizer, C.W., Buchanan, S.J., Vogel, H. D., Nichols, C.E., 1935. Studies of River Bed Materials and Their Movement, With Special Reference to the Lower Mississippi River. In: Technical Report Paper 17. U.S. Waterways Experiment Station.
Thorn, C.E., Welford, M.R., 1994. The equilibrium concept in geomorphology. Ann. Am. Assoc. Geogr 84, 666–696.
Tognacca, C., 1997. Debris-flow initiation by channel-bed failure. In: Chen, C.L. (Ed.), First International Conference on Debris Flow Hazards Mitigation. ASCE, San Fransisco, pp. 44–53.
Tranmer, A.W., Caamaño, D., Goodwin, P., 2020. Identifying dynamic equilibrium of an undeveloped alluvial stream by extremal hypotheses. CATENA 194, 104680.
Tsujimoto, T., 1991. Bed-load transport in steep channels. In: Armanini, A., Di Silvio, G. (Eds.), Fluvial Hydraulics of Mountain Regions. Springer, Berlin, pp. 89–102.
Turcotte, D.L., 1995. Scaling in geology: Landforms and earthquakes. Proc. Natl. Acad. Sci. U. S. A. 92, 6697–6704.
Turowski, J.M., Rickenmann, D., Dadson, S.J., 2010. The partitioning of the total sediment load of a river into suspended load and bedload: a review of empirical data. Sedimentology 57, 1126–1146.
Turowski, J.M., Badoux, A., Rickenmann, D., 2011. Start and end of bedload transport in gravel-bed streams. Geophys. Res. Lett. 38, L04401.
Turowski, J.M., Badoux, A., Leuzinger, J., Hegglin, R., 2013. Large floods, alluvial overprint, and bedrock erosion. Earth Surf. Process. Landf. 38, 947–958.
Valyrakis, M., Diplas, P., Dancey, C.L., 2013. Entrainment of coarse particles in turbulent flows: An energy approach. J. Geophys. Res. Earth Surf. 118, 42–53.
van Rijn, L., 1984a. Sediment transport, part I: bed load transport. J. Hydraul. Eng. 110, 1431–1456.
van Rijn, L., 1984b. Sediment transport, part III: bed forms and alluvial roughness. J. Hydraul. Eng. 110, 1733–1754.
Van Rijn, L.C., 1993. Principles of Sediment Transport in Rivers, Estuaries and Coastal Seas, vol. 1006. Aqua publications Amsterdam.
Venditti, J.G., Dietrich, W.E., Nelson, J., Wydzga, M.A., Fadde, J., Sklar, L.S., 2010. Mobilization of coarse surface layers in gravel-bedded rivers by finer gravel bed load. Water Resour. Res. 46, W07506.
Vericat, D., Church, M., Batalla, R.J., 2006. Bed load bias: Comparison of measurements obtained using two (76 and 152 mm) Helley-Smith samplers in a gravel bed river. Water Resour. Res. 42, W01402.
Vericat, D., Wheaton, J.M., Brasington, J., 2017. Revisiting the morphological approach: opportunities and challenges with repeat high-resolution topography. In: Tsutsumi, D., Laronne, J.B. (Eds.), Gravel-Bed Rivers: Process and Disasters, 121. Wiley, New York, pp. 121–158.
Wainwright, J., Parsons, A.J., Cooper, J.R., Gao, P., Gillies, J.A., Mao, L., Orford, J.D., Knight, P.G., 2015. The concept of transport capacity in geomorphology. Rev. Geophys. 53, 1155–1202.
Wang, X., Zheng, J., Li, D., Qu, Z., 2008. Modification of the Einstein bed-load formula. J. Hydraul. Eng. 134, 1363–1369.
Wang, L., Cuthbertson, A., Pender, G., Zhong, D., 2019. Bed load sediment transport and morphological evolution in a degrading uniform sediment channel under unsteady flow hydrographs. Water Resour. Res. 55, 5431–5452.
Warburton, J., 1992. Observations of bed load transport and channel bed changes in a proglacial mountain stream. Arct. Alp. Res. 24, 195–203.
Whiting, P.J., King, J.G., 2003. Surface particle sized on armoured gravel streambed: effects of supply and hydraulics. Earth Surf. Process. Landf. 28, 1459–1471.
Wilcock, P.R., 1990. Bed-load transport of mixed-size sediment. Ph.D. thesis. Massachusetts Institute of Technology.
Wilcock, P.R., Crowe, J.C., 2003. Surface-based transport model for mixed-size sediment. J. Hydraul. Eng. 129, 120–128.
Wilcock, P.R., McArdell, W., 1997. Partial transport of a sand/ gravel sediment. Water Resour. Res. 33, 235–245.
Willgoose, G., 2005. Mathematical modeling of whole landscape evolution. Annu. Rev. Earth Planet. Sci. 33, 443–459.
Williams, G.P., 1970. Flume width and water depth effects in sediment-transport experiments. Technical Report Professional Paper 562-H. USGS.
Williams, R.D., Brasington, J., Hicks, D.M., 2016. Numerical modelling of braided river morphodynamics: review and future challenges. Geogr. Compass 10, 102–127.
Wilson, K.C., 1966. Bed-load transport at high shear stress. J. Hydraul. Div. ASCE 92, 49–59.
Wilson, K.C., 1989. Mobile-bed friction at high shear stress. J. Hydraul. Eng. 115, 825–830.
Wohl, E., Scott, D.N., 2017. Wood and sediment storage and dynamics in river corridors. Earth Surf. Process. Landf. 42, 5–23.
Wong, M., Parker, G., 2006. Reanalysis and correction of bed-load relation of Meyer-Peter and Müller using their own database. J. Hydraul. Eng. 132, 1159–1168.
Wu, W., Wang, S.S.Y., 2007. One-dimensional modeling of dam-break flow over movable beds. J. Hydraul. Eng. 133, 48–58.
Xu, G., Zhao, L., Yang, C.T., 2016. Derivation and verification of minimum energy dissipation rate principle of fluid based on minimum entropy production rate principle. Int. J. Sediment Res. 31, 16–24.
Yager, E.M., Schmeeckle, M.W., 2013. The influence of vegetation on turbulence and bed load transport. J. Geophys. Res. Earth Surf. 118, 1585–1601.
Yager, E.M., Kirchner, J.W., Dietrich, W.E., 2007. Calculating bed load transport in steep boulder bed channels. Water Resour. Res. 43, W07418.
Yager, E.M., Turowski, J.M., Rickenmann, D., McArdell, B.W., 2012. Sediment supply, grain protrusion, and bedload transport in mountain streams. Geophys. Res. Lett. 39, L10402.
Yager, E.M., Schmeeckle, M.W., Badoux, A., 2018. Resistance is not futile: grain resistance controls on observed critical Shields stress variations. J. Geophys. Res. Earth Surf. 123, 3308–3322.
Yager, E.M., Venditti, J.G., Smith, H.J., Schmeeckle, M.W., 2019. The trouble with shear stress. Geomorphology 323, 41–50.
Yalin, M.S., Ferreira Da Silva, A.M., 1999. Regime channels in cohesionless alluvium. J. Hydraul. Res. 37, 725–742.

Yalin, M.S., Ferreira Da Silva, A.M., 2000. Computation of regime channel characteristics on thermodynamic basis. J. Hydraul. Res. 38, 57–63.
Yang, C.T., 1971. Potential energy and stream morphology. Water Resour. Res. 7, 311–322.
Yang, C.T., 1984. Unit stream power equation for gravel. J. Hydraul. Eng. 110, 1783–1797.
Yang, C.T., 1992. Force, energy, entropy, and energy dissipation rate. In: Singh, V.P., Fiorentino, M. (Eds.), Entropy and Energy Dissipation in Water Resources. Springer, Dordrecht, pp. 63–89.
Yang, C.T., 1994. Variational theories in hydrodynamics and hydraulics. J. Hydraul. Eng. 120, 737–756.
Yang, C.T., 1996. Sediment Transport:Theory and Practice. McGraw-Hill, New York.
Yang, C.T., Molinas, A., 1982. Sediment transport and unit stream power function. J. Hydraul. Div. ASCE 108, 774–793.
Yang, J.Q., Nepf, H.M., 2019. Impact of vegetation on bed load transport rate and bedform characteristics. Water Resour. Res. 55, 6109–6124.
Yang, C.T., Song, C.C.S., Woldenberg, M.J., 1981. Hydraulic geometry and minimum rate of energy dissipation. Water Resour. Res. 17, 1014–1018.
Zhang, Q., Deal, E., Perron, J.T., Venditti, J.G., Benavides, S.J., Rushlow, M., Kamrin, K., 2022. Fluid-driven transport of round sediment particles: from discrete simulations to continuum modeling. J. Geophys. Res. Earth Surf. 127 e2021JF006504.